UNIVERSITÀ
DEGLI STUDI
DI PADOVA

Sede Amministrativa: Università degli Studi di Padova

Dipartimento di SCIENZE BIOMEDICHE SPERIMENTALI

SCUOLA DI DOTTORATO DI RICERCA IN : BIOSCIENZE
INDIRIZZO: NEUROBIOLOGIA
CICLO XXIII

Study of the nerve terminal regeneration in neuromuscular junction intoxicated with different presynaptic neurotoxins

Direttore della Scuola: Ch.mo Prof. Giuseppe Zanotti
Coordinatore d'indirizzo: Ch.mo Prof. Daniela Pietrobon
Supervisore: Dott. Ornella Rossetto

Dottorando: Erik Tedesco

SOMMARIO

La giunzione neuromuscolare (GNM) e' una struttura fondamentale in biologia e la sua organizzazione e' stata recentemente complicata dall' aggiunta delle cellule di Schwann perisinaptiche (CSP), portando al concetto di sistema tripartito. Le CSP rappresentano la glia della GNM e sono coinvolte nel suo recupero in seguito a danno. Infatti, le CSP dedifferenziano in seguito a danno al terminale nervoso (TN), rimuovono i detriti derivanti della sua degenerazione e protrudono una serie di prolungamenti che guidano la reinnervazione. Alcuni mediatori implicati nell'attivazione dell CSP sono stati individuati (es. ATP, ACh) ma noi ipotizziamo che anche l'acido arachidonico e I suoi derivati possano portare all'attivazione dell CSP. I modelli di danno al nervo usati fino ad ora forniscono un sistema non controllabile dal momento che portano alla degenerazione Walleriana, un processo degenerativo e infiammatorio. L'iniezione intramuscolare di tossine presinaptiche (α-LTX and SPANs), provocando un danno limitato al solo TN, rappresenta il nostro sistema sperimentale. Dal momento che le SPANs conducono alla degenerazione del TN mediante differenti azioni, per determinare il contributo relativo dell'influsso di Ca^{2+} abbiamo effettuato una comparazione con α-LTX, la quale provoca degenerazione del TN attraverso un massiccio ingresso di Ca^{2+}. Tutti I parametri analizzati sono simili per le due classi di neurotossine. Questo indica che il sovraccarico di Ca^{2+} gioca un ruolo di rilievo nella degenerazione del TN indotta da SPANs. Non sono state osservate differenze nella cinetica di degenerazione/rigenerazione dei TN tra muscoli veloci (EDL) e lenti (soleo). α-LTX provoca una degenerazione sincrona in completo accordo con i dati derivanti dal saggio di funzionalita' muscolare (saggio DAS). La degenerazione dei TN indotta da SPANs, nel caso specifico βBtx, presentano un motivo a chiazze e i dati derivati dal saggio DAS non correlano con le osservazioni immunoistologiche. Una differenza nel

comportamento delle CSP e' stato osservato tra EDL iniettati con α-LTX e denervati. Una diminuzione dell'intensita' del segnale delle CSP marcate con S100 e' stato osservata dopo trattamento con α-Ltx e denervazione, indicandone l'attivazione, ma non e' stata osservata la protrusione di prolungamenti se non nei muscoli denervati. Al fine di caratterizzare meglio questo peculiare comportamento dell CSP, abbiamo esteso l'analisi ad *marker* di attivazione delle CSP, quali Nestina and *Glial Fibrillaric Acidic Protein* (GFAP). Non sono state osservate differenze tra i controlli e i campioni intossicati. Considerando che le CSP acquisiscono un'attivita' simil-macrofagica in seguito ad attivazione e possiedono recettori in grado di individuare pattern molecolari associati a patogeni, ci siamo chiesti se peptidi formilati e DNA mitocondriale, derivanti dai mitocondri in degenerazione, possano attivare le CSP. Abbiamo provato a testare con diversi approcci la nostra ipotesi su colture primarie di cellule di Schwann ma, a causa di problemi sperimentali, i risultati non sono al momento conclusivi.

ABSTRACT

The neuromuscular junction (NMJ) is a fundamental structure in biology and its organization have been complicated by the addiction of perisynaptic Schwann cells (PSCs), leading to the tripartite system concept. PSCs are the glia of the NMJ and they are implicated in its recovery after damage. Indeed, PSCs dedifferentiate upon nerve terminal (NT) damage, remove NT debries and protrude prolongations to guide reinnervation. Some PSCs activation mediators have been found (ATP, ACh) but we hypothesized that also arachidonic acid and its derivates could lead to PSCs activation. Nerve damage models used till now provide a non controllable system since they lead to Wallerian degeneration, a degenerative/inflammatory process. The intramuscular injection of presynaptic neurotoxins (α-LTX and SPANs), provoking damage limited to the NTs, represents our experimental model. Since SPANs leads to NTs degeneration via different action, to unravel Ca^{2+} influx relative contribution we performed a side-by-side comparison with α-LTX, which provoke degeneration through massive Ca^{2+} influx. All analyzed parameters are similar for the two neurotoxin classes. This indicates that Ca^{2+} overloading plays a major role in NTs degeneration induced by SPANs. No differences were observed in NTs degeneration/regeneration kinetic between fast (EDL) and slow muscle (soleus). α-LTX provoke a synchronous degeneration of NTs in agreement with muscle functional assay (DAS assay). NTs degeneration induced by a SPAN such as βBtx present a "patch-like" pattern and DAS score do not parallels immunohistological observations. A difference in PSCs behaviour was observed between α-LTX-injected and denervated EDL. A decrease in signal intensity of S100-labeled PSCs was observed after α-Ltx treatment, indicating their activation, but no prolongations were observed except in denervated sample. To characterize PSCs behavior we extended the analysis to Nestin and Glial Fibrillaric Acidic Protein (GFAP), that label only activated PSCs. No differences between control and intoxicated

NTs were observed. Considering that PSCs acquire macrophagic-like activity and possess receptors sensing pathogen-associated molecular patterns we wondered if formylated peptides and mitochondrial DNA, coming from degenerating mitochondria, could activate PSCs. We tried to address this question on Schwann Cells primary culture with different approaches but, up to now, the results are not conclusive due to experimental problems.

Table of Contents

1 INTRODUCTION 1

1.1 THE NEUROMUSCULAR JUNCTION 1

1.2 SCHWANN CELLS 2

1.2.1 MYELINATING SCHWANN CELLS 3

1.2.2 NON-MYELINATING SCHWANN CELLS 4

1.3 PERISYNAPTIC SCHWANN CELLS FUNCTIONS AT NMJ 5

1.3.1 THE ROLE OF PSCS IN THE DEVELOPMENT OF NMJ 5

1.3.2 THE ROLE OF PSCS IN THE MAINTENANCE OF THE ADULT NMJ 7

1.3.3 THE ROLE OF PSCS IN SYNAPTIC TRANSMISSION AT ADULT NMJ 8

1.3.4 PSCS IN NERVE DEGENERATION AND REGENERATION 9

1.4 PROBES FOR PSCS 17

1.5 THE IMMUNOCOMPETENCE OF SCHWANN CELLS 18

1.5.1 PATTERN RECOGNITION RECEPTORS 18

1.6 PRESYNAPTIC NEUROTOXINS 21

1.6.1 α- LATROTOXIN (α-LTX) 22

1.6.2 PRESYNAPTIC SNAKE NEUROTOXIN ENDOWED WITH PLA2 ACTIVITY (SPANS) 28

2 AIM 31

3 MATERIAL AND METHODS 33

3.1 MATERIAL 33

3.2 METHODS 34

3.2.1 ANIMAL CARE AND TREATMENT 34

3.2.2 CELLULAR BIOLOGY 36

3.2.3 CALCIUM IMAGING 41

3.2.4 BIOCHEMICAL TECHNIQUE 43

3.2.5 IMMUNOFLUORESCENCE 45

4 RESULTS AND DISCUSSIONS 49

4.1 RESULTS (PART I) 49

4.1.1 SPANS AND α-LTX INDUCE SIMILAR BULGING ON RAT PRIMARY NEURONS 49

4.1.2 SPAN AND α-LTX-INDUCED BULGES ACCUMULATE SYNAPTIC VESICLE MARKERS 50
4.1.3 SPANS AND α-LTX INDUCE EXPOSURE OF SYNAPTIC VESICLE LUMINAL PROTEINS IN CULTURED NEURONS 50
4.1.4 SPANS AND α-LTX INDUCE ENTRY OF CALCIUM INTO CULTURED NEURONS 52
4.1.5 DEGENERATION OF PRESYNAPTIC NERVE TERMINALS AT NMJ AFTER SPAN OR α-LTX EXPOSURE 53
4.2 DISCUSSION 55
4.3 RESULTS (PART II) 57
4.3.1 NERVE TERMINAL DEGENERATION / REGENERATION KINETICS IN MUSCLES INTOXICATED WITH PRESYNAPTIC NEUROTOXINS 57
4.3.2 NERVE TERMINAL DEGENERATION AND REGENERATION IN α-LTX INTOXICATED MUSCLES 57
4.3.3 NERVE TERMINAL DEGENERATION AND REGENERATION IN B-BTX INTOXICATED MUSCLES 61
4.3.4 α-LTX DIFFUSION IN INJECTED EDL 64
4.3.5 PERISYNAPTIC SCHWANN CELLS RESPONSE TO NMJ INTOXICATION BY α-LTX IN EDL MUSCLE 65
4.3.6 PERISYNAPTIC SCHWANN CELLS RESPONSE TO SURGICAL DENERVATION IN EDL MUSCLE 67
4.4 DISCUSSION AND PERSPECTIVES 71
4.5 RESULTS (PART III) 75
4.5.1 PRIMARY SCHWANN CELLS CULTURE PURITY 75
4.5.2 MORPHOLOGICAL AND CYTOSKELETAL MODIFICATION IN MTDS AND FMLP-TREATED SCHWANN CELLS 75
4.5.3 IMMUNOCYTOCHEMICAL LOCALIZATION OF TLR9 AND FPR1 IN SCHWANN CELLS 78
4.5.4 TLR9 COLOCALIZATION WITH ENDOSOMES AND ENDOPLASMIC RETICULUM MARKER 78
4.5.5 WESTERN BLOT ANALYSIS 79
4.5.6 CALCIUM RESPONSE OF SCS TREATED WITH FMLP AND MTDS. 82
4.5.7 CALCIUM RESPONSE OF PSCS TO ATP AND ACETYLCHOLINE 84
4.5.8 CALCIUM RESPONSE OF PSCS TO α-LTX 88
4.6 DISCUSSION AND PERSPECTIVES 89

5 REFERENCES 93

Abbreviations

NMJ	NeuroMuscular Junction
AChRs	AcetylCHoline Receptors
PSCs	Perisynaptic Schwann Cells
SCs	Schwann Cells
SCPs	Schwann Cell Precursors
ACh	AcetylCHoline
ATP	Adenosine TriPhosphate
BzATP	Benzoil-ATP
GFAP	Glial Fibrillary Acidic Protein
GAP-43	Growth Associated Protein-43
NT	Nerve Terminal
PAMPs	Pathogen-Associated Molecular Patterns
DAMPs	Damage-Associated Molecular Patterns
MTDs	Mitochondrial DAMPs
TLR	Toll-Like Receptor
FPR	Formyl Peptide Receptor
ER	Endoplasmic Reticulum
PNA	PeaNut Agglutinin
LTX	LatroToXin
SPAN	Snake Neurotoxin endowed with PLA2 activity
PLA2	Phospholipase Activity 2
BTX	BungaroToXin
EDL	Extensor Digitorum Longus
FMLP	Formyl-Met-Leu-Phe
BSA	Bovine Serum Albumin

1 Introduction

1.1 The Neuromuscular Junction

The neuromuscular junction (NMJ) is a specialized chemical synapse designed to transmit electrical impulse from the nerve to the skeletal muscle via the neurotransmitter acetylcholine and much of our knowledge about how a synapse works comes from the study of this kind of synapse.

The vertebrate NMJs, similar to other chemical synapse in the central nervous system (CNS), have been previously considered composed of two active components: 1) the presynaptic nerve terminal, characterized by specialized sites, the so called active zones, where neuroexocytosis occurs and 2) the postsynaptic specialization on the muscle fiber containing the nicotinic receptor for acetylcholine (nAChRs). Though it has long been noticed that glial cells named perisynaptic Schwann cells (PSCs) are intimately associated with the nerve-muscle contact, these synapse-associated glial cells were considered merely passive supporting players at the synapse. However, a flurry of recent studies have unraveled the active roles of PSCs in formation, function, maintenance, and repair of NMJ,

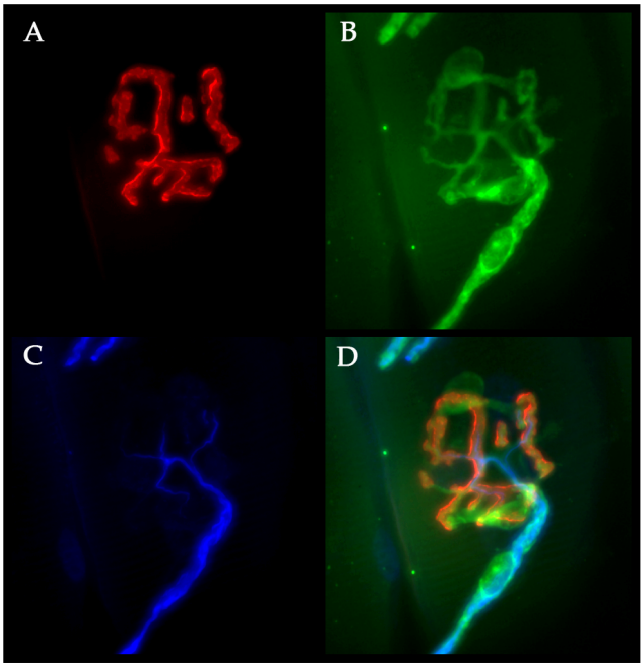

Figure 1 The Organization of the NMJ. A) The postsynaptic specialization labeled with α-BTX conjugated with Alexa 555 (red); B) the perisynaptic Schwann cells labeled with an antibody against S100 (green); C) the nerve terminal labeled with an antibody against neurofilaments (NF200) (blu). D) Merge. The interdigitation of the nerve terminal with the "pretzel"-like structure of the postsynaptic specialization is shown, moreover the PSCs branches completely cover the nerve terminal.

demonstrating that PSC s are indeed integral and essential components of the NMJ. Taken together, these considerations led to the concept of "tripartite" synapse (Fig. 1).

1.2 Schwann Cells

Schwann cells (SCs) are the principal glia of the peripheral nervous system (PNS). Named after the German physiologist Theodor Schwann, SCs are a variety of glial cell that keep peripheral nerve fibres (both myelinated and unmyelinated) alive.

SCs are of neural crest origin (Fig. 2) [1]. During mouse embryonic development, neural crest cells first differentiate into Schwann cell precursors (SCPs) at around embryonic day (E) 12-13 [2]. These precursor cells subsequently differentiate into immature SCs at approximately E15-16, persisting until birth. The postnatal fate of the immature Schwann cell depends on its random association with axons. In a process called radial sorting, whereby SCs segregate axons by extending processes into axon bundles, the SCs that happen to associate with a large diameter axon (>1 μm) will develop into myelinating SCs. Small diameter axons become entrenched in the invaginations of non-myelinating SCs, also called Remak bundles. A further class

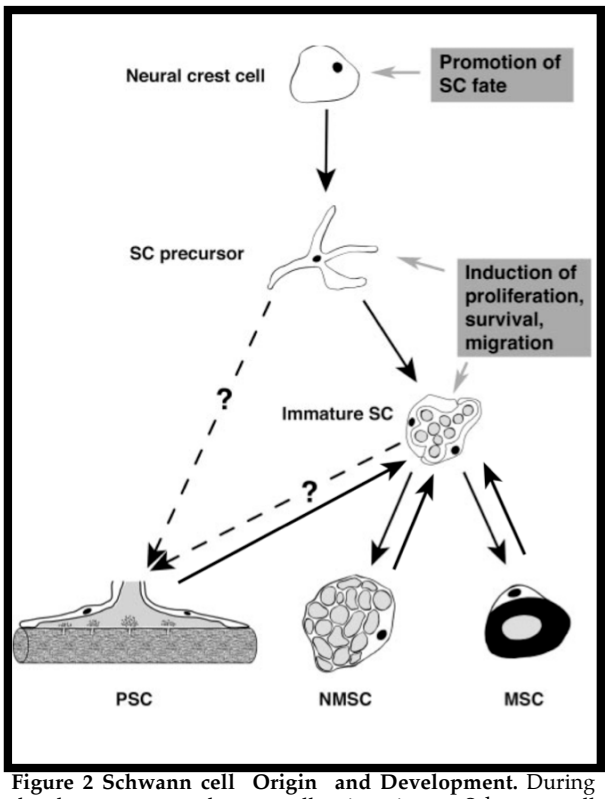

Figure 2 Schwann cell Origin and Development. During development, neural crest cells give rise to Schwann cell precursors, which then develop into the three adult phenotypes: PSCs, NMSCs, or MSCs. During their differentiation into MSCs and NMSCs, the precursors proceed through a stage called immature Schwann cell, whereas the direct precursor of PSCs remains unknown. NRG1– erbB signaling regulates important aspects of Schwann cell biology at each step of their development

of non-myelinating Schwann cell, the terminal (or perisynaptic) Schwann cell, exists at the neuromuscular junction, in close proximity to the neuron-muscle synapse (Fig. 2).

The transition from immature Schwann cell to myelinating/non-myelinating Schwann cell is reversible (Fig. 2). After nerve injury, SCs can dedifferentiate to a cell type resembling the immature Schwann cell, often referred to as a denervated or dedifferentiated Schwann cell. This allows them to re-enter the cell cycle in order to proliferate and aid nerve regeneration [3].

1.2.1 Myelinating Schwann Cells

In myelinated axons, SCs form the myelin sheath. The sheath is not continuous. Individual myelinating SCs cover about 100 micrometres of an axon. This equates to approximately 10,000 SCs along a 1 meter length of the axon. The gaps between adjacent SCs are called nodes of Ranvier (Fig. 3). The vertebrate nervous system relies on the myelin sheath for insulation and as a method of decreasing membrane capacitance in the axon. The action potential jumps from node to node, in a process called saltatory conduction, which can increase conduction velocity up to ten times, without an increase in axonal diameter. Unlike oligodendrocytes, each myelinating Schwann cell provides insulation to

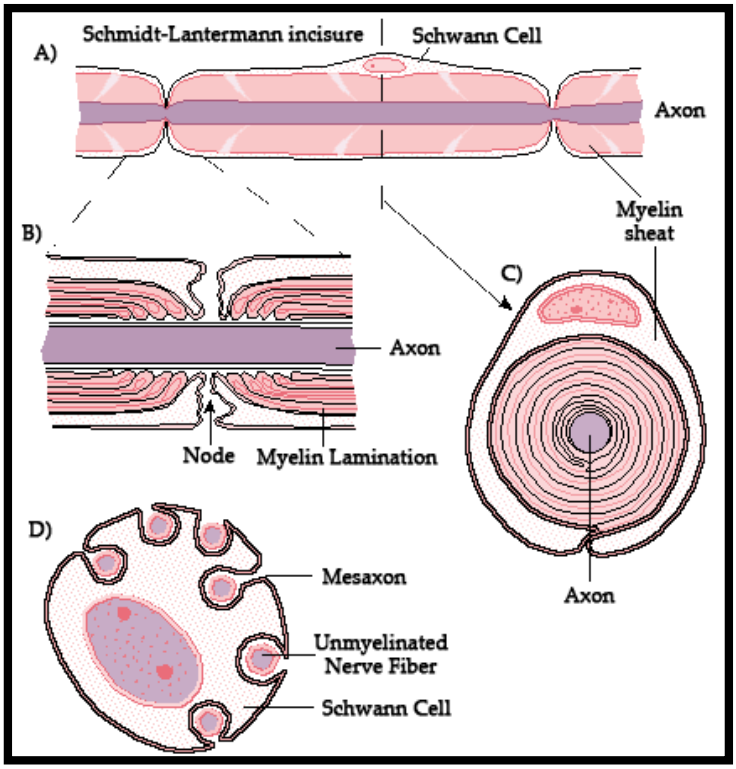

Figure 3 The Myelinating Schwann cells. A) Organization of myelinating Schwann cells along the axon. To be noted the strict 1:1 ratio between mSCs and axon. mSCs cytoplasm is in contact with the axon via the Schmidt-Lantermann incisures. B) The interruption between contiguous mSCs, called Node of Ranvier allows the saltatory conduction of the action potential. C) Transversal section of a myelinated nerve. D) The Remark bundles.

only one axon (Fig. 3). This arrangement permits saltatory conduction of action potentials with repropagation at the nodes of Ranvier. In this way, myelination greatly increases speed of conduction and saves energy.

Myelinating SCs begin to form the myelin sheath in mammals during fetal development and work by spiraling around the axon, sometimes with as many as 100 revolutions. A well-developed SC is shaped like a rolled-up sheet of paper, with layers of myelin in between each coil. The inner layers of the wrapping, which are predominantly membrane material, form the myelin sheath while the outermost layer of nucleated cytoplasm forms the neurolemma. Only a small volume of residual cytoplasm communicates the inner from the outer layers, the Schmidt-Lantermann incisure (Fig. 3).

1.2.2 Non-Myelinating Schwann Cells

1.2.2.1 Remak Bundles Schwann Cells

C fiber axons are grouped together into what is known as Remak bundles. These occur when an unmyelinated SCs bundles the axons close together by surrounding them. The Schwann cell keeps them from touching each other by squeezing its cytoplasm between the axons (Fig. 3). The condition of Remak bundles varies with age. The number of C fiber axons in each Remak bundle varies with location. Multiple neurons contribute axons to the Remak bundle with an average ratio of about 2 axons contributed per bundle. Remak bundles in the distal peripheral nerve are clustered with other Remak bundles. The Remak Schwann cells have been shown to be electrochemically responsive to action potentials of the axons contained within them.

In experiments where nerve injury is caused but nearby C fibers remain intact, increased spontaneous activity in the C fibers is observed. This phenomenon supports the theory that damaged nerve fibers may release factors that alter the function of neighboring undamaged fibers. Study of Remak bundles has important implications in nerve regeneration after sustaining injury. Currently, recovery of distal C fiber function takes months and may still only regain incomplete function. This may result in

abnormal sensory function or neuropathic pain. Remak bundles are thought to release certain trophic factors that promote the regeneration of the damaged axons.

1.2.2.2 Perisynaptic Schwann Cells

A further class of non-myelinating SCs, the terminal (or perisynaptic) Schwann cell, exists at the neuromuscular junction, in close proximity to the neuron-muscle synapse (Fig. 1). As descrive above, PSCs exert a very important role in formation, maintenance, maturation, function and repair of the NMJs.

1.3 Perisynaptic Schwann cells functions at NMJ

1.3.1 The role of PSCs in the development of NMJ

PSCs are present at developing NMJs soon after the initial formation of nerve-muscle contacts [4,5,6]. The number of PSCs per NMJ increases before the period of rapid synaptic growth and also correlates with the length of the NMJ [4,7,8]. At developing NMJs, the survival of Schwann cell relies on axonal supply of neuregulin-1 (NRG-1). Thus, SCs both in the peripheral nerves and NMJs are absent in transgenic mice lacking NRG-1 or its receptors (ErbB2 or ErbB3) (Fig. 4) and undergo apoptosis in denervated developing muscle of young mice in which the NMJ is still in formation [9,10,11,12,13]. It is noticeable that apoptosis can be rescued by applying exogenous NRG-1 to neonatal rat muscle or by conditionally inducing the expression of constitutively active ErbB2 receptors in neonatal mouse SCs [14,15].

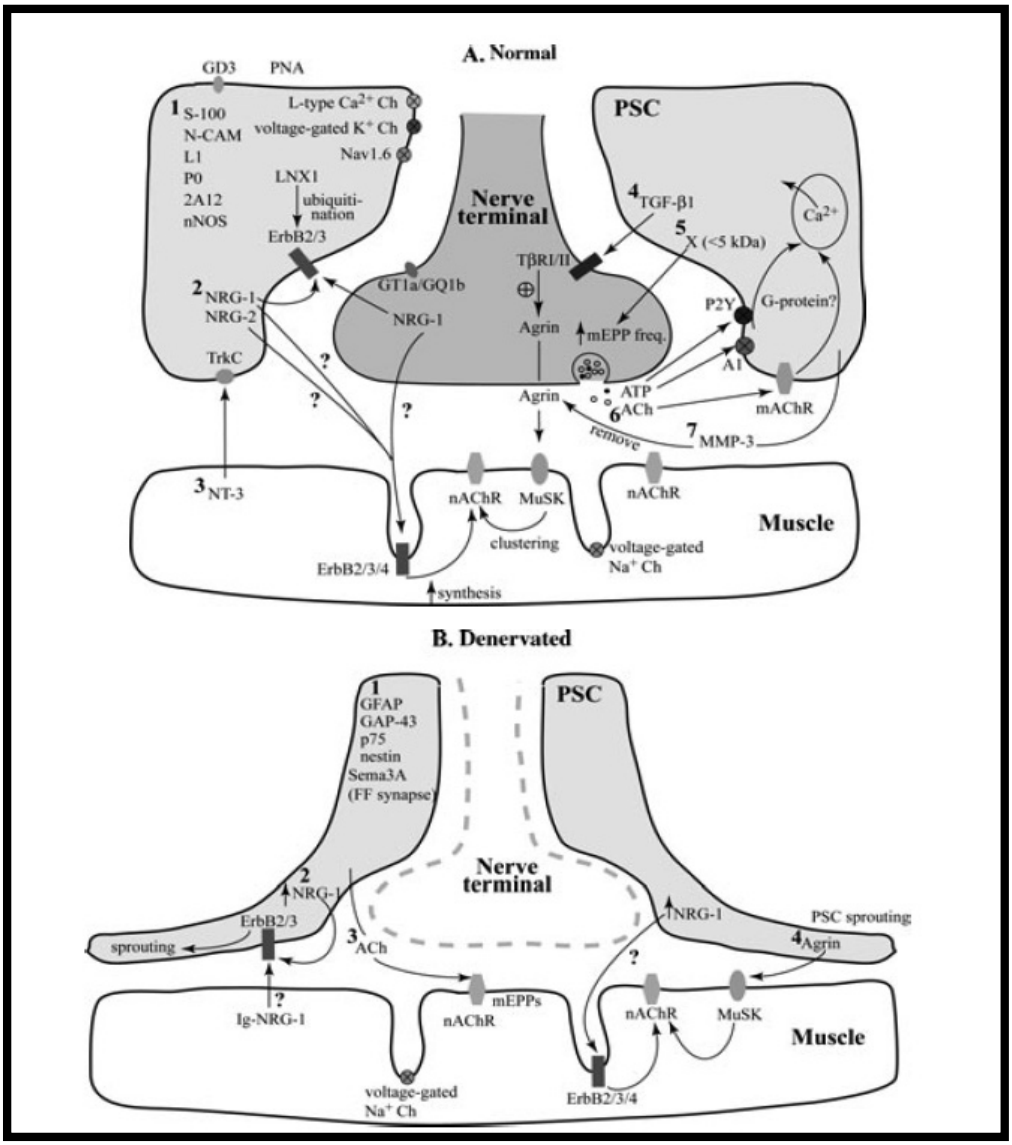

Figure 4 A schematic diagram depicting some of the interactions between PSCs and nerve–muscle contacts in intact muscles. 1. PSCs express a variety of molecules, including S100, N-CAM, L1, and myelin-associated protein P0. Frog PSCs also express unknown molecules recognized by mAb 2A12. In addition, several ion channels, such as L-type calcium channel, voltage-gated potassium channel, and voltage-gated sodium channels Nav1.6, have been shown to be localized on PSCs. 2. PSCs also express neuregulin (NRG)-1, NRG-2, and their receptors ErbB2/3. Nerve-derived NRG-1 is required for the serviva of developing PSCs. NRG-1 and NRG-2 derived from PSCs, together with NRG-1 derived from the nerve terminal, may play a role in regulating the synthesis of nicotinic acetylcholine receptors (nAChRs) in postsynaptic muscle fibers. 3. NT-3 receptor TrkC is localized on PSCs. Muscle-derived NT-3 may be a survival or mitogenic factor for developing PSCs. 4. Schwann cell–derived molecules, one of which has been suggested to be transforming growth factor (TGF)-β1, enhance synaptogenesis via upregulating the expression of neuronal agrin during development. 5. Unknown factor(s) (molecular weight <5kDa) released from Schwann cells potentiate(s) spontaneous synaptic activity during development. 6. Synaptic activity increases intracellular calcium level in PSCs via activating muscarinic AChRs (mAChRs) by ACh or P2Y and A1 receptors by ATP. 7. PSCs may release and activate matrix metalloproteinase 3 (MMP3),which may be involved in removing agrin from synaptic basal lamina. (B) A schematic diagram depicting some of the interactions between PSCs and nerve–muscle contacts in denervated muscles. 1. The expressions of several molecules are upregulated in PSCs after denervation, including GFAP, GAP-43, p75, nestin, and Semaphorin (Sema) 3A (only at fast-fatigable synapses). 2. Upregulated NRG-1 in PSCs may play a role in inducing PSC sprouting upon denervation. 3. ACh, released from PSCs, can induce spontaneous synaptic activity at denervated NMJs. 4. PSC-derived agrin may play a role in inducing AChR clusters underneath PSC sprouts in denervated muscles.

Despite the absence of Schwann cell, motor axons still project to muscle, indicating that SCs are dispensable for axon navigation towards their target muscles. However, nerve terminal retract after transiently contracting muscle fibers, suggesting that SCs may play a maintenance role at developing NMJs. This observation has been further confirmed by SCs *in vivo* complement-mediated immunocytolysis in tadpole muscles [16]. Moreover, PSCs sprouts induced by NRG-1 are sufficient to trigger nerve terminal sprouts in developing mammalian muscle [14,17].

It has been shown recently that besides axon-derived NRG-1, muscle-derived NT-3 might also serve as a survival or mitogenic factor for developing SCs and might regulate the number of PSCs at the NMJ (Fig. 4) [18].

1.3.2 The role of PSCs in the maintenance of the adult NMJ

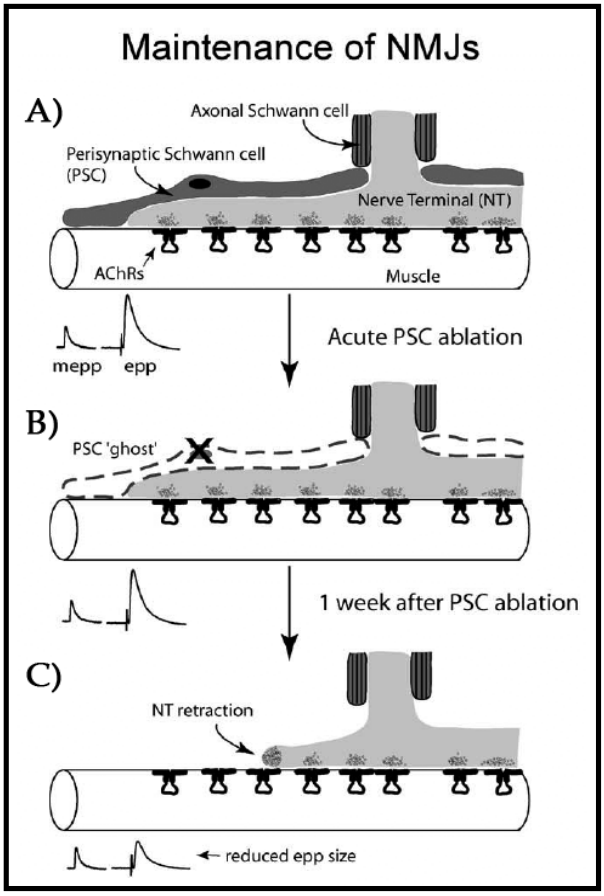

Figure 5 A schematic diagram summarizing the effects of removal of PSCs from adult (a–c) NMJs. (A) The intact NMJ with presynaptic nerve terminal, postsynaptic muscle membrane specializations, and the glial component, the PSCs. (B) NMJs after acute (5 hr) PSC ablation. Normal morphology and neurotransmission in the acute absence of PSCs suggests that PSCs are not required for the short-term maintenance of NMJs. (C) NMJs
1 week after PSC ablation. Nerve terminals retracted while AChR clusters remained unchanged, epps were reduced in size while mepp size was unchanged, and nerve-evoked muscle twitch tension was decreased 1 week after PSC ablation. Thus, PSCs are essential for the long-term maintenance of the presynaptic structure and function of the adult neuromuscular synapse.

The close association of PSCs with nerve-muscle contacts suggests that PSCs may also be required for the maintenance of the adult NMJ. To investigate the role of PSCs in maintaining adult NMJs, *in*

vivo complement-mediated immunocytolysis of these cells has been applied at frog (by using a monoclonal antibody, 2A12, which recognizes the plasma membrane of PSCs) and mammalian NMJs (by using a group of antidisialosyl antibodies recently found in Miller Fisher syndrome (MFS) that preferentially bind to PSCs) [16,19,20].

In frog, shortly after PSCs ablation (within 5 h), synaptic function as well as ultrastructure of nerve-muscle contact are not significantly affected. Neither is short-term plasticity including paired-pulse facilitation and synaptic depression. Thus, PSCs are dispensable for the short term maintenance of mature NMJ and do not seem to play an acute role in synaptic transmission (Fig. 5). In contrast to the lack of short-term effect, transmitter release is reduced by half in 1 week after PSC ablation. The morphology of NMJs is also affected, as shown by partial or total retraction of nerve terminals at NMJs that lack PSCs. The retraction of nerve terminals does not seem to have resulted from nerve degeneration, as no signs of Wallerian degeneration have been observed. Taken together, the finding from the PSCs ablation study implicates an essential role for PSCs in the long-term, but not short term, maintenance of mature NMJs (Fig. 5). Whether this role is dependent on a "glue" effect of PSCs or to their trophic support to nerve terminals (PSCs express a variety of trophic factors and extracellular matrix (ECM) molecules) is not known but the latter seems more likely [21,22,23].

Similar to acute PSCs ablation in frog muscles, mouse NMJs do not show any acute changes in synaptic structure or function in the absence of PSCs. The long term effect of PSCs ablation at mammalian NMJs remains to be studied.

1.3.3 The role of PSCs in synaptic transmission at adult NMJ

Though being closely associated with nerve-muscle contacts, PSCs were thought not to actively participate in synaptic transmission at the NMJ, partly due to the fact that glial cells are electrically nonexcitable. However, PSCs express a group of ion channels and neurotransmitter

receptors suggesting that PSCs may be responsive to at least the synaptic activity in forms other than action potential [24,25,26]. Indeed, PSCs increase intracellular calcium level in response to high-frequency nerve stimulation at both amphibian and mammalian NMJs [27,28,29]. The neurotransmitter acetylcholine (ACh), as well as purinergic agonists, such as ATP and adenosine, are suggested to be responsible for this PSC calcium response (Fig. 4) [27,29,30,31,32]. Altogether, PSCs possess a different form of excitability, such as "calcium excitability", in response to synaptic activity. In addiction, this response can be modulated by molecules other than neurotransmitters, including the trophic factors BDNF and NT3, substance P and nitric oxide (NO) [30]. Whether the PSC calcium increase in response to high-frequency nerve stimulation can in turn modulate synaptic transmission has been studied by pharmacologically manipulating intracellular calcium level in PSCs [33].

The calcium increase may not be the only response of PSCs to synaptic activity. Other signaling pathways might also be activated in PSCs during synaptic transmission. For example, several receptor including muscarinic AChRs, ATP receptors, and adenosine receptors, all of which are G-protein coupled receptors, are activated on PSCs during synaptic transmission (Figure 4). The involvement of PSCs G-protein signaling in modulating synaptic transmission has been tested by microinjecting nonhydrolysable analogues of GTP or GDP into PSCs.

Recently, it has been demonstrated that PSCs, not only respond to high-frequency synaptic transmission, but are able to discriminate patterns of motor nerve activity and influence plasticity at the NMJs accordingly [34].

1.3.4 PSCs in Nerve Degeneration and Regeneration

Despite the important fuctions exerted by PSCs in the formation, development, maturation and maintenance of the NMJ, they play, along with myelinating Schwann cell, a key role in nerve terminal degeneration and regeneration. Considering that myelinating e PSCs work in concert

during nerve terminal degeneration and regeneration, it is not possible to describe separately their activities.

When a nerve fiber is cut or crushed as a consequence of a traumatic injury (ie. motorcycle crash), the part of axon separated from the neuronal cell body undergoes a degenerative process called **Wallerian degeneration**, also called **anterograde** or **orthograde degeneration** [35].

1.3.4.1 Nerve Degeneration

Although most injury responses include a calcium influx that promotes the resealing of severed parts [36,37,38,39], axonal injuries initially lead to acute axonal degeneration (AAD), which is a rapid separation of the proximal (the nearer to the cell body) and distal ends within 30 minutes of injury [40]. Degeneration proceeds with swelling of the axolemma, and eventually leads to bead-like formation (Fig. 6). The process takes about roughly 24 hours in the PNS, and longer in the CNS. The signaling pathways leading to axolemma degeneration are currently unknown. However, research work has shown that this AAD process is calcium–independent [41].

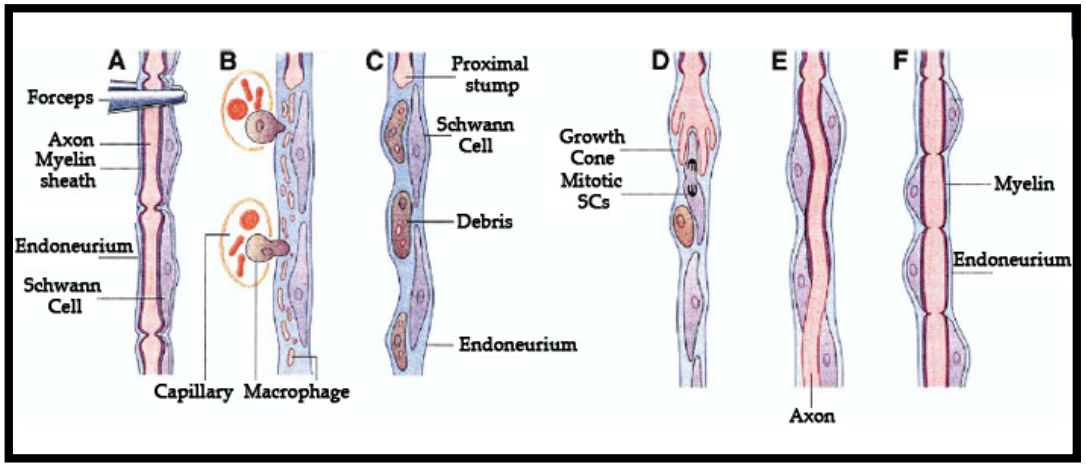

Figure 6 Principals Steps of Wallerian Degeneration. A) Damage of the axon (in the specific case a compression); B) degeneration of the distal stump and activation of Schwann cells (dedifferentiation and re - entry in the cell cycle), secretion of cytokines and chemokines with recruitment of macrophages; C) debris removal by macrophages and SCs; D) growth cone formation; E) bands of Büngner organization; F) complete recovery.

Granular disintegration of the axonal cytoskeleton and inner organelles occurs after axolemma degradation. Early changes include

accumulation of mitochondria in the paranodal regions at the site of injury (Fig. 6). Endoplasmic reticulum degrades and mitochondria swell up and eventually disintegrate, leading to the release of mitochondrial DNA and formylated peptide which represent both PAMPs (Pathogen-Associated Molecular Patterns), since mitochondria are of bacterial origin, and DAMPS (Damage-Associated Molecular Patterns) because they are release from damaged cells [42]. These could lead to the activation of macrophages and, probably, of SCs which possess Toll-like Receptor (TLR) 2,3,4 [43,44,45,46,47]. Depolymerization of microtubules occurs and is soon followed by degradation of the neurofilaments and other cytoskeleton components. The disintegration is dependent on Ubiquitin and Calpain proteases (activated by influx of calcium ion), suggesting that axonal degeneration is an active process and not a passive one as previously misunderstood [48]. Thus the axon undergoes complete fragmentation. The rate of degradation is dependent on the type of injury and is slower in the CNS than in the PNS. Degradation rate is also dependent on axon diameter: larger axons require a longer time for the cytoskeleton to degrade and thus take a longer time to degenerate.

The response of SCs to axonal injury is rapid. The time period of response is estimated to be prior to the onset of axonal degeneration. Neuregulins are believed to be responsible for the rapid activation. They activate ErbB2 receptors in the Schwann cell microvilli (Fig. 4), which results in the activation of the mitogen-activated protein kinase (MAPK) [49]. The *sensing* is followed by decreased synthesis of myelin lipids and that eventually stops within 48 hrs. The myelin sheaths separate from the axons and then rapidly deteriorate and shorten to form bead-like structures. SCs continue to clear up the myelin debris by degrading their own myelin, phagocytosing extracellular myelin and attracting macrophages to myelin debris for further phagocytosis (Fig. 6) [41]. However, the macrophages are not attracted to the region for the first few days; hence SCs have a major role in the early myelin cleaning.

SCs have been observed to recruit macrophages by releasing cytokines and chemokines after *sensing* of axonal injury. The recruitment of macrophages helps to improve the clearing rate of myelin debris. The

resident macrophages of the nerves further release chemokines and cytokines to attract more macrophages. The degenerating nerve also produces chemotactic molecules for macrophages. Another source of macrophage recruitment factors is serum. These signaling molecules together cause an influx of macrophages, which peaks during the third week after injury. While SCs mediate the initial stage of myelin debris clean up, macrophages come in to finish the job.

Murinson et al. [50] observed that PSCs and myelinated SCs in contact with an injured axon dedifferentiates and enter cell cycle thus leading to proliferation (Fig. 2 and 6) . Possible sources of proliferation signal are attributed to the ErbB2 receptors and the ErbB3 receptors. This proliferation could further enhance the myelin cleaning rates and plays an essential role in regeneration of axons observed in PNS.

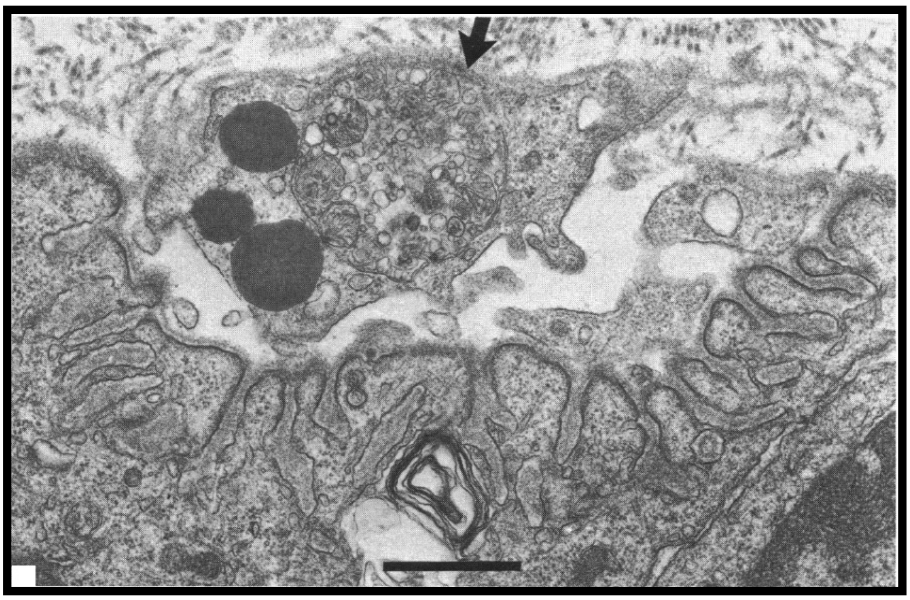

Figure 7 Macrophagic-like activity of PSCs. 24 h after black widow spider venom a denervated end-plate with intact post-synaptic sarcolemma still coated by basal lamina can be seen. Profiles of Schwann cell cytoplasm lie close to the end-plate and contain debris and a degenerated axon (arrow). Calibration bar: 1 μm.

During the degenerative process PSCs, as well as myelinating Schwann cell, dedifferentiate, acquire a macrophagic-like activity and contribute to remove the debris originating from the degenerating nerve terminal (Fig. 7) [51]. It has been demonstrated that, once the debris are removed, PSCs cover the post synaptic specialization of the muscle fiber membrane and start to secrete acetylcholine [52], but the physiological

meaning of this behavior has yet been explained. This release seems to be non quantal and not dependent on the presence of Ca^{2+} ions in the external medium.

1.3.4.2 Nerve Regeneration

Regeneration follows degeneration. Regeneration is rapid in PNS, allowing for rates of up to 1 millimeter a day of regrowth [53]. It is supported by SCs through growth factors release and structural guidance. CNS regeneration is much slower, and is almost absent in most species. The primary cause for this could be the delay in clearing up myelin debris. Myelin debris, common in both CNS and PNS, contain several inhibitory factors. The elongated presence of myelin debris in CNS could possibly hinder the regeneration [54]. An experiment conducted on Newts, animals which have fast CNS axon regeneration capabilities, showed that Wallerian degeneration of an optic nerve injury took up to 10 to 14 days on average, further suggesting that slow clearance inhibits regeneration [55].

Immediately after injury, the axon portion proximal to the site of damage and still connected to the nerve's cell body undergoes a Ca^{2+}-dependent reorganization which will lead to the formation of a fundamental structure in the process of nerve regeneration: the growth cone (Fig. 6 and 8).

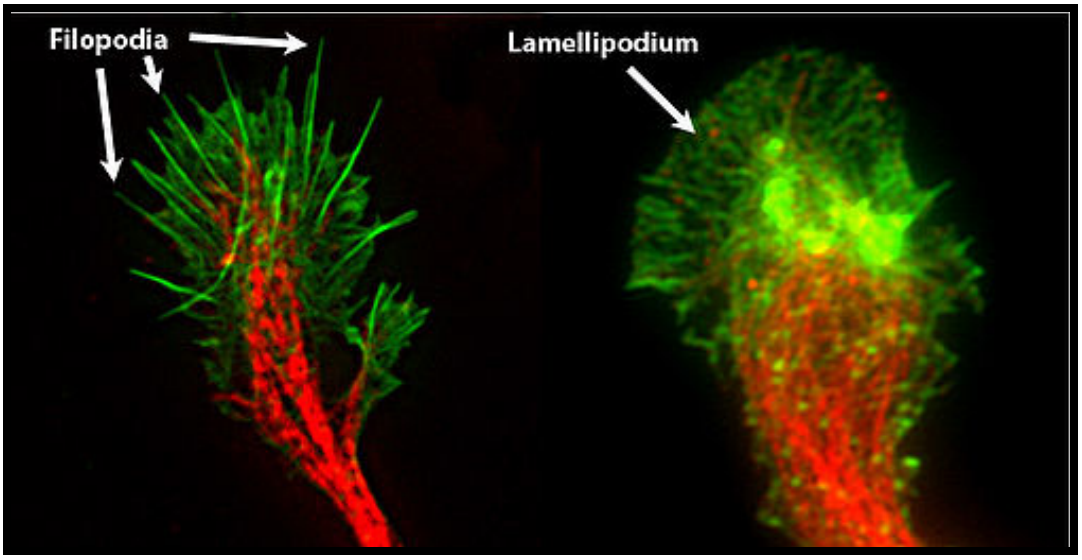

Figure 8 Two fluorescently-labeled growth cones. The growth cone on the left (green) is an example of a "filopodial" growth cone, while the one on the right is a "lamellipodial" growth cone. Typically, growth cones have both structures, but vary in sizes and number.

The growth cone is a specialized structure at the end of a growing nerve fiber that guides the fiber to its destination during the development of the nervous system or after nerve damage by means of interaction with

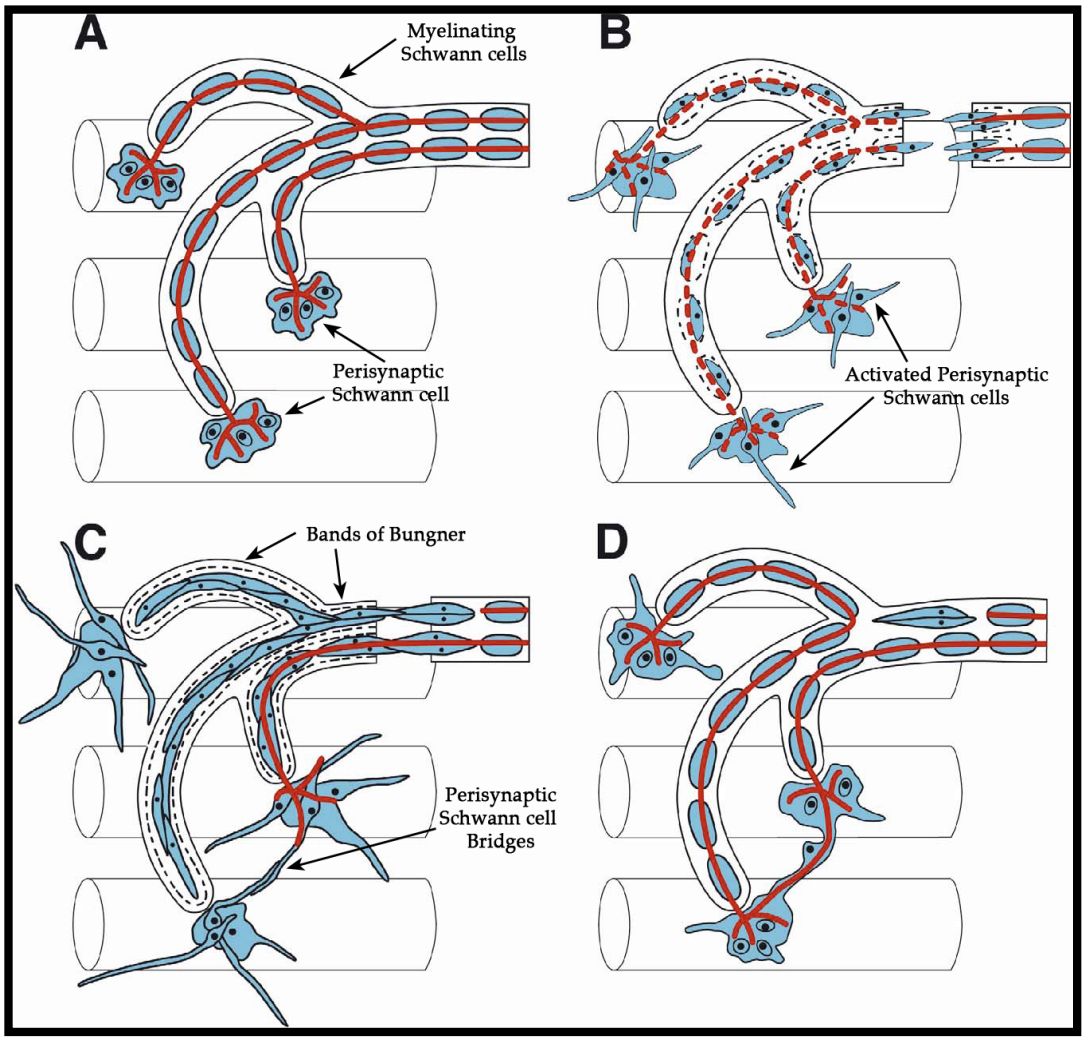

Figure 9 Cartoon depiction of the role of Schwann cells in the reinnervation of neuromuscular junctions. A) 3 muscle fibers and their innervation by myelinated axons in a branch of the intramuscular nerve. Axons are red; Schwann cells are blue. The top and the bottom muscle fibers are shown to be innervated by branches of the same motor axon. B) The consequences of denervation; a resection of a piece of nerve is shown on the upper right. The myelin surrounded the axons distal to the site of injury is destroyed and the Schwann cells producing this myelin become activated and begin to extend processes up and down the endoneurial tubes. Processes are extended from each end of the lesion site and will eventually grow to provide a pathway for axons to regenerate across the lesion. Similarly, terminal Schwann cells begin to extend processes away from the synaptic sites, but these do not yet "bridge'' between synaptic sites. C) Asynchronous reinnervation of synaptic sites that is commonly observed. An axon arrives at the lower site by following the endoneurial tube. As it reinnervates this site, Schwann cell bridges form with one of the neighboring sites. The activate myelinating Schwann cell form a tube", the Bands of Bungner, along which the axon regenerates. D) The growth of an escaped fiber from the lower site, along the Schwann cell bridge, to reinnervate the adjacent site. The axon is shown continuing to grow in a retrograde direction up the endoneurial tube of the lower muscle fiber and then down the endoneurial tube of the upper muscle fiber to reinnervate this fiber as well. Schwann cells seem to function to provide a means of rapid reinnervation of all the synaptic sites in the muscle. Cartoon is modified from Son and Thompson (1995a).

signaling and adhesive molecules in its surroundings and its own motile mechanism. The transient elevation of the free intracellular Ca^{2+}

concentration observed after injury leads to calpain activation and localized proteolysis of submembranal spectrin. These events are associated with the formation of distinct microtubule (MT)-based vesicle traps that accumulate anterogradely transported vesicles that fuse with the spectrin free plasma membrane in support of the growth process (Fig. 10).

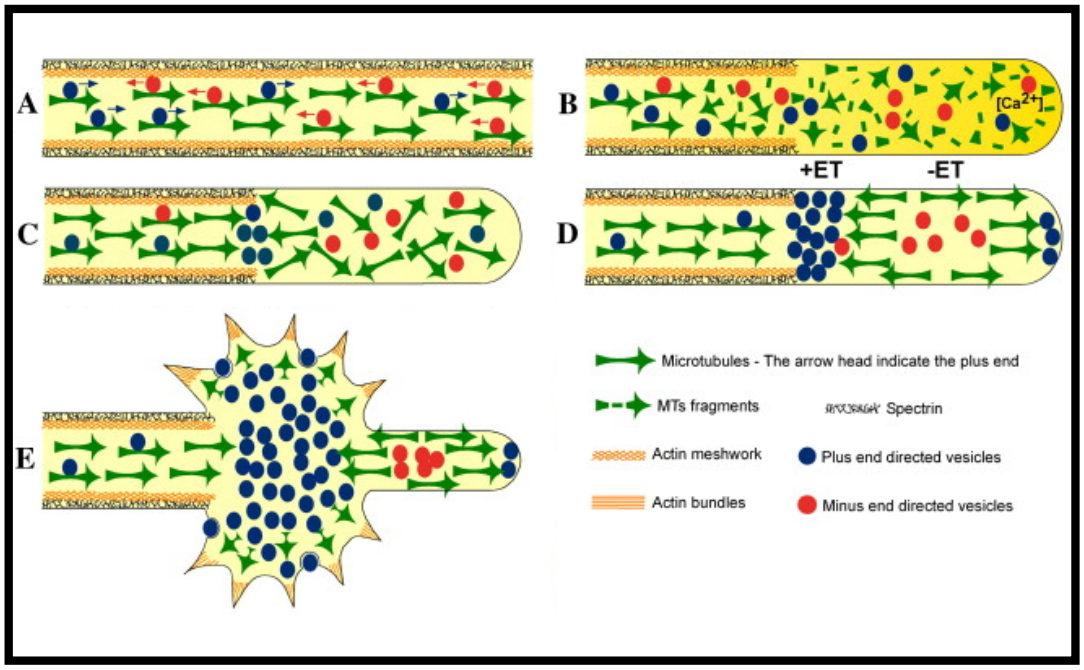

Figure 10 Diagrammatic summary of the structural events leading to the formation of an endbulb. The diagram illustrates the sequence of changes leading to the formation of a competent growth cone. (A) In intact neurons the MTs orient their plus ends distally (arrows) towards the tip of the axon. Vesicles are transported along the MTs (blue anterograde, and red retrograde transport). Axotomy (B), leads to calcium influx (yellow background) through the cut axonal end. The incoming calcium wave leads to MT depolymerization along the tip of the transected axon, activation of calpain and cleavage of the submembrane spectrin. The MT depolymerization wave ends when a membrane seal is formed over the cut axonal ends and the free intra-axonal calcium concentration recovers to its control level. (C) When the free intra-axonal calcium concentration recovers, the MTs repolymerize. Following axotomy the MTs repolymerize initially in all directions and subsequently form two vesicle traps, a plus-end trap (+ET) in which plus-ends oriented molecular motors and cargo accumulate and a minus-end trap (−ET) where minus-end oriented molecular motors and cargo accumulate (D). With time (E), vesicles trapped within the+ET, of a transected axon, fuse with the spectrin free plasma membrane, and an actin network and filaments polymerize to generate the mechanical force to extend a growth cones lamellipodium.

In healthy nerves, Nerve growth factor (NGF) is produced in very small amounts. However, upon injury, NGF mRNA expression increases by five to sevenfold within a period of 14 days. Nerve fibroblasts and SCs play an important role in increased expression of NGF mRNA [56]. Macrophages also stimulate SCs and fibroblasts to produce NGF via macrophage-derived interleukin-1 [57]. Other neurotrophic molecules produced by SCs and fibroblasts together include Brain-derived neurotrophic factor, Glial cell line-derived neurotrophic factor, Ciliary

neurotrophic factor, Leukemia inhibitory factor, Insulin-like growth factor, and Fibroblast growth factor. These factors together create a favorable environment for axonal growth and regeneration [41]. Apart from growth factors, SCs also provide structural guidance to further enhance regeneration. During their proliferation phase, SCs begin to form a line of cells called *Bands of Bungner* within the basal laminar tube (Fig. 9).

Growth cone of regenerating axons have been observed to move along these bands [58]. SCs upregulate the production of cell surface adhesion molecule ninjurin further promoting growth [59]. These lines of cell guide the axon regeneration in proper direction. The possible source of error that could result from this is possible mismatching of the target cells.

During the process of reinnervation the dynamic behavior of PSCs become even more evident. After denervation PSCs, upon an extensive cytoskeletal reorganization probably due to the upregulation of GFAP, consequent to ACh release blockade [60], sprout profusely after denervation (Fig. 9), and the regenerating nerve terminals extend sprouts along the proceeding PSCs to innervate adjacent denervated junctions. The importance of PSC sprouting in nerve regeneration has been demonstrated after partial denervation. When nerve inputs to the same muscle are partially damaged, PSC from the denervated junctions extend processes and form PSC "bridges" by contacting PSC processes from adjacent innervated junction (Fig. 9) [61]. As a result of this process an increase in the average dimension of motor units is observed. The formation of PSC bridges triggers nerve terminals from the innervated endplates to grow along PSC bridges to innervate the original yet denervated endplates (Fig. 9). The essential role of PSC sprouting in triggering terminal sprouting is absent following partial denervation in neonatal mice, possibly due to the apoptosis of developing SCs induced by denervation [62]. Furthermore, the deficiency in PSC bridge formation impairs the efficiency of nerve reinnervation as well as the functional recovery of muscle, as demonstrated in aging muscle and mdx mice (a model of Duchenne Muscular Dystrophy) [63,64].

1.4 Probes for PSCs

As described above, PSCs are nonmyelinating SCs and can be labeled with SCs markers, such as antibodies raised against S100 (a calcium-binding protein), GFAP (glial fibrillary acidic protein), N-CAM (neural cell adhesion molecule), and L1 [65]. Unexpectedly, PSCs also express several myelin-associated proteins, including P0, galactocerebroside, 2',3'-cyclic nucleotide-3'-phosphodiesterase (CNPase), and myelin-associated glycoprotein [66]. Moreover, antibodies to the neurotrophin receptor p75, GAP-43, and nestin label PSCs only at denervated or inactivated NMJ (Figure 4) [67,68,69].

One limitation of the molecules mentioned above is that they cannot be used for in vivo labeling of PSCs since they are cytoplasmatic and their labeling by antibodies requires membrane permeabilization. The problem of visualizing PSCs in living animals have been partially overcome by the generation of transgenic mice expressing green fluorescent protein (GFP) under the control of human S100B gene [70]. However, at present, it is not possible to generate transgenic mice in which only PSCs are genetically manipulated since S100B gene is not specific for PSCs (its protein product, S100, is a general SCs marker). Recently, several molecules, such as LNX1 (an E3 ubiquitin ligase) and homocysteine-responsive ER-resident protein, have been shown to be specifically expressed in PSCs (Fig. 4) [71,72]. It would be important to find whether antibodies to this proteins could be used to selectively label PSCs and whether the identification of the promoter for these molecules may help generate knockout for PSCs or proteins specific for PSCs.

To visualize PSCs in vivo two other vital probes have been developed: peanut agglutinin (PNA) (Fig. 4) [73], which label the extracellular matrix associated with PSCs, and a monoclonal antibody (mAb) 2A12 [20]. Unfortunately, they represent a feasible method to label in vivo PSCs only at frog NMJs since neither mAb 2A12 nor PNA are able to recognize PSCs in mammalian NMJs.

1.5 The Immunocompetence of Schwann Cells

SCs shares with macrophages more than their ability to phagocyte nerve degeneration debries. In fact a growing body of evidences seems to indicate that SCs possess a certain degree of immunocompetence, that can in part explain the interaction of these cells with the immune system, which is involved in diseases of the peripheral nervous system. Up to now, different immunomodulating abilities could be ascribed to SCs: 1) facultive antigen presentation, 2) regulation of the immune response through secretion of different mediator (ie. chemokines), 3) termination of an immune response and 4) facultive antigen recognition [74]. In particular the latter is very important because it could lead to SCs activation.

Recently, Zhang and collegues [42] demonstrated that the aseptic systemic inflammatory response shock (SIRS) observed in heavily traumatized patience without guts injury is due to neutrophil activation by formylated peptides, via Formyl Peptide Receptor (FPR1), and mitochondrial DNA (mDNA), throught Toll-Like Receptor 9 (TLR-9), leaking from damaged cells at the injuries sites. Formylated proteins and mDNA represents well known pathogen-associated molecular patterns (PAMPs) but in this case they are also danger-associated molecular patterns (DAMPs) since they are released from damaged cells. Therefore, Zhang and collegue named them mitochondrial DAMPs (MTDs)

Considering the strong parallels between SCs and innate immunity cells it would be interesting to investigate on a possible activation of the former by formylated proteins and mDNA.

1.5.1 Pattern recognition receptors

The strategy of the innate immune response is to focus on a few highly conserved structures present in large groups of microorganisms known as PAMPs and the corresponding receptors of the innate immune system are called pattern recognition receptors [75]. Examples of this molecules are the lipopolysaccharide (LPS) and the mitochondrial DNA (mDNA).

1.5.1.1 Toll-Like Receptors (TLRs)

The family of TLRs belongs to the group of pattern-recognition receptors that recognize specific conserved components of microbes [76] and that have been implicated to play a critical role in various inflammatory disorders [77,78]. To date, 11 TLRs have been identified in humans and 7 in rats [79] and they are usually found on antigen-presenting cells.

A schematic representation of TLRs signalling is shown in Fig. 11.

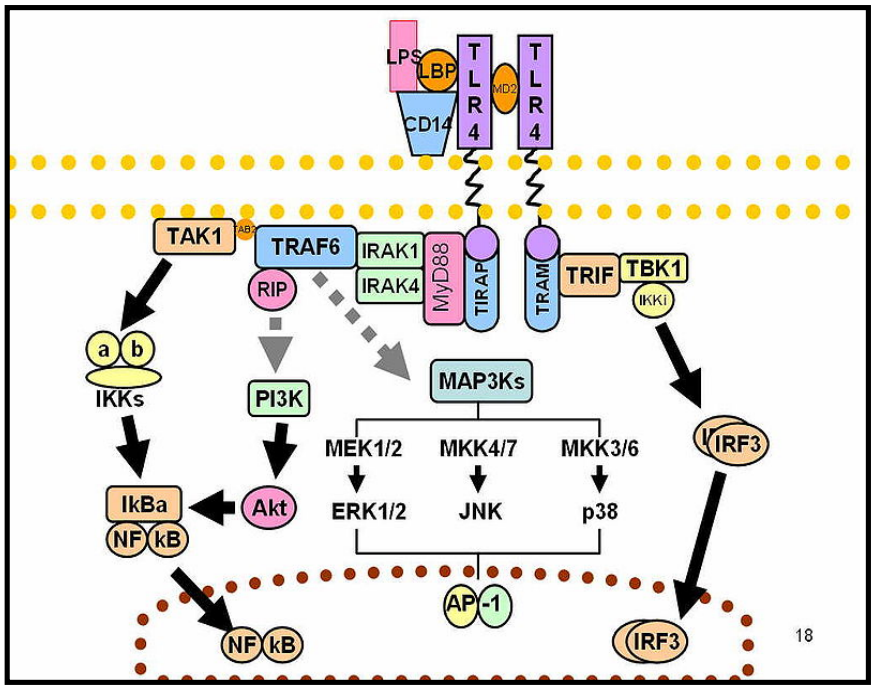

Figure 11 Schematic representation of TLRs signalling. Toll-like receptors (TLRs) recognize microbial products during infection and initiate signalling pathways that culminate in the increased expression of immune and inflammatory genes. TLRs that recognize nucleic acids signal from endosomes, whereas cell-surface TLRs sense lipids and proteins. Two major signalling pathways have been detailed. The core pathway activated by most TLRs leads to activation of the transcription factor nuclear factor-κB (NF-κB) and the mitogen-activated protein (MAP) kinases p38 and JNK. These signalling cascades increase the expression of many pro-inflammatory genes. The second pathway is activated by TLR3 and TLR4 and leads to activation of both NF-κB and another transcription factor interferon regulatory factor 3 (IRF3), allowing for an additional set of genes to be induced, including antiviral genes such as interferon-β (*IFN-β*). In this way, TLRs can tailor the innate response to pathogens.

The presence of three TLRs have been already demonstrated in SCs. TLR-2, which recognize multiple glycoprotein, lipoproteins and lipopeptides, is constitutively expressed on primary human and rat Schwann cells and it is the probable target receptor for *Mycobacterium leprae* [43,80]. TLR-3 and 4, recognizing respectively double-stranded DNA and lipopolysaccharide, are induced in SCs under inflammatory conditions [46].

1.5.1.2 Formyl-Peptide Receptor (FPR1)

The formyl peptide receptors (FPR) are a members of a class of G protein-coupled receptors involved in chemotaxis [81,82]. These receptors where originally identified by their ability to bind N-formyl peptides such as *N*-formylmethionine produced by the degradation of either bacterial or host cells [83,84]. Hence formyl peptide receptors are involved in mediating immune cell response to infection. These receptors may also act to suppress the immune system under certain conditions [85]. aa schematic representation of FPR signalling is shown in Fig. 12.

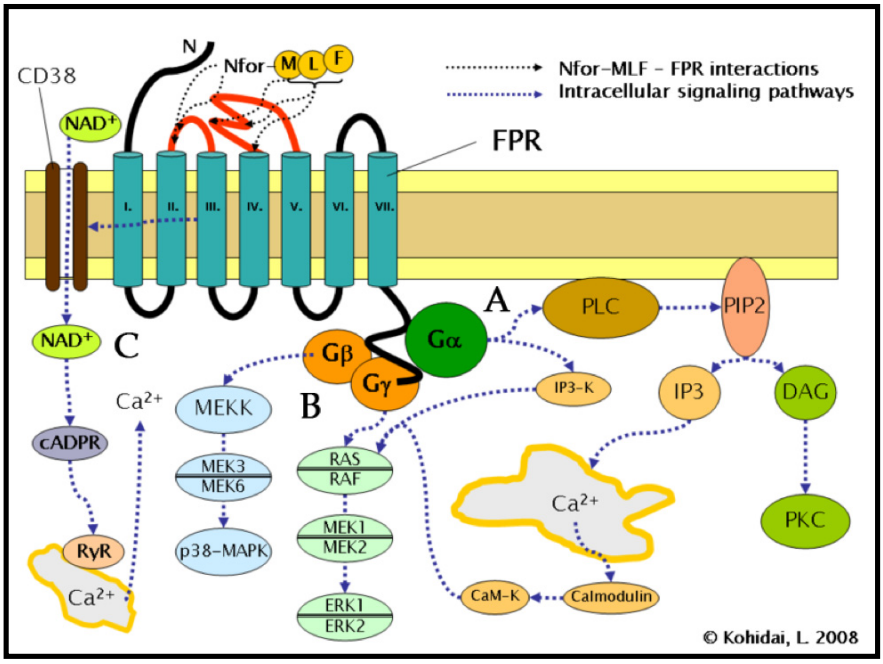

Figure 12 Schematic representation of FPR1 signalling. G protein dependent activation of phospholipase C (PLC) which results in the breakdown of the membrane constituent phospholipid, phosphatidylinositol (4,5)-bisphosphate (PIP2) into phosphatidylinositol (3,4,5)-trisphosphate (IP3) and diacyl glycerol (DAG). IP3 is one of the most effective inducer of Ca^{2+} increase from cytoplasmic pools and from outside the cell via opening Ca^{2+} channels. DAG in turn is an inducer of protein kinase C (PKC). B) Activation of the regulatory small GTPase, RAS. The active RAS can in turn activate RAF, a Ser/Thr kinase. In the next step mitogen-activated protein kinases (MAP kinases) are activated. As a result of the last step, ERK1 and ERK2 are activated. The phosphorylated forms of ERKs can continue the cascade by triggering activation more interacting kinases which results in altered transcriptional activity in the nucleus. C) Ligand binding to FPR can also induce the activation of CD38, an ectoenzyme of the surface membrane. As a result of activation NAD^+ molecules will enter the cytoplasm. NAD^+ is converted into cyclic ADP ribose (cADPR), a second messenger which interacts with ryanodine receptors (RyR) on the surface of the rough endoplasmic reticulum. The overal result of the process is increased cytoplasmic Ca^{2+} levels via the direct pathway described above and also via indirect pathways such as opening of Ca^{2+} channels in the cell membrane. The sustained increase of Ca^{2+} is required for directed migration of the cells.

1.6 Presynaptic neurotoxins

Considering the difficulty of working with nerve terminal degeneration/regeneration process we needed an experimental system as controllable as possible. The surgical techniques used till now to study the role of PSCs in the process of nerve terminal degeneration/regeneration, respectively the cut and the crush of sciatic nerve, are not controllable at all, because they activate the Wallerian degeneration. The ideal condition is to provide a very specific and localized damage to the nerve terminal in order to avoid the activation of many cell types (including myelinating SCs) and the production of inflammatory mediators (cytokine, chemokine, ecc). Moreover, this localized damage should mimic as much as possible the cascade of events that leads to nerve terminal degeneration in injured patients (increase of the cytoplasmatic calcium concentration, mitochondrial swelling and degeneration cytoskeleton following activation of calpain and other Ca^{2+}- dependent protease). So, we decided to use presynaptic neurotoxins to provide an extremely localized damage to the nerve terminal. In particular we focused our attention on α-Latrotoxin (α-LTX), a pore forming toxin, and SPANs, which are phospholipases with PLA2 activity. We demonstrated with a side by side comparison that both kind of toxin exert their degenerative action via a massive calcium influx [86].

1.6.1 α- Latrotoxin (α-LTX)

The notorious black widow spider (Latrodectus genus) venom contains at least 86 unique proteins [87], including several homologous LTXs which play a role in its toxicity towards insects and crustaceans [88], with only one component, α-LTX, targeting vertebrates specifically [89].

1.6.1.1 Sequence and High-Order Structures:

1.6.1.1.1 Sequence

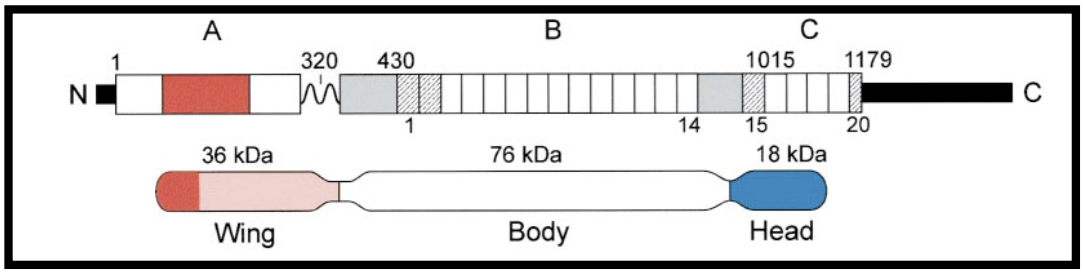

Figure 13 Diagram of the LTX sequence (top) and a linear representation of the domain structure of LTX (bottom). The numbers above the diagram mark amino acid positions of region boundaries. Narrow boxes numbered 1–20 correspond to ankyrin repeats (imperfect or incomplete repeats are hatched); grey, sequence regions lacking homology with other proteins; wavy line, coiled coil region; red, fragment used for the isolation of the N-terminal Ab; thick black lines, fragments proteolytically removed during LTX maturation. Note that the relative sizes and positions of the 3D domains are similar to those of the LTX sequence regions.

α-LTX is synthetized as a 157 kDa polypeptide (Fig. 13) [90] in the cytosol of secretory epithelial cells of the venom gland [91]. These cells disintegrate [92] and expel toxin into the gland lumen together with various proteases [87]. Here, it is cleaved at both termini by a furin-like protease [93], producing an active α-LTX of 131 kDa [90,94]. The most striking feature of the α-LTX primary structure is a series of 22 ankyrin repeats (Fig. 13). The N-terminal of the toxin shows no significant homology to other proteins and contains three conserved cysteines important for structural stability and activity of all LTXs [94,95].

1.6.1.1.2 High-Order Structure

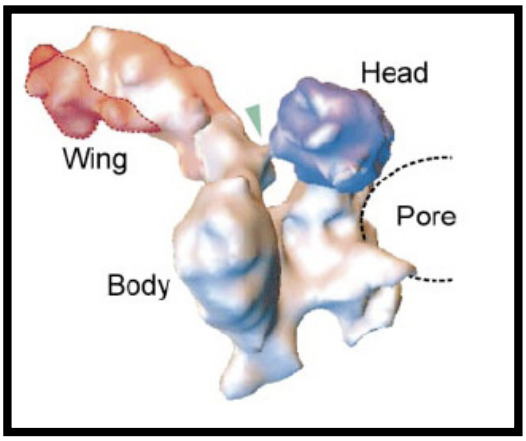

Figure 14 View of the monomer illustrating the three structural domains of the molecule: wing (pink), body (silver), and head (blue). The position of the central pore within the tetramer is indicated by the dotted line; binding sites for the N-terminal Ab are dark red. The arrowhead points at a connection between the head and the body.

Although some monomers, consisting of a wing, a body and a head domain (Fig. 13 and 14), have been observed by cryo-EM in EDTA-treated α-LTX, the toxin almost always exists as a stable dimer [96,97] in which the monomers are associated "head to tail". Association of dimers, strongly catalyzed by divalent cations produces a bowl-like structure that can contain four monomers (Fig. 15).

The bottom part of the bowl-like structure is important for penetration into lipid bilayer and it is probable that structural arrangements leading to tetramer formation cause the exposition of surface region favorable to interaction with lipid bilayers. The four heads at the center of the bowl form a cylindrical assembly, restricted at one point to 10 Å. This constriction most probably correspond to the cation binding site (selectivity filter) of α-LTX channel (Fig. 15).

1.6.1.1.3 Membrane pore formation and features

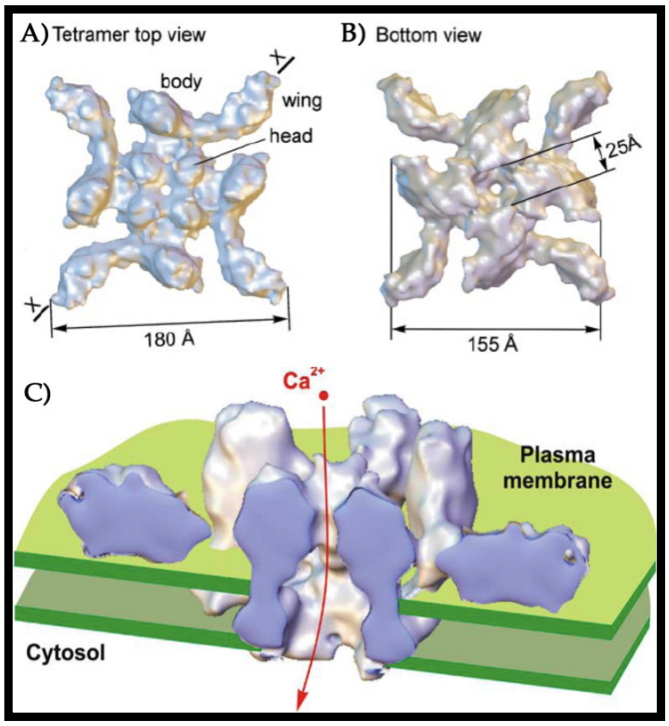

Figure 15 The 3D reconstruction of the LTX oligomers. A) The top and B) bottom views of the tetramer. C) A model of the α-LTX pore in the membrane bilayer. The tetramer is cut open to show the channel. The base of the tetramer fully penetrates the membrane, whilst the wings are attached to the outer membrane surface. Cations can enter the cytosol through the channel, as shown by the arrow.

Once formed, the α-LTX channel mediates only cationic currents, probably because negatively charged acidic side chains line the channel [98]. Most significantly, the α-LTX channel is permeable to Ca^{2+} [98,99,100].

However, this channel is not very selective, and Ba^{2+}, Sr^{2+}, Mg^{2+} and Na+ and K+ currents are also carried by the channel [99,100]. Moreover, due to the relatively wide selectivity filter, small molecule as cytplasmatic acetylcholine can pass through [101,102,103]. The channel is open most of the time but closure events have been observed [98,104,105], and several channels can open and close in concert. The molecular basis of gating is currently unknown, but is likely to involve head domains (Fig. 14).

The formation of α-LTX membrane pore consists of at least three steps: toxin tetramerization, interaction with a specific cell-surface receptor and membrane insertion.

1.6.1.1.4 Receptors

Althoug α-LTX is able to insert into pure lipid membranes [98], reconstituted receptors greatly enhance the rate of insertion [106]. Receptors, thus, confer specificity to the pore mediated effects of α-LTX. It is not clear whether receptors are directly involve in membrane insertion, simply concentrate the toxin close to the membrane , or organize membrane lipid domains. At present, three receptors have been identified to be selectively bound by α-LTX: neurexin (NRX) (Ca^{2+}-dependent interaction), latrophilin 1 (LPH1) and protein tyrosin phosphatase σ (PTPσ). Interestingly, three point α-LTX mutants, in which the conserved cysteins in the C- terminal of the toxin have been replaced, are unable to bind α-LTX receptors Accordingly, chemical reduction of disulphide bonds in α-LTX abolishes receptor binding [94].

Neurexin Ia, a neuronal protein with a single transmembrane domain, is the first receptor to be discovered [107]. Multiple form of NRXs have been identified; however, all of them bind α-LTX only in the presence of Ca^{2+} [108,109]. Because α-LTX was also shown to act in the absence of this cation, this clearly indicated that another Ca^{2+}-indipendent toxin receptor must exist. Such a protein was later discovered and termed latrophilin (LPH) [110] , or CIRL (Ca1+-independent receptor for LTX) [111]. LPH is a heptahelical transmembrane protein that belongs to the secretin/calcitonin family of G protein-coupled receptor [112,113]. Three isoforms of LPH have been found up to now and LPH 1 is the only homologue that binds α-LTX with high affinity [114,115,116].

Recently a third receptor for α-LTX , protein tyrosine phosphatase σ (PTPσ) [117], has been described; it binds the toxin in a Ca^{2+}-independent manner. However, PTPσ appears to represent a minor receptor component: much less of it is purified from brain extracts on a-LTC columns compared to NRX or LPH, and its affinity for the toxin has not been determined [117].

1.6.1.1.5 Mechanisms of Action

α-LTX causes Ca^{2+}-dependent and –independent release of neurotransmitters. Dense core vesicles require Ca^{2+}, while synaptic vesicle can be stimulated in its absence. However, in presence of Ca^{2+}, transmitter is stronger overall due to initially perturbed vesicle recycling.

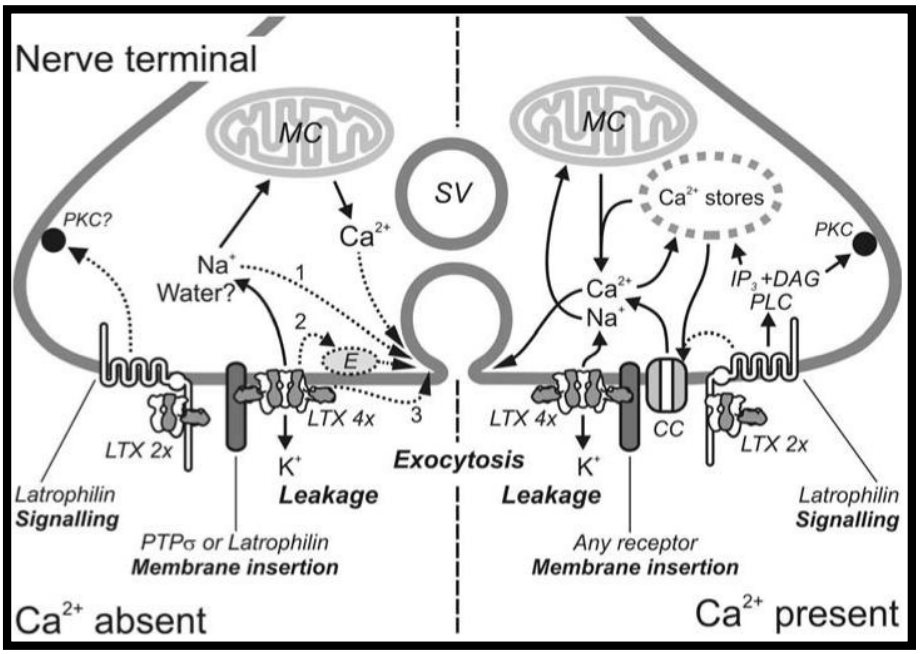

Figure 16 Diverse mechanisms of α-LTX action. Right, Ca^{2+} is present in the medium. The pathways shown are described in the text. CC; Ca^{2+} channels; DAG, diacyl glycerol; LTX 4x, α-LTX tetramers; MC, mitochondria. **Left,** Ca^{2+}-free conditions. For main comments, see text. The possible pathways for Ca^{2+}-independent exocytosis shown include: (1) high concentrations of Na^+ mimicking Ca^{2+}; (2) the internalised domains of α-LTX interacting with components of the exocytotic machinery (E); (3) α-LTX exerting direct fusogenic action.

All α-LTX actions in biological systems require receptors, which provide binding sites for the toxin on the cell surface. Once the toxin is bound, part of its Ca^{2+} dependent action is due to pore formation and influx of Ca^{2+}. This mechanism triggers the release of both readily releasable and reserve pool of vesicles (Fig. 17) [118]. Another action is based on receptor-mediated signaling, which involves stimulation of PLC, production of IP_3 and diacyl glycerol, with respective release of stored Ca^{2+} and activation of PKC (Fig. 16). This mechanism, most likely mediated by LPH1, affects readily releasable vesicle only. Both the pore- and the receptor- mediated signal can be amplified by the release of $Ca^{2+}{}_i$ and influx of $Ca^{2+}{}_e$, producing calcium waves. Mitochondria can contribute to the increase in $[Ca^{2+}]_I$ (Fig. 16).

In the absence of Ca^{2+}_{e}, α-LTX only binds to LPH1 and PTPσ. Ca^{2+}-independet exocytosis requires the presence of Mg^{2+} and toxin insertion into the plasma membrane, but these conditions also induce formation of α-LTX channels. Influx of Na+ and efflux of K+ through these channels and associated efflux of small molecules (acetylcholine for example) and influx/efflux of water may cause secretion. In addition, transmitter release can be caused by membrane perturbation or direct interaction with secretory machinery (Fig. 16). Some secretion may be non vesicular (leakage) [119].

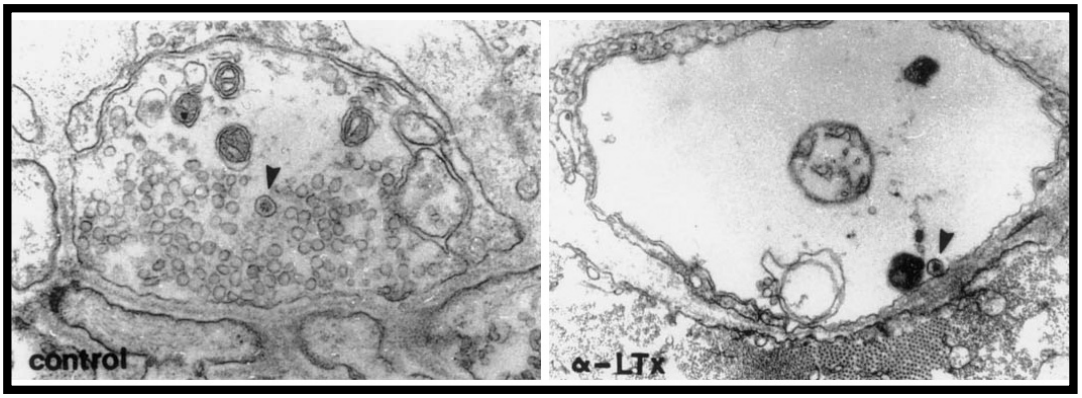

Figure 17 Frog neuromuscular junction treated with a-latrotoxin (α-LTX). Exposure to high amounts of toxin for hours causes a massive release of small synaptic vesicles. This results in an enlargement of the plasmalemma and a total depletion of the neurotransmitter containing vesicles, but not of the large dense-core vesicles containing neuropeptides (arrow). Nerve terminal is swollen as consequence of a toxin mediated entry of cations. From [118]

The massive calcium influx inside the nerve terminal leads to the activation of Ca^{2+}-dependent proteases as calpains, mitochondria swelling, microtubule disassembly, ect leading to a necrotic-like degeneration of the terminal. It is also important to note that α-LTX intoxication never leads to neuronal death but the nerve terminal regenerates leading to a structural and functional recovery of the intoxicated NMJs [86].

1.6.2 Presynaptic Snake Neurotoxin endowed with PLA2 activity (SPANs)

Presynaptic snake neurotoxin endowed with PLA2 activity are major components of the venom of four families of venomous snake (Crotalidae, Elapidae, Hydrophiidae and Viperidae (Figure 16)). These neurotoxins play a major role in the envenomation of the prey by causing a persistent blockade of neurotransmitter release from nerve terminal. Several venom components are biologically active but, almost invariabily, most of neurological signs and symptoms are due to SPANs' action.

Figure 18 *Notechis scutatus* (top left), *Bungarus multicinctus* (top right), *Oxyuranus scutellatus* (bottom left), and *Pseudonaja textilis* (bottom right) are elapid snakes originary from Australia and South East of Asia. Their venom contains the highly neurotoxic phospholipases A2 responsible for the neuromuscular paralysis of their prey.

1.6.2.1 Structure and Activity

SPANs show a wide range of structural complexity and of PLA2 activity. The crystallographic structures of few of the simpler toxins have been determined (Fig. 19) [120]. They include a phospholipase A2 domain with a calcium atom that stabilizes and activates the enzyme. Their typical feature is a hydrophobic channel that accommodates the fatty acid chain of the phospholipid molecule and places the ester bond to be cleaved into the active site. The key residues directly involved in catalysis are a histidine residue, which hydrogen-binds the water molecule used for hydrolysis and an aspartate, which positions the Ca^{2+} ion coordinating both the phosphate and the sn-2 carbonyl groups of the phospholipid molecule (Fig. 19). In addition, chemical modification studies have identified two segments of the PLA2 subunit involved in neurotoxicity [121].

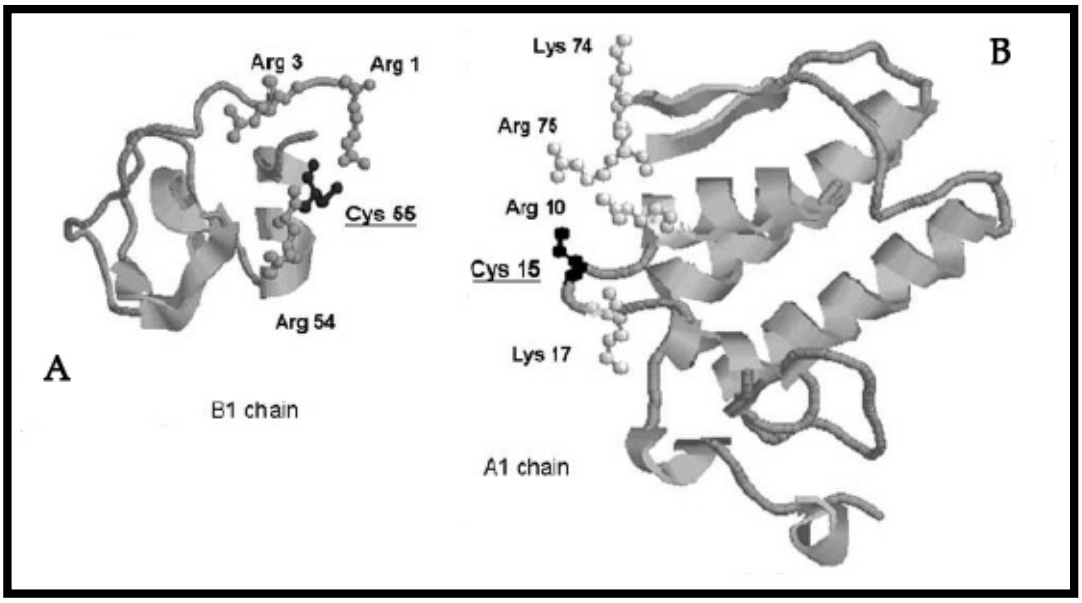

Figure 19 Tertiary structure of A1 chain and B1 chain of β-BTX. A) The B1 chains is the subunit responsable for binding to K^+ channels while B) A1 chain is the subunit endowed with PLA2 activity. Resolution: 2.45 Å.

However, additional regions and/or subunits may be implicated, particularly in the case of multisubunit toxins; this still awaits detailed investigations. Indeed, SPANs vary greatly in terms of quaternary structure, ranging from the single subunit notexin (from the Australian tiger snake *Notechis scutatus*), to β-bungarotoxin (from the Taipan snake *Bungarus multicinctus*), which consists of two covalently linked subunits, the larger of which is a PLA2. Only one of the three subunits of taipoxin

(from the elapid *Oxyuranus scutellatus*) has PLA2 activity; in contrast, textilotoxin (from the Australian elapid *Pseudonaja textilis*) consists of five subunits, all endowed with PLA2 activity [122].

SPANs present a wide heterogeneity, both in structure, enzymatic activity and neurotoxicity (Table 1); up to now, no direct relationship has been found between the relative enzymatic activities of snake PLA2 neurotoxins and their lethal potencies. Nevertheless, neurotoxicity results from the coexistence of two factors: (1) the capacity of hydrolyzing efficiently the phospholipids of the presynaptic membrane, and (2) the ability to recognize the nerve terminal, to bind efficiently to it, and to concentrate in that site the enzymatic activity.

Table 1 Comparison of subunit composition, molecular weight, toxicity and enzymatic activity of the four investigated snake PLA_2 neurotoxins.

$sPLA_2$	Subunits	MW (kDa)	mouse LD_{50} * (μg/kg)	PLA_2 activity *,†
Notexin	1	14	17	19.460
β-Bungarotoxin	2	21	14	1281
Taipoxin	3	42	2	18
Textilotoxin	5 (6)	70 (84)	1	224

*from Kini, 1997. Lethal Potency of Snake Venom Phospholipase A_2 Enzymes

† in nmols of PL hydrolysed / min / nmol of toxin

1.6.2.2

1.6.2.3 Receptors

Differently from α-LTX, at present no receptor/s for SPANs (except for α-BTX) have been identified at the level of presynaptic membrane; however the kinetics of paralysis of the prey after snake bite and after SPAN injection suggest that they rapidly find their way to peripheral nerve terminals, to which they bind quickly and specifically [123,124,125]. A very interesting proposal for the binding of SPANs comes from Montecucco et al, 2004 [126]. In this paper the concept of 'Array of Presynaptic Receptors' (APR) developed for botulinum neurotoxins (BoNTs) was extended to SPANs.

APRs are proposed to be dynamic microdomains of the presynaptic membrane where several molecules endowed with neurotoxin-binding properties are localized. The oligosaccharide portions of polysialogangliosides are suggested to act as initial neurotoxin-binding factors because of their high local concentration on the presynaptic membrane, their high lateral mobility and the ability of the oligosaccharide moiety to act as 'antennas' that can engage multiple bonds and thus effectively capture neurotoxin molecules present in the intersynaptic fluid. This initial neurotoxin–antenna interaction is expected to be reversible and to have a fast on-rate, with a moderate affinity, and recent data support this possibility for BoNTs [127,128]. Binding involves the transition from the three dimensional water solvent to the two-dimensional membrane surface, and such reduction of dimensionality brings with it a high concentration of the reagents because of a decrease of the reaction volume. Accordingly, even weak interactions among the neurotoxin and other membrane components may become relevant. Thus, following its entry in an APR, a neurotoxin can be engaged in binding to different receptor molecules, each one possibly present in several copies. At this stage, the neurotoxin–membrane binding is characterized by very high affinity as it involves multiple interactions, making it almost irreversible – hallmark of the action of both BoNTs and SPANs at nerve terminals. In the light of the blockade of neurotransmission by the toxins, it is tempting to speculate that APR coincide with the active zones of the presynaptic membrane where synaptic vesicle fusion takes place.

1.6.2.4 The mode of action of PLA2 snake presynaptic neurotoxins

SPANs do not directly affect proteins involved in neuroexocytosis. They act on phospholipids. Indeed, within few minutes from their addition to neurons in culture, phosphatidylcholine is hydrolyzed to lysophosphatidylcholine and fatty acid with minor production of lysophosphatidyl-ethanolamine and –serine [129]. Under physiological conditions, such lipids are present only in minute amounts, as their molecular shape is not compatible with the bilayer membrane structure.

Lysophosphatidylcholine is an inverted cone-shaped lipid which forms spheroidal micelles, whereas fatty acids are cone-shaped. As a consequence of their shapes, these lipids alter the curvature of the membrane [130,131]. Moreover, it should be considered that lysophosphatidylcholine does not flip-flop across the lipid bilayer of the membrane, whereas fatty acids are capable of a very rapid trans-bilayer movement [132]. Consequently, as fatty acids are produced by SPANs on the external layer of the plasma membrane, they redistribute among the two membrane layers, whereas lysophosphatidylcholine remains outside. It has been theoretically predicted, and experimentally documented in the case of viral membrane fusion, that the presence of an inverted cone-shaped lipid in trans, and of cone-shaped lipids in cis, with respect to the

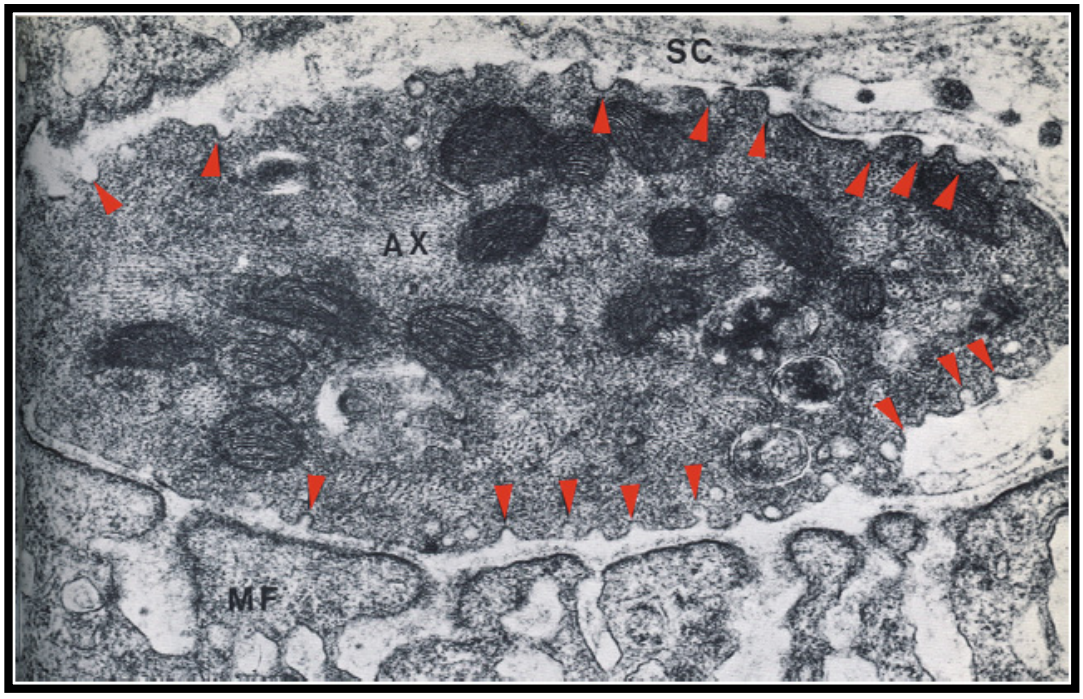

Figure 20 Electron microscopy of a mouse neuromuscular junction from phrenic nerve-hemidiaphragm preparation intoxicated with taipoxin (46,000x). The axon terminal is almost devoid of synaptic vesicles and shows numerous axolemmal indentations (red arrowheads). Adapted from [136].

site of membrane fusion, promotes the process, whereas it inhibits the opposite process of membrane fission [131,133]; Chernomordik and Kozlov 2003). Such membrane configuration favors the membrane fusion via pore opening from an hemifusion lipid intermediate which develops by intermixing of the two cis monolayers of the two membranes that have come together. In a later stage, intoxicated NMJs show enlarged axon

terminals with depletion of synaptic vesicles (Fig. 20). There are several clathrin-coated Ω-shaped plasma membrane invaginations, also in areas not facing the muscle membrane foldings indicating an unbalance in exo-endocytotic process. Mitochondria are swollen with altered cristae and large vacuoles are also observed (Fig. 20) [123,124,134,135,136,137,138]. It should be emphasized that even at this late stage of SPAN intoxication no damage of muscle, fibroblasts and Schwann cells is noticeable. Observations made at later stages (several hours after treatment) both in frog and rat muscles show that the nerve terminal of the motor neuron axon virtually disappears from the endplate. Prasarnpun et al. 2005 [125] documented a substantial axonal degeneration with loss of mitochondria, neurofilaments and synaptophysin staining. The robust extracellular matrix structure of the NMJ remains in place.

2 AIM

Perisynaptic Schwann Cells, the specialized glia of the neuromuscular junction, are well known for their role in formation, maturation, maintenance and function of the NMJ. Moreover, upon nerve terminal damage, PSCs dedifferentiate, acquire a macrophagic-like activity that contribute to the removal of degenerative debries and facilitate reinnervation by protrusion of sproutings. Canonical mediators of PSCs phenotypical and functional activation are ACh and ATP . It is however possible that other molecules such as inflammatory mediators and immunoactive substances released during nerve terminal degeneration contribute to PSCs activation.

The aim of this project is to investigate the role of inflammatory mediators as well as mitochondrial danger associated molecules (MTDs), comprising formylated proteins and mitochondrial DNA released upon nerve terminal degeneration, on PSCs activation.

We employed a novel model of degeneration, achieved by muscle injection of presynaptic neurotoxins (α-LTX or SPANs), that represent a more controllable system for the study of Schwann behaviour following nerve terminal damage.

Moreover, we tried to test MTDs potential role as SCs activators through calcium imaging experiments on both *in vitro* and *ex vivo* models.

The results of this study aim to unravel the possible contribution of these mediators on PSCs activation and to provide clinical insights for the therapy of patients. The current therapy protocols for crush injured patients imply the somministration of a wide range of anti-inflammatory drugs that could potentially hinder the healing process by delaying PSCs activation.

3 Material and Methods

3.1 Material

Toxins: β-Bungarotoxin (β-BTX) was obtained from SIGMA, taipoxin (TPX) and textilotoxin (TETX) were purchased from Venom Supplies, notexin (NTX) from Latoxan. α-LTX was purified from the venom of *Latrodectus tredecimguttatus* (Ushkaryov and Grishin, 1986). The neuroparalytic activity of the toxins was tested using the mouse phrenic nerve-hemidiaphragms preparation, as described previously (Rigoni et al., 2005). The enzymatic activity of SPANs was checked with a commercial kit based on the use of 1,2-dithio analogue of di-heptanoyl phosphatidylcholine as substrate (Cayman Chemicals).

Primary Antibodies: Polyclonal antibody against vesicle-associated membrane protein 2 (VAMP2) (Rossetto et al., 1996) was used at 1:300 dilution; monoclonal antibody against synaptophysin I (SypI) (DAKO) was used at a dilution of 1:10; monoclonal antibody against synaptotagmin I (SytI) luminal domain (Synaptic Systems) was used at a working dilution of 1:100; monoclonal antibody anti-NF (SIGMA) and polyclonal antibody anti-VAChT (Synaptic Systems) were diluted 1:500; polyclonal antibody agains myelin basic protein (MBP) (Abcam) was used at a working dilution of 1:500; polyclonal antibody against S100 (Dako) was used at a working dilution of 1:400; polyclonal antibody against GFAP (Dako) was used at a working dilution of 1:300; monoclonal Nestin antibody (Developmental Studies Hybridoma Bank (DSHB), University of Iowa) (1:100); monoclonal antibody against actin (Sigma) was used at a working dilution of 1:5000; monoclonal antibody against TLR9 (Cayman) was used at a working dilution of 1:400 for immunocytochemistry and 1:1000 for western blot; polyclonal antibody against FPR1 (Santa Cruz) was used at a working dilution of 1:100 in immunocytochemistry and 1:500 in western blot.

Secondary antibodies: Alexa555-, Alexa488- and Alexa647-conjugated α-Bungarotoxin (Molecular Probes) were used at a working dilution of 1:200; Alexa555, Alexa350 and Alexa488 secondary antibodies (Molecular Probes) were used at a dilution of 1:200. Horseradish Peroxidase (HRP)-conjugated secondary antibodies were used at a working dilution of 1:10000 (anti-mouse, Calbiochem) and 1:1000 (anti-goat, Santa Cruz).

Reagents: All salts, FMLP, Mowiol, trypsin, trypsin inhibitor, gentamicin, L-glutamine, AraC, 2-mercaptoethanol, glutammic acid, collagenase, poly-lisine, forskolin, heregulin, BES buffer, cocarboxilase, ionomycin, monensin, tubocurarine, DTT, SDS and phosphatase inhibitor mix I and II were purchased from Sigma; BSA, Triton X100, Tween-20, DNase I ad proteases inhibitor cocktail were purchased from Roche; Fura-2AM, pluronic acid, sulfynpirazone and Fluo-4AM were puchased from Invitrogen; Blotto was purchased from Santa Cruz; Percoll was purchased from GE Healthcare.

Cell Medium: Cell medium were from Invitrogen.

3.2 Methods

3.2.1 Animal Care and Treatment

3.2.1.1 Intramuscular Injection of Presynaptic Neurotoxins

All experiments were performed in accordance with Italian animal care guidelines, law no. 116/1992. Adult CD11 mice, weighting between 35 and 37 g, were anaesthetized by intraperitoneal injection of 15 mg/kg of a combination of tiletamine hypochloride and zolazepam hypochloride (Laboratories Virbac, Carros, France) and 3 mg/kg of xylazine hydrochloride (Laboratoires Calier, Barcelona, Spain). 50 μl of α-LTX or SPANs (5 μg/kg and 3–10 μg/kg respectively), dissolved in physiological saline (NaCl 0.9% in bidistillated water), were injected intramuscularly in the mouse tibialis anterior, EDL or soleus muscles of the left hind limb; an equal amount of physiological saline was injected in the contra-lateral hind limb as a control.

3.2.1.2 Sciatic nerve surgery

Denervation of the distal muscles group (tibialis anterior, soleus, plantar and gastrocnemius) of the hind limb was obtained via the surgical cut of the sciatic nerve at the level of the coxo-femoral articulation. Briefly, the mouse was anaesthetized with a mixture of air and isofluorane. The fur at the level of the site of operation was removed and the skin sterilized with absolute ethanol. The skin at the level of the coxo-femoral articulation was cut and the sciatic nerve exposed via a small incision of the muscle above. A portion of 5 mm of the sciatic nerve was removed in order to prevent nerve regeneration. Once the cut is done, the skin is suturated and disinfected with Betadine. The operated mice were kept under strict control to prevent the stitch removal. All surgical instruments were kept in absolute ethanol during operation to avoid any possible infection.

3.2.1.3 Digit Abduction Score assay

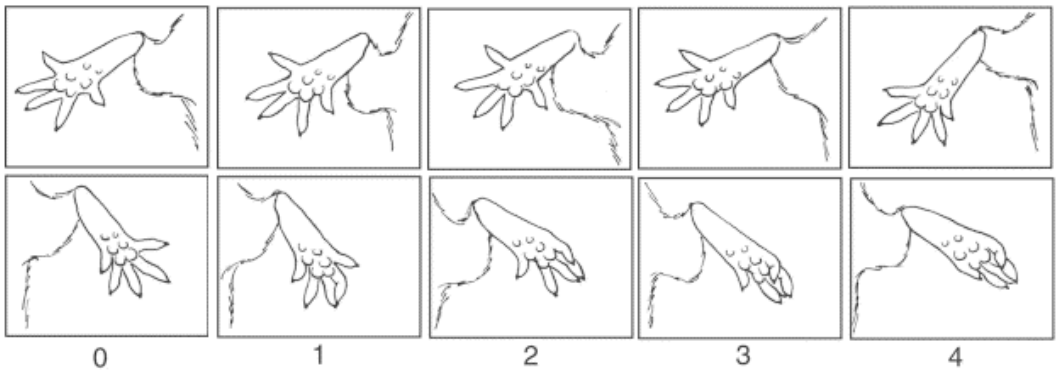

Figure 21 DAS assay. A schematic representation of the different degree of leg paralysis and the releative score based on [126]

Following the injection of the neurotoxins (α-LTX or SPANs) in mice hind limb, the functional recovery and the degree of paralysis were estimated with the Digit Abduction Score assay [139]. This assay is based on the extension reflex of the hind limbs and of the fingers after the posterior part of the animal was lifted. To the degree of extension is assigned a score ranging from 0 to 4, with 0 representing a normal condition (full functionality) and 4 to the highest degree of paralysis (Fig. 21).

3.2.2 Cellular Biology

3.2.2.1 Primary cultures

3.2.2.1.1 CGNs (cerebellar granular neurons) primary culture

For this preparation the following solutions are used:

- Solution A: NaCl 120 mM, KCl 5.3 mM, glucose 14 mM, phenol red 30 μM, NaH_2PO_4 X H_2O 1 mM, Hepes 20 mM, $MgSO_4$ 0.5 mM, BSA 40 μM in bidistillated water, pH 7.4
- Solution B: solution A + trypsin 30 μM (Sigma)
- Solution C: solution A + DnaseI 3 μM (Roche), trypsin inhibitor 30 μM (Sigma), $MgSO_4$ 1.6 mM
- Solution D: 16% of solution C + 84% solution A
- Solution E: solution A + $MgSO_4$ 1.2 mM, $CaCl_2$ 0.1 mM

The culture medium used was BME added with gentamicin (50 mg/l) (Sigma), L-glutamine (2 mM) (Sigma), KCl (20 mM) and 10% FBS.

CGNs were prepared from P5-P7 Wistar rat. After decapitation, the skin and the cartilage of the head were cut and removed. The portion including bridge-cerebellum-bulb was removed and immediately transferred in a petri dish containing Solution A. Once transferred under a dissection microscope, blood vessels and meninges were removed from the cerebellum which is then separated from bridge and buld and placed in a ice-cooled petri dish containing Solution A.

After aspiration of the solution A, cerebellum were minced with a lancet and resuspended in 10 ml of Solution B. The obtained suspension was transferred in a sterile tube (N) and incubated at 37°C in constant agitation to facilitate trypsin action. After 15', 10 ml of Solution D was added. The suspension was centrifuged at 900 rpm for 2'. The supernatant was eliminated and the pellet resuspended with 3 ml of Solution C. At this point, the separation of CGNs from connective tissues was further improved by repeated cycle of aspiration and espiration through a

micropipette tip. The suspension was left resting for 1' to let settle the debris. The clear portion of the suspension was transferred in a sterile tube (S) and an equal volume of Solution E was added. 3 ml of Solution C was added to the suspension in tube N and previous steps repeated. The suspension in tube S was then centrifuged at 900 rpm at RT for 8'. Once the supernatant was discarded, the resulting pellet was resuspended with culture medium and neurons counted with a Bürker chamber.

Neurons were then seeded onto poly-L-lysinated-coverslips (10 μg/ml poly-L-Lysine (Sigma) for 45'at RT) at the following concentration:

- 1.4 x 10^6 cell/well in 6-well plates with 24 mm diameter coverslips
- 0.3 x 10^6 cell/well in 24-well plates with 13 mm diameter coverslips

The day after the seeding, neurons were treated with the anti-mitotic agent AraC 10 μM (Sigma) in order to obtain a culture as pure as possible. Cells were used 6 to 8 days after seeding.

3.2.2.1.2 SCMs (spinal cord motoneurons) primary culture

The primary culture of embrionic spinal motoneurons was prepared from E14 Wistar rats as previously described [140]. The spinal cords of 4 to 6 embryos were dissected under a dissection microscope and minced with a lancet. Fragments were transferred in a tube containing PBSA (PBS without Ca^{2+} and Mg^{2+}) added with trypsin (0.025%) and incubated for 10'at 37°C. After the first 5' the tube was agitated. During the incubation with trypsin the following solution was prepared : 800 μl of L-15 medium, 100 μl of BSA 4%, 100 μl di DNase I 1 mg/ml. Immediately after trypsin incubation, the spinal cord fragments were transferred into the prepared tube. The tube was then agitated vigorously by hand until the tissue fragments were disaggregated. To further improve the disaggregation, the fragments were triturated twice with a micropipette

tip. After this step, the resulting suspension was left to settle for 2' and the supernatant transferred into a fresh tube. To the tube containing the settled fragments 900 µl of L-15 medium, 100 µl of BSA 4% and 20 µl of Dnase I (1 mg/ml) were added. The resuspended fragments were triturated 6 times with a micropipette tip. The remaining fragments were left to settle and the supernatant transferred to the fresh tube.

By using a long Pasteur pipette, we applied a BSA 4% cushion (1.5 ml) onto the bottom of the tube containing the pooled supernatants. The suspension was then centrifuged for 5' at 370 g at RT.

The supernatant was discarded and the pellet resuspended in 1 ml L-15 medium. Then, the obtained SCMs were seeded in complete Neurobasal medium (Neurobasal added with B27, horse serum 2%, L-glutamine 0.5 mM, 2-mercaptoethanol 25 µM (Sigma), glutamic acid 25 µM) (Sigma). SCMs were used 6 to 8 days after seeding.

Glass coverslips preparation: coverslips were left in a mixture of nitric and solphonic acid for 24 h; after extensive washes with bidistillated water coverslips were kept in absolute ethanol. Before SCMs seeding, acid- washed coverslips were coated with 1X polyornithine in sterile water for 2 h. The solution was removed and coverslips left to dry. When completely dryed, they were covered with 1X laminin in neurobasal medium and incubated for at least 2 h in a humidified 5% CO_2 incubator at 37 °C. Finally, before seeding laminin solution was removed and replaced with complete neurobasal medium.

3.2.2.1.3 Schwann Cells primary culture

The primary culture of SCs was prepared from 6 P3 rat. Pups were anaesthetized with isofluorane and sacrificed by decapitation. The skin at the level of the hind limbs were carefully removed and muscle near the head of the thigh-bone cut in order to expose the sciatic nerve. The cut was progressively enlarged along the thigh-bone and the sciatic nerve freed from connective tissues. The portion of sciatic nerve comprised between the spinal chord and the insertion point in the muscle was removed and immediately moved in ice-cooled Preparation Medium (L15 medium added with BSA 0.3%) . After nerve collection was completed, remaining

connective tissues and endoneurium were removed and cleaned nerve transferred in Digestion Solution (Collagenase 0.1% (Sigma), Trypsin in Preparation Medium). The obtained suspension was incubated at 37°C for 1 h, gently shaking every 10', filtered with a Nylon Net Filters (80 µm cut-off) (Millipore) to remove undigested fragments; 5 ml of FBS 10% in DMEM were added and the solution centrifuged at 1400 rpm for 3'. Supernatant was discarded, the pellet resuspended with DMEM supplemented with 10% heat inactivated FBS and resulting cells seeded in non-coated Petri dishes. 24 h after seeding, the medium was replaced with fresh medium added with AraC 10 µM to prevent macrophages and fibroblasts mitosis. To improve the purity of the culture we performed an immunocytolysis step 5 days after seeding (in order to get rid of the majority of fibroblasts). Briefly, culture medium was replaced with DMEM supplemented with 10% FBS and a anti-Thy 1.1 monoclonal antibody (Sigma) (1:500) for 30' at 37°C. Subsequently, rabbit complement (Sigma), diluited 1/10, was added to the medium and the culture incubated for futher 2 h. Finally, cells were washed two times with DMEM FBS 10%. The purified SCs were subsequently plated in poly-L-lysine-coated 10 cm dishes and allowed to grow in Expansion Medium consisting of DMEM, supplemented with 10% FBS , 2 µM forskolin (Sigma) and 10 nM neuregulin (Sigma).

SCs were induced to acquire a differentiated phenotype by exposure for 3–4 days to Forskolin 20 µM [141] and were seeded in collagen-coated glass coverslips as follow:

- 100,000 cells in 24 mm diameter glass coverslips
- 10-15,000 cells/well in 96 well plate
- 30,000 cells in 13 mm diameter glass coverslips.

3.2.2.1.4 Monocyte isolation from Buffy coat

Human monocytes were obtained from healthy donors-derived buffy coat, from the Transfusional Centre of the Universitary Hospital of Padova.

Blood was diluted 1:4 with sterile phosphate buffer (PBS) without Ca^{2+} and Mg^{2+}; then dextran 5% was added, and erytrocytes sedimented for 30'. The supernatant was recovered and washed with sterile PBS for 15' at 50g. The pellet was resuspended in 15 ml of sterile PBS, stratified on Ficoll and centrifuged 30' at 400g without brake and accelerator.

Lympho-monocytes were recovered and washed 15' at 311g, and then stratified on Percoll (GE-Healthcare) gradient (15,76 ml RPMI 1640, 10% FCS (v/v), HEPES 4 mM (Gibco), 50 μg/ml gentamycin, 285 mOsm; 15,54 ml 10% Percoll in 10x sterile PBS 285 mOsm), and centrifuged 30' at 400g without brake and accelerator.

Monocytes were recovered and washed 15' at 311 g, then the cells were risuspended in RPMI 1640, 2% FBS, 50 μg/ml gentamycin, seeded $2x10^6$ cells in 24 well plates and separated from contaminating lymphocytes by adherence (1 h at 37°C). Adherent monocytes were extensively washed with medium to remove residual non adherent cells.

3.2.2.1.5 Purification of Rat Brain Mitochondria and MTDs Preparation

Two adult Wistar rat forebrains were used for each mitochondrial preparation. Rats were killed by cervical dislocation and forebrains immediately transferred into ice-cold isolation medium (250 mM sucrose, 10 mM Tris-HCl, pH 7.4, 0.1 mM EGTA). Dissected forebrains were chopped with scissors and homogenized with 5–7 strokes of a loose-fitting Wheaton pestle. The homogenate was centrifuged for 3' at 2,000 × g in isolation medium added with 0.5% bovine serum albumin to precipitate the nuclei, and the supernatant was centrifuged twice for 8' at 12,000 × g. The resulting pellet was resuspended in isolation medium without albumin and centrifuged for 8' at 12,000 × g. The resulting surnatant was

discarded and the pellet resuspended in 6 ml of isolation medium without BSA. Protease inhibitor cocktail (1:100) was added to the suspension which was then sonicated on ice (VCX130-Vibra Cell, Sonics and Materials) at 100% amplitude (ten times, 30" each time with 3"- intervals). The disrupted mitochondrial suspensions were then centrifuged at 12,000*g* for 10' at 4°C followed by 100,000*g* at 4°C for 30'. Residual supernatants were used for experiments. Protein concentrations of the MTD solutions were determined by BCA Protein Assay (Pierce).

3.2.2.1.6 Cytotoxicity Assay

SCs grown in 96-well plates were exposed to FMLP 50 and 100 nM (Sigma) for 1, 6 and 18 h; their viability was then measured with the MTS (3-(4,5-dimethylthiazol-2-yl-5-(3-carboxymethoxyphenyl-2-(4-sulfonphenyl)-2H-tetrazolium, inner salt) assay. The CellTiter 96 AQueous One Solution Cell Proliferation Assay (Promega) was used and instructions from the manufacturer were followed.

3.2.3 Calcium Imaging

3.2.3.1 Calcium imaging of cultured Schwann cell and CGNs

Neurons and Schwann cells grown on 24 mm coverslips were incubated in complete medium with 3 μM Fura-2AM and 0.02% pluronic (Invitrogen) for 30' at 37 °C and then washed. To prevent Fura-2 leakage and sequestration, 250 μM sulfinpyrazone (Sigma) was present throughout the loading procedure and $[Ca^{2+}]_i$ measurements. After loading, cells were bathed in Krebs-Ringer buffer (KRH, in the case of CGNs and SCs) . KRH composition was the following: 125 mM NaCl, 5 mM KCl, 1.2 mM $MgSO_4$, 2 mM $CaCl_2$, 1.2 mM KH_2PO_4, 6 mM glucose, and 25 mM HEPES, pH 7.4. Coverslips were mounted on a thermostated chamber (Medical System Corp.), placed on the stage of an inverted epifluorescence microscope (Axiovert 100 TV; Zeiss), equipped for single cell fluorescence measurements and imaging analysis [142]. Samples were

alternatively illuminated at 340 and 380 nm (every 15″ for 20-30′ after SPAN and α-LTX addition, every 1″ for 300″ after BzATP addiction to SCs and every 15″ for 30′ after MTDs or FMLP addiction to SCs) through a ×40 oil immersion objective (numerical aperture 1.30; Zeiss), exposure times of 100 ms. Data were analyzed with TillVision and ImageJ software.

3.2.3.2 Calcium imaging and analysis in PSCs

Dissected soleus muscles were pinned in Rees saline solution (Rees, 1978) as follows (in mM): NaCl 110 mM; KCl 5 mM; MgCl2 1 mM; NaHCO3 25 mM; CaCl2 2 mM glucose 11 mM; glutamate 0.3 mM; glutamine 0.4 mM; BES buffer (Sigma), 5 mM; cocarboxylase 0.4 μM (Sigma); and choline chloride 36 M and bubbled with 95% O2/5% CO2. The dissected muscles were incubated for 1h at RT with 0.6 μM α-BTX conjugated to an Alexa-647 fluorophore. After 3 washes, muscles were incubated in 10 μM Fluo-4AM (Invitrogen) containing 0.02% pluronic acid for 1.5 h at room temperature. NMJs were located on the surface of muscle fibers using Alexa-647 conjugated α-LTX labeling of the postsynaptic specialization and were chosen for experiment when PSCs, loaded with Fluo-4AM, were superimposed to α-BTX labeling. ATP (1 mM, Sigma) or acetylcholine chloride (20 μM, Sigma) puff was provided with a picospritzer apparatus (puff parameters: time=300ms; pressure= 0.5 atm) and checked with Alexa-633 (7 μM) loaded in the puffed solution. Images were acquired at a rate of one image per second with an integration time of 400 ms. Fluorescence was quantified by subtracting the background fluorescence from the neighboring muscle fiber and then performing the calculation $(F-F_0/F_0)*100$ to give the percentage $\Delta F/F_0$. Experiments were discarded when focal drift occurred. For the duration of the experiment, the preparation was continuosly perfused with Rees saline added with tubocurarine 10 μM (Sigma) in order to prevent muscle contraction.

3.2.4 Biochemical Technique

3.2.4.1 Sample Preparation

Total cell lysates were prepared by resuspending the cells in a buffer consisting of 50 mM Tris, 150 mM NaCl, 1% SDS (Sigma), and 0.5 mM DTT (Sigma) along with protease inhibitors cocktail (Roche) and phosphatase inhibitors (phosphatase mixtures I and II, Sigma). Protein lysates were combined with SDS sample buffer (400mM Tris/HCl,pH6.8, 10% SDS, 50% glycerol, 500mM DTT, 2 μg/ml bromophenol blue), followed by 10 min of boiling.

3.2.4.2 SDS-PAGE

All SDS-PAGE electrophoresis was performed using NuPAGE® Novex® Bis-Tris pre-cast protein gradient gels (4-12%), XCell *SureLock*™ Mini-Cell System (Invitrogen) and NuPAGE® MOPS SDS Running Buffer (Invitrogen). Briefly, each well of the gel was carefully washed to eliminate residues of polymerized polyacrylammide. Inner and outer chamber of the electrophoresis system were filled with MOPS running buffer to provide an effective medium for electrical current conduction. Samples and molecular weight markers (Chemichrome (Sigma) and Magik Marker (Invitrogen)) were loaded and the electrophoresis performed.

3.2.4.3 Western Blot

All electrotransfer was performed using the Invitrogen apparatus mentioned above and Transfer Buffer (Invitrogen). After the transfer, the nitrocellulose immobilizing membrane was washed with PBST (Tween 20 0.05% in PBS) and stained with Ponceau Red to check for correct transfer. The dye was removed with extensive washings with bidistillated water and the membrane was saturated with Saturating Solution (Blotto 5% (Santa Cruz) in PBST) for 1h at RT; the membrane was then incubated overnight with primary antibodies against epitope of the interested protein diluited in Saturating solution. After 3 washings with PBST, the membrane was incubated with the corresponding secondary antibodies diluited in Saturation Solution; secondary antibodies are conjugated with

HRP (Horseradish Peroxidase) that, in the presence of a chemiluminescent substrate, is able to oxidate the luminol emitting radiation in the visible spectrum (ECL Plus-Amersham). The membrane is then washed first with PBST and then with PBS and the labeled proteic bands detected with the Chemidoc apparatus (BioRad). The densitometric analysis of the bands was performed with Quantity one software (BioRad)

3.2.4.4 BCA Protein Quantification method

The BCA method allows to determine the proteic concentration of a sample tha contains detergents that interfere with the Bradford method. It is based on the biuret reaction. In alkaline condition Cu^{2+} ions form a complex with the peptidic bonds of proteins and they are reduced to Cu^{+}. The bicinclonilic acid (BCA) in alkaline condition is a highly sensitive and stable reactive for Cu^{+} with which forms a purple chemical complex. Depending on the proteic concentration of the sample, a colorimetric variation detectable at a wavelenght of 562 is observed. Therefore, the absorbance value of the sample at 562 nm is proportional to the proteic concentration of the sample.

The determination of the proteic concentration of the samples was performed using the Microplate procedure of the kit mentioned above. Briefly, 25 µl of each standar or unknown sample replicate was pipetted into a microplate well (worling range 20-2,000 µg/ml). To each loaded well were then added 200 µl of the working solution, prepared by mixing 50 parts of Reactive A and 1 part of Reactive B, and the plate was mixed thoroughly on a plate shaker for 30 s. The plate was then covered and incubated at 37°C for 30'. Once the incubation period was terminated, the plate was left cooling to RT (around 10'). The absorbance of standard and unknown samples was measured at 562 nm on a plate reader.

To the obtained values, the average 562 nm absorbance measurements of the blank standard was subtracted. Next we prepared a standard curve by plotting the average blank-corrected 562 nm measurement for each BSA standard versus its concentration in µg/ml. The standard curve was used to determine the protein concentration of each unknown sample.

3.2.5 Immunofluorescence

3.2.5.1 Immunofluorescence protocol for CGNs

The experiments were performed with CGNs after 6-8 days in culture. Cells seeded in 24 well plate were incubated with neurotoxins (α-LTX 0.1 nM and SPANs 6 nM) for 20' (α-LTX) and 60' (SPANs) at 37°C in serum-free medium. After treatment, CGNs were extensively washed with KRH at 37°C, fixed for 20' ar RT with a PFA 4% in PBS, treated with quenching solution (glicine 0.38%, NH_4Cl 0.24% in PBS) for 20' at RT and permeabilazed for 20' at -20°C with acetic acid 5% in absolute ethanol. After washing with PBS, CGNs were saturated with BSA 0.5 % in PBS for 30' and then incubated for 90' at RT with the primary antibodies diluited in BSA 3% in PBS; subsequently CGNs were washed with BSA 0.5% in PBS at RT (5' for 3 times) and were incubated with the corresponding secondary antibodies conjugated with Alexa 555 or 488 fluorophore. Glass slices were then mounted with mounting solution (glycerol 90%, N-propilgallate 3% in PBS) and observed with an epifluorescence microscope (Leica DMIRE2). The acquired images were analyzed and processed with ImageJ software.

To test the effect of neurotoxin on synaptic vesicle recycling (a method to determine if there is an imbalance in the process of exo-endocytosis), either control and samples exposed to neurotoxin (same concentration and time described above) were incubated with a primary antibody against the Synaptotagmin I intraluminal epitope; the incubation lasted for 5' at 37°C, then the samples were washed, fixed, treated with quenchin solution, non permeabilized and incubated with an Alexa 555 conjugated secondary antibody. Samples were mounted, observed and analyzed ad described above.

3.2.5.2 Immunofluorescence protocol for Spinal Cord Motoneurons

The experiments were performed with SCMs after 6-8 days in culture. As for CGNs SCMNs seeded in 24 well plate were incubated with neurotoxins (α-LTX 0.1 nM and SPANs 6 nM) for 20' (α-LTX) and 60'

(SPANs) at 37°C in serum-free medium. The immunofluorescence protocols were the same adopted for CGNs but cells were permeabilized with Triton X-100 0,1 % in PBS for 3' and saturated with a different solution (normal goat serum 10%, BSA 2%, gelatin 0.2 % in PBS).

3.2.5.3 Immunofluorescence protocol for Schwann cells

All experiments were performed using SCs from passages 2–4. The immunofluorescence protocols were the same adopted for CGNs but SCs were permeabilized with Triton X-100 0,3 % in PBS for 10' and saturated with a different solution (BSA 1% in PBS).

3.2.5.4 Immunofluorescence Protocol for Muscle Preparation

Mice were sacrificed by cervical dislocation and injected muscles of both hind limbs were dissected. Muscles were then processed in skinning solution (137 mM NaCl, 5 mM KCl, 1 mM MgCl2, 24 mM NaHCO3, 1 mM NaH2PO4, 11 mM glucose and 5 mM EGTA, pH 7.4), washed and fixed for 30 min at room temperature with PFA 4% in PBS. Samples were quenched with 50 mM NH_4Cl in PBS for 10 min and incubated with saturation solution (0.1% Triton X-100, 3% BSA, 10% normal goat serum in PBS) for 60 min. Processed muscles were incubated with primary antibodies in 5% BSA, 0.1% Triton X-100 in PBS for 3 h at room temperature, washed with PBS and then incubated with the correspondent secondary antibodies plus α-Btx conjugated with Alexa488 or Alexa555 in 5% BSA in PBS for 90 min. Samples were mounted in Mowiol after extensive washing with PBS (20’ for 3 times) and examined by Nikon Eclipse 80i Video-Confocal microscope, Nikon SP2 confocal microscope or Leica DM 6000 B epifluorescence microscope.

To improve the labelling of S100 at the level of PSCs and myelinating SCs we modified the protocol described above. Briefly, fixed and quenched muscles were permeabilized in BSA 3%, Triton X-100 0.5% in PBS for 45’, washed and saturated with BSA 3%, goat serum 10% in PBS for 1 h. After washing, samples were incubated overnight with primary

antibodies in BSA 10%, Triton X-100 10% in PBS at RT. Subsequently, samples was incubated with secondary antibodies and Alexa555 or 488 conjugated α-BTX diluted in BSA 10% in PBS for 2 h at RT. Samples were then mounted and examined as described above.

Nestin was labelled using a protocol described by Son Y.J. e Thompson W.J., 1996 [143]. Briefly, after being processed, fixed and quenched, muscles were incubated with Alexa-555 or -488 conjugated α-BTX in BSA 0.5% in PBS for 90′ at RT and permeabilized in absolute methanol for 20′ at -20°C. Samples were then washed with PBS and incubated overnight with primary antibodies at RT. Muscles were then incubated with corresponding secondary antibodies for 2h at RT. Mounting and examination of the processed muscle was performed as described above.

4 RESULTS AND DISCUSSIONS

4.1 RESULTS (Part I)

4.1.1 SPANs and α-LTX induce similar bulging on rat primary neurons

SPANs induce a defined phenotype in different types of neurons in culture [144]. Within few minutes from toxin addition, bulges appear as defined rounded swellings of the plasma membrane at neurons' terminals and extensions (right panels of Fig. 22). The left panels of Fig. 22 show that α-LTX induces, at very low concentration, a similar phenotype in both cerebellar granular neurons and in spinal cord motoneurons. Neuronal bulges induced by SPANs and α-LTX were similar in size, appearance and distribution. These findings indicate that also the activity of α-LTX can be tested with this sensitive and easy to perform cellular assay.

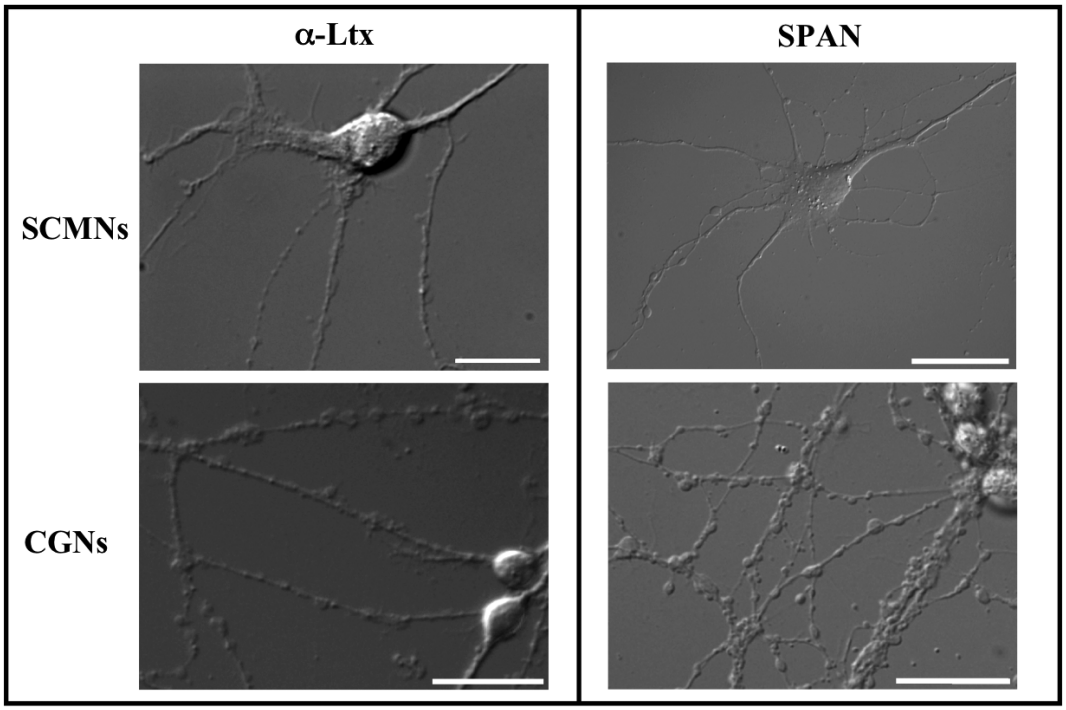

Figure 22 Morphological changes induced by α-LTX and SPANs in primary neurons in culture. Spinal cord motoneurons (SCMNs, upper panels) and cerebellar granule neurons (CGNs, lower panels) were treated with α-LTX 0.1 nM for 20 min (A) or with β-BTX 6 nM for 30 min (B). Both toxins induce closely similar membrane enlargements of neuronal processes (bulges). Very similar results were obtained with taipoxin, notexin and textilotoxin. Scale bar: 20 mm.

4.1.2 SPAN and α-LTX-induced bulges accumulate synaptic vesicle markers

We have previously established that the neuronal bulges induced by SPANs are sites of accumulation of synaptic vesicles (SVs), whose presence could be shown by labelling with antibodies specific for SV proteins such as the vesicle-associated membrane protein 2 (VAMP2) or synaptophysin I (SypI) [144]. Fig. 23 shows examples of such accumulation caused by SPANs (right panels) and that the action of α-LTX (central panels) is very similar also in this respect, as previously found in hippocampal neurons [145]. These pictures were obtained in permeabilised neurons and do not allow one to distinguish between an internal localization or a surface exposure of the antigens. Therefore the action of the toxins was also analysed in non-permeabilised cells (see next paragraph).

4.1.3 SPANs and α-LTX induce exposure of synaptic vesicle luminal proteins in cultured neurons

According to the electron microscopy analyses discussed in the introduction, SVs are largely reduced, or absent, in the cytosol after the action of α-LTX or SPANs. The most likely possibility is that SVs were induced to fuse and that exocytosis was not followed by SV retrieval, owing to an impairment in the exo–endocytic balance. If this is the case, the luminal domains of the SV membrane proteins have to be permanently exposed on the surface of the neurons.

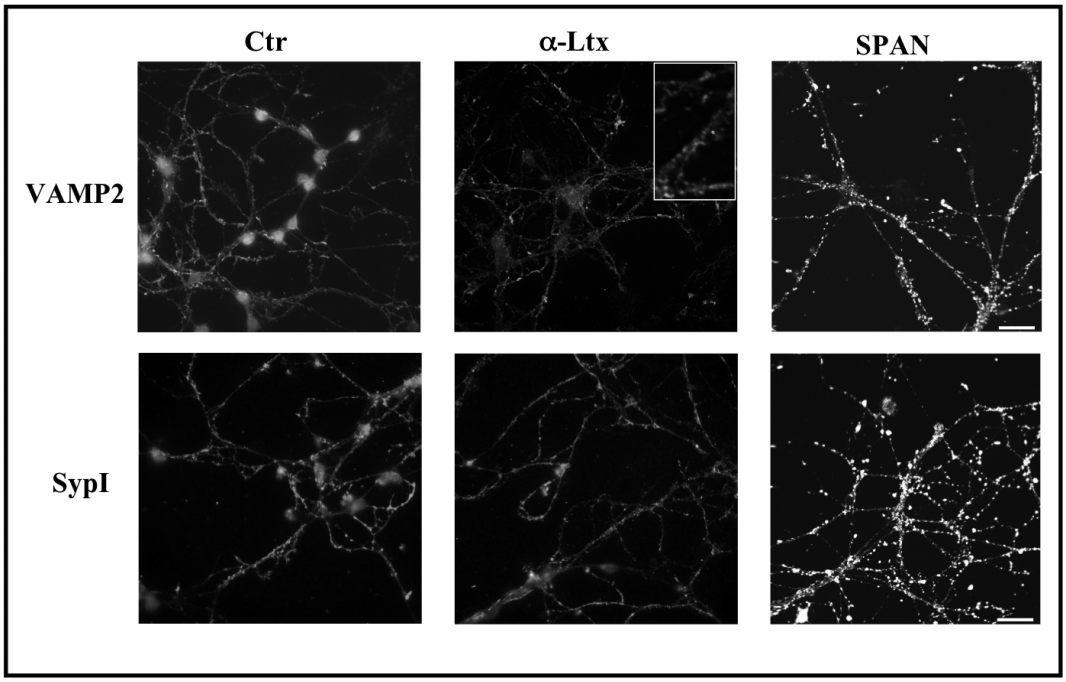

Figure 23 Effect of α-LTX and SPANs on the distribution of synaptic vesicle markers in primary neurons in culture. Cerebellar granule neurons were incubated with α-LTX and β-BTX (0.1 nM for 20 min and 6 nM for 60 min respectively) and the distribution of the vesicular proteins VAMP2 and synaptophysin I was analysed by indirect immunofluorescence. In both cases the staining of the two proteins changes with respect to the control, showing an accumulation within the toxininduced membrane enlargements. Overlapping results were obtained with spinal cord motoneurons and with taipoxin, notexin and textilotoxin. Scale bar: 20 mm.

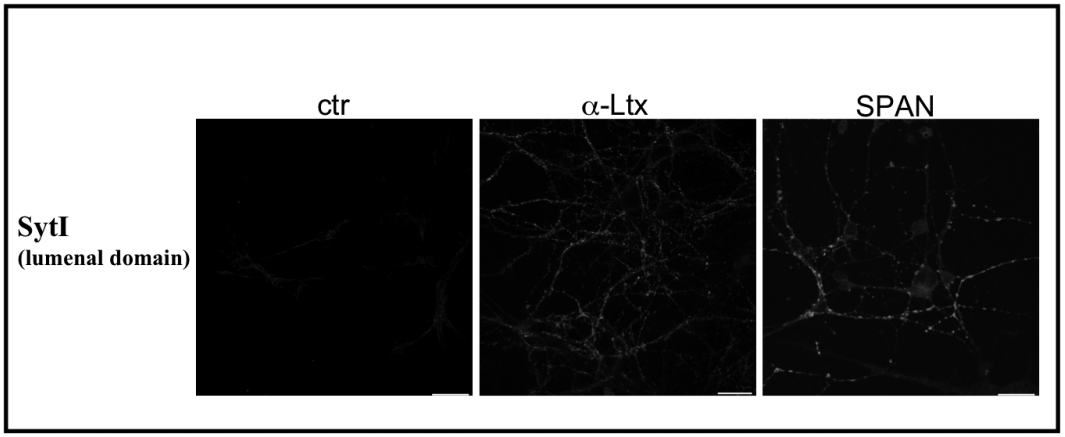

Figure 24 Effect of α-Ltx and SPANs on synaptic vesicle recycling of cultured neurons. Cerebellar granule neurons were exposed to α-LTX and TPX (0.1 nM for 20 min and 6 nM for 60 min respectively) and then incubated for 5 min at 37 °C before fixation and permeabilization with a monoclonal antibody that specifically recognizes a luminal epitope of the vesicular protein synaptotagmin I and then processed for indirect immunofluorescence. In both cases the fluorescent signal is brighter than the control and accumulates within the membrane enlargements, indicating that these bulges are sites of unbalanced exo–endocytosis. Similar results were obtained in SCMNs and with β-BTX, NTX and TeTX. Scale bar: 20 mm.24

Fig. 24 shows that, whilst the luminal part of the SV membrane marker synaptotagmin I is very little stained in control non-permeabilised neurons, it is intensively stained on the surface of bulges induced by both α-LTX and SPANs.

Such intense surface fluorescent signal indicates that SVs are incorporated in the plasma membrane at sites of bulging following the exposure to both types of neurotoxins.

4.1.4 SPANs and α-LTX induce entry of calcium into cultured neurons

Previous studies have established that a very large Ca^{2+} influx is induced at nerve terminals by α-LTX [88,89,119] and that SPAN-induced bulges are sites of Ca^{2+} influx that can be monitored by Ca^{2+} imaging (Rigoni et al., 2007). It remained to show that the α-LTX induced bulges are as well sites of Ca^{2+} entry. The left panel of Fig. 25 shows that this is indeed the case, but the time course of this Ca^{2+} influx is different from that observed in SPAN-treated neurons (middle and right panels). In cerebellar granular neurons exposed to 0.1 nM α-LTX Ca^{2+} ions begin to enter about 700 s after toxin addition and this timing is very similar in all terminals that we have analysed. This is in agreement with the notion that the ions enter through a tetrameric channel made by the α-LTX on the plasma membrane [97], and indicates that several hundreds of seconds are needed to assemble a functional toxin channel on the plasma membrane. Fig. 25 shows that calcium imaging in a homogeneous population of neurons such as CGNs is very useful in the study of the kinetics of the action of this toxin in vivo. In contrast, SPANs induce a progressive increase of Ca^{2+} entry and this is in agreement with the proposal that this influx is mediated by transient lipidic pores made by lysophospholipids and fatty acids in the plasma membrane [146,147]. The end result is, however, in both cases the same, i.e. toxin-induced bulges accumulate Ca^{2+} and this calcium overload may set in motion a series of degenerative events.

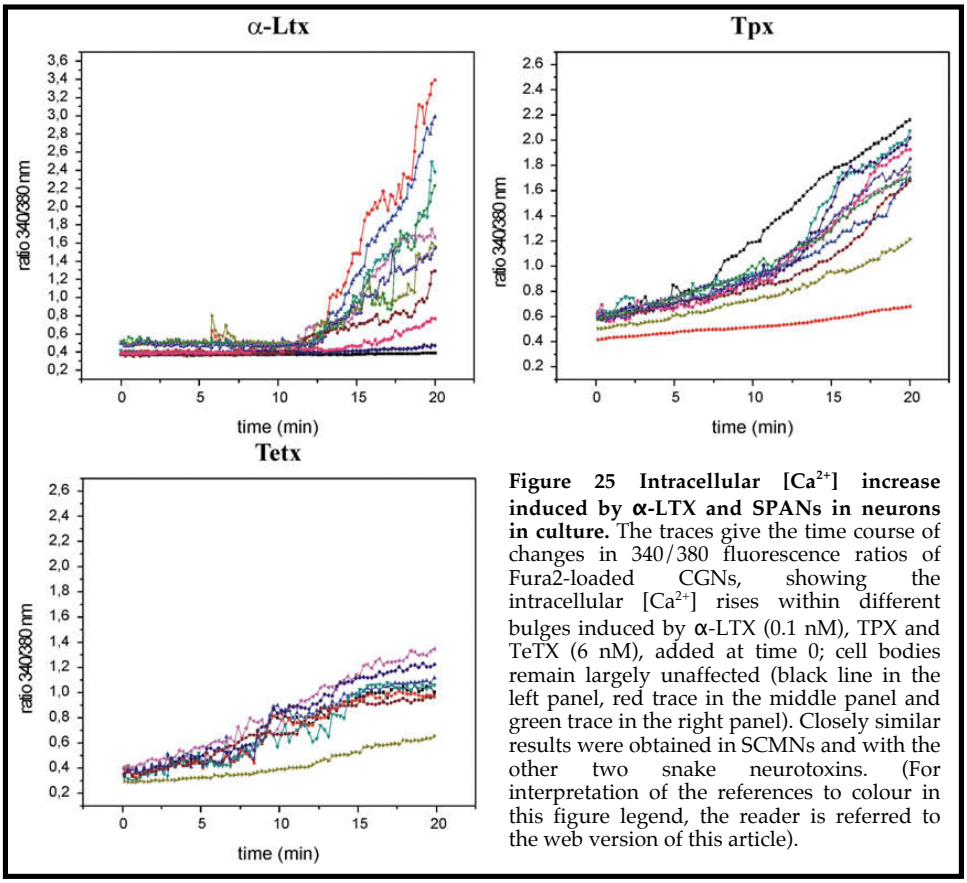

Figure 25 Intracellular [Ca^{2+}] increase induced by α-LTX and SPANs in neurons in culture. The traces give the time course of changes in 340/380 fluorescence ratios of Fura2-loaded CGNs, showing the intracellular [Ca^{2+}] rises within different bulges induced by α-LTX (0.1 nM), TPX and TeTX (6 nM), added at time 0; cell bodies remain largely unaffected (black line in the left panel, red trace in the middle panel and green trace in the right panel). Closely similar results were obtained in SCMNs and with the other two snake neurotoxins. (For interpretation of the references to colour in this figure legend, the reader is referred to the web version of this article).

4.1.5 Degeneration of presynaptic nerve terminals at NMJ after SPAN or α-LTX exposure

An end result of the chain of events started by the $Ca^{2?}$ influx caused by SPANs and α-LTX is the degeneration of nervous terminal [51,123,135,136,137,138,148,149,150]. Fig. 26 compares the staining of neurofilaments and vesicular acetylcholine transporter (VAChT), which are essential components of nerve terminals, in control and toxininjected mice muscles. With both SPANs and α-LTX there is an evident loss not only of neurofilaments but also of the specific nervous terminal marker VAChT. One may conclude that also in this respect the two types of toxins share a similar pharmacological/pathophysiological endpoint. As expected from presynaptic neurospecific toxins, there is no evident modification of the postsynaptic component of the NMJ (except for notexin, which is well known to cause also myotoxic effects).

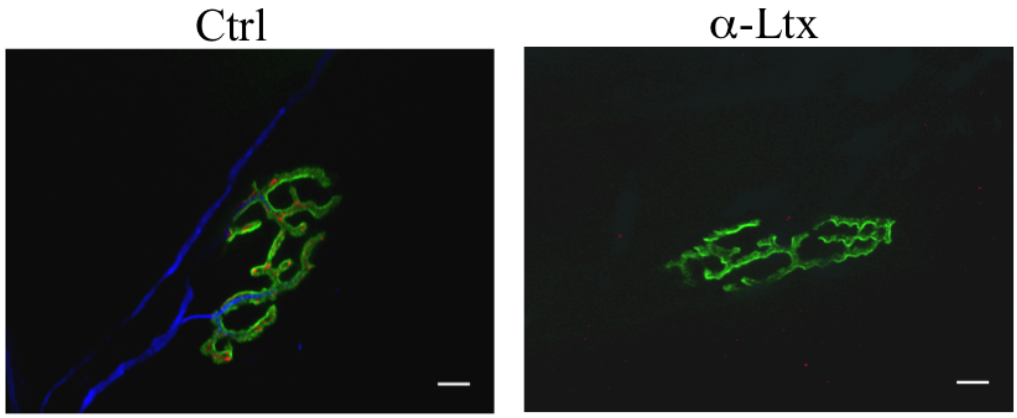

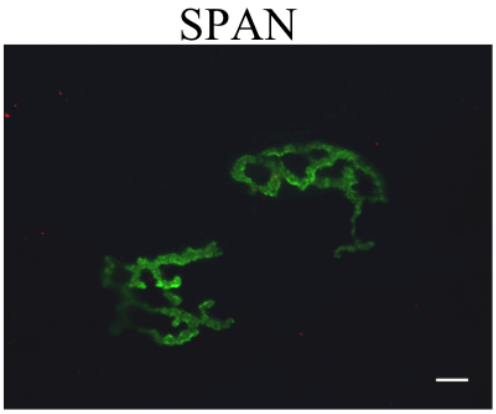

Figure 26 Effect of α-LTX and SPANs on mouse neuromuscular junction. Mice hind limbs were injected with α-LTX and TPX and processed for indirect immunohistochemistry after 12 and 24 h respectively. Both neurotoxins cause degradation of neurofilaments (blue) and disappearance of vesicular acetylcholine transporter staining (red). No morphological modifications of the postsynaptic element of the NMJ stained with a-Btx (green) were observed. Scale bars: 10 mm. Similar results were obtained with the three other SPANs (with the exception of NTX that caused also muscle damage). (For interpretation of the references to colour in this figure legend, the reader is referred to the web version of this article).

4.2 Discussion

The main purpose of the present work was the comparison of the action of snake presynaptic PLA2 neurotoxins with that of the black widow spider α-LTX. Apart from that such a side-by-side comparison was not performed before, the rationale for such a work is based on the fact that the molecular pathogenesis of the degeneration of nerve terminals induced by the snake presynaptic PLA2 neurotoxins is not yet defined [151,152], whilst that caused by α-LTX is well established to be due mainly to the large influx of Ca^{2+} which induces mitochondrial collapse and activation of many degradative enzymes [119]. The present work documents that the two types of presynaptic neurotoxins cause similar alterations in neurons in culture and in vivo. Both of them cause bulging of neurons in culture and these bulges expose on their surface the luminal domain of proteins of the synaptic vesicle membrane. Bulges accumulate calcium although with different kinetics, which are accounted for by the different biochemical activities of the two types of toxins, i.e. PLA2 activity for SPANs and ion channel activity for α-LTX. A high cytosolic [Ca^{2+}] is known to trigger a series of degradative events and, as a marker, we followed here the degradation of neurofilaments and the disappearance of VAChT. Here, we found that neurofilaments and VAChT disappear at the motoneuron endings of mice injected with the two types of neurotoxins, similarly to what previously found with β-BTX [124]. Taken together, all these similarities suggest that a major role in the degeneration of the nerve terminals caused by SPANs is the calcium overloading that follows the change in membrane composition caused by the PLA2 activity of SPANs. The fact that Ca^{2+} ions appear to enter into nerve terminals soon after SPANs addition and that they accumulate within bulges are indications that the toxin hydrolytic activity may be, at least in the beginning of the process, concentrated close to their binding sites and that the concentration of the phospholipids hydrolysis products may reach significant values such as to change the plasma membrane permeability. The precise localization of the binding sites of SPANs within the nerve

termini remains to be determined and should throw light on this ill-defined, but fundamental, aspect of the process.

4.3 RESULTS (Part II)

4.3.1 Nerve Terminal Degeneration/Regeneration Kinetics in muscles intoxicated with Presynaptic Neurotoxins

To study the involvement of PSCs in the regeneration process following selective damage of NTs we first needed to determine the "time window" between the beginning of the nerve terminal degeneration, the onset of paralysis and their complete recovery in NMJs of EDL and soleus muscles injected with presynaptic neurotoxins (α-LTX and β-BTX).To this aim sublethal doses of α-LTX (5 μg/Kg) or β-BTX (10 μg/Kg) were injected in the left hind limb of anaesthetized CD11 mice, whereas the right one was injected with the same volume (50 ul) of saline solution and used as control.

At given times, the degree of paralysis was estimated with the DAS assay and a score assigned (see Material and Methods). Mice were then sacrificed and the muscle of interest dissected and processed for immunohistochemical analysis. Intoxicated NMJs were compared with the control ones by staining the presynaptic marker VAChT and the postsynaptic marker α-BTX. The degree of colocalization between these two markers was used to assess the nerve terminal degeneration/regeneration stage.

4.3.2 Nerve Terminal Degeneration and Regeneration in α-LTX intoxicated muscles

30′ after α-LTX injection the mouse leg is almost completely paralyzed (DAS score 1) and this is confirmed by the partial co-labelling of VAChT and α-BTX in either EDL and soleus (Fig. 27 and 28). The rapid paralysis of injected muscle is expected since the massive influx of Ca^{2+} provoked by this pore-forming toxin leads to a fast degeneration of the nerve terminals [86]. The paralysis is complete 6 h after the toxin injection with a DAS score of 4 and with the absence of VAChT labelling which implies the complete degeneration of the nerve terminals. This condition is

maintained till the second day after injection. The lack of differences in α-BTX staining between intoxicated and control NMJs indicates that, at this concentration, α-LTX does not alter the postsynaptic element (Fig. 27 and 28).

Three days post injection the leg shows a partial recovery of the motility, with a weak extension of the fingers upon stimulation (DAS score 1-2). VAChT and α-BTX colocalization is almost recovered confirming the beginning of nerve terminal regeneration. At the following considered time, day 6 and 8, the extension reflex is completely recovered with a DAS score of 0 as the untreated control leg, and with the VAChT and α-BTX colocalization (Fig. 27 and 28).

We observed no difference between fast (EDL) and slow (soleus) muscles in terms of DAS assay and immunohistological data and the results of the kinetics are summarized in Table 2. The kinetic data obtained with our experimental model parallels those obtained in previous works [51,153]. There is a complete superimposition between functional and immunohistological data. Therefore, the time window between 6 h and 3 days has been chosen to monitor PSCs activation following α-LTx intoxication.

Table 2 Summary of the degeneration/regeneration time-course of nerve terminal in α-LTX intoxicated EDL and soleus. ✔ indicate presence of labeling while ✖ its complete absence. The functionality score assigned with DAS assay at each time point is correlated to immunohistological observations.

Time	VAChT	β-BTX	DAS
30 min	✔ (partial)	✔	**2**
6 h	✖	✔	**4**
1 d	✖	✔	**4**
2 d	✖	✔	**4**
3 d	✔ (partial)	✔	**1**
4 d	✔ (less intense)	✔	**0**
6 d	✔ (as control)	✔	**0**

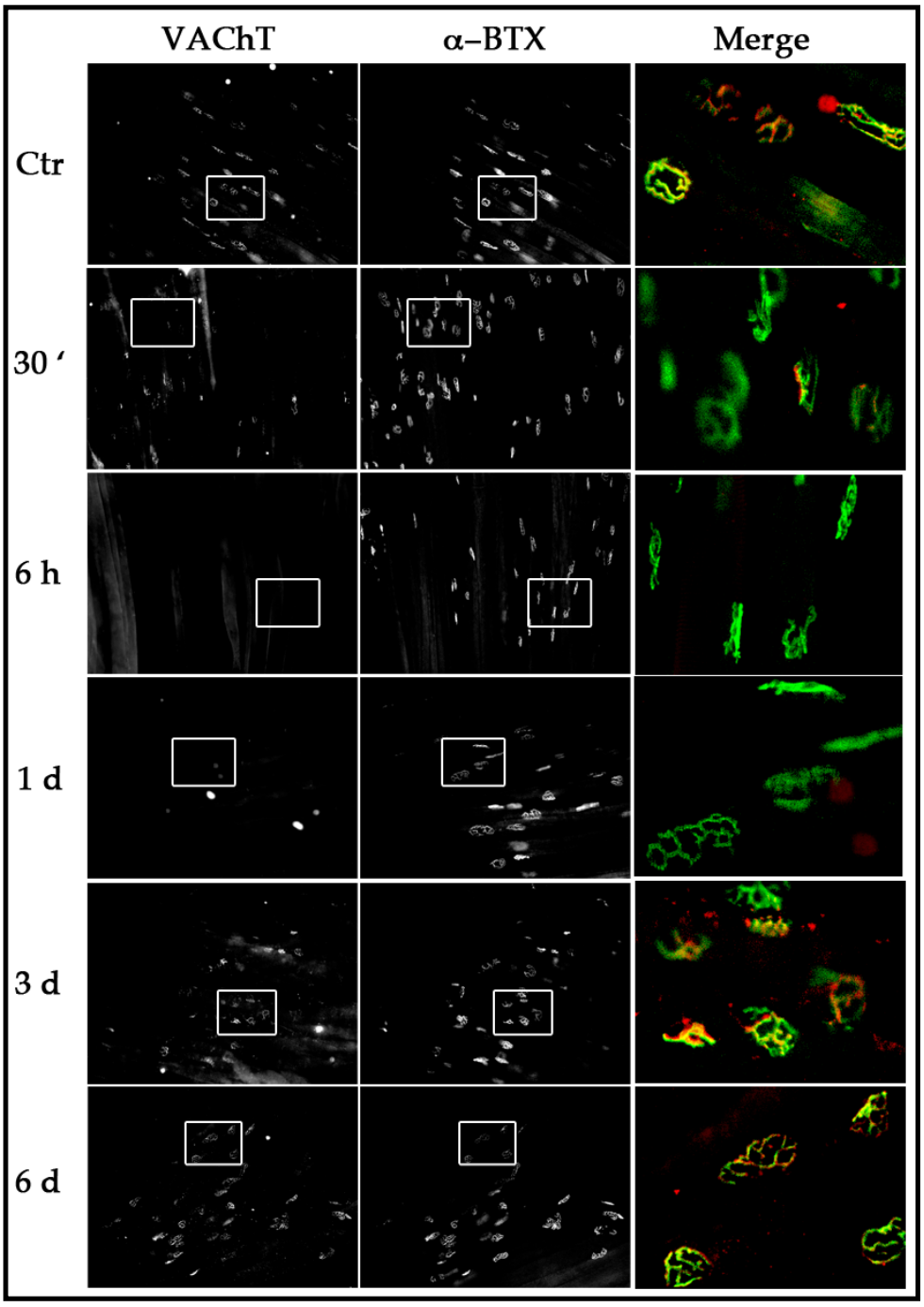

Figure 27 Kinetic of degeneratio/regeneration of nerve terminals in EDL intoxicated with α-LTX. Mice hind limbs were injected with α-LTX (5μg/Kg), dissected at considered time points and processed for indirect immunohistochemistry. VAChT staining (left column) reveal a fast and syncronous degeneration of nerve terminals starting 30′ post-injection. At 3 d, almost all NMJs are reinnervated. No morphological modifications of the postsynaptic element of the NMJ stained with α-BTX (middle column) were observed. Colocalization of pre- and postsynaptic markers is shown in the right column (magnification of the highlighted region). Scale bars: 20 μm

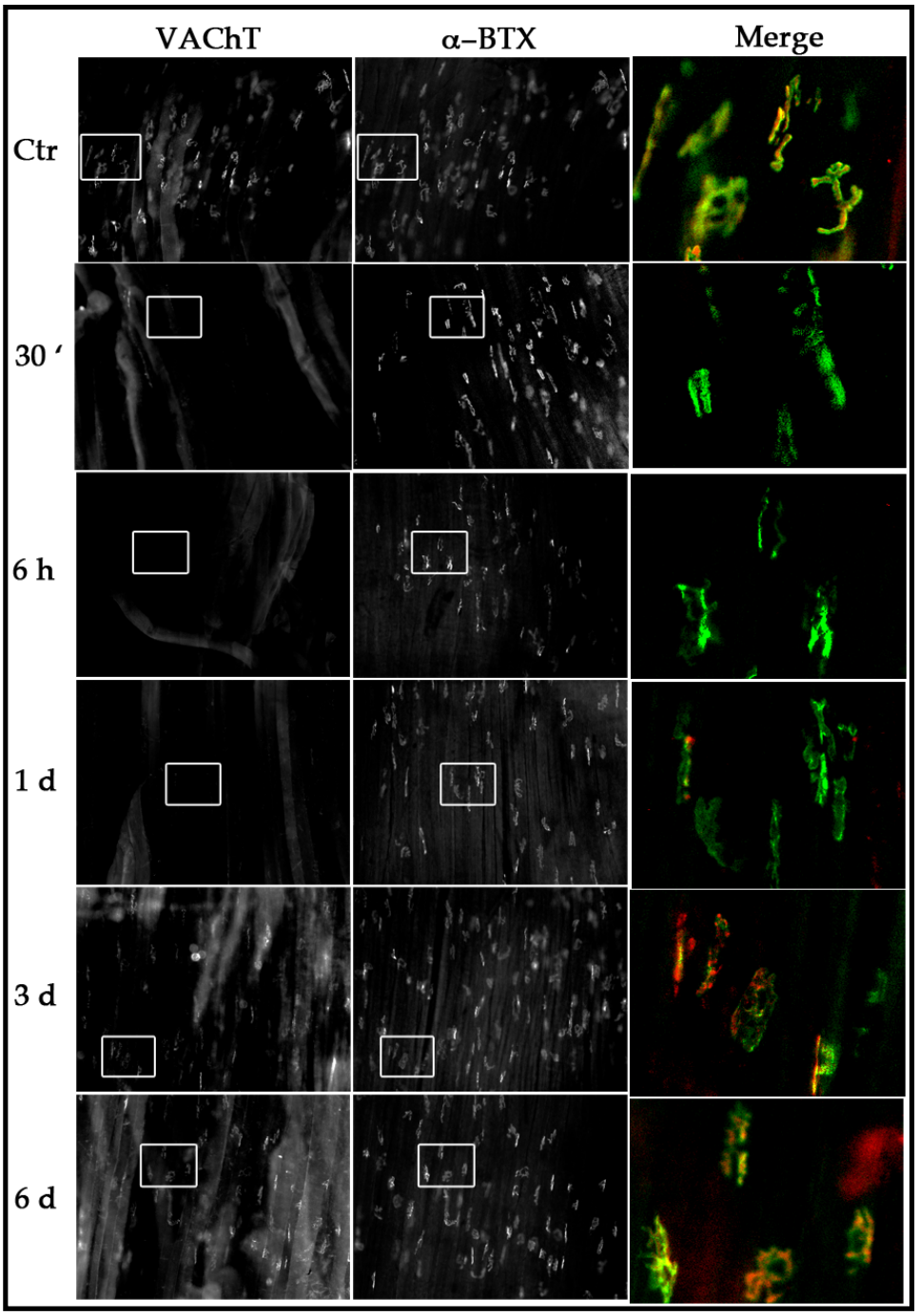

Figure 28 Kinetic of degeneratio/regeneration of nerve terminals in soleus intoxicated with α-LTX. Mice hind limbs were injected with α-LTX (5μg/Kg), dissected at considered time points and processed for indirect immunohistochemistry. VAChT staining (left column) reveals a fast and syncronous degeneration of nerve terminals starting 30′ post-injection. At 3 d, almost all NMJs are reinnervated. No morphological modifications of the postsynaptic element of the NMJ stained with α-BTX (middle column) were observed. Colocalization of pre- and postsynaptic markers is shown in the right column (magnification of the highlighted region). Scale bars: 20 μm

4.3.3 Nerve Terminal Degeneration and Regeneration in β-BTX intoxicated muscles

Differently from α-LTX , the paralysis induced by β-BTX presents some discrepancies between the functional and immunohistological data. The onset of paralysis is observed 4 h post injection but, even if the score assigned based on the extension reflex is 3-4, VAChT and α-BTX labelling still colocalize, at least in part, in a "patch-like" pattern. The same situation is present also at later time (until day 4) (Fig. 29).

The extension reflex is partially recovered (DAS 1-2) at 6 d. At that time VAChT labelling looses its patch-like pattern to become more homogeneous, even if still partial, probably confirming the beginning of nerve terminals regeneration. The extension reflex is completely recovered 8 day post injection as VAChT labelling overlaps that of α-BTX (Fig. 29) .

Table 3 Summary of degeneration/regeneration process of nerve terminals in β-BTX intoxicated EDL an soleus. ✔ indicate presence of labelling while ✖ its complete absence. The functionality score assigned with DAS assay at each time point is correlated to immunohistological information.

Time	VAChT	β-BTX	DAS
30 min	✔	✔	**n. d.**
1 h	✔	✔	**n. d.**
2 h	✔	✔	**n. d.**
6 h	✔ (partial)	✔	**4**
12 h	✔ (patch-like)	✔	**4**
1 d	✔ (patch-like)	✔	**4**
2 d	✔ (patch-like)	✔	**4**
3 d	✔ (patch-like)	✔	**4**
4 d	✔ (partial)	✔	**3**
6 d	✔ (less intense)	✔	**1**
8 d	✔ (as control)	✔	**0**

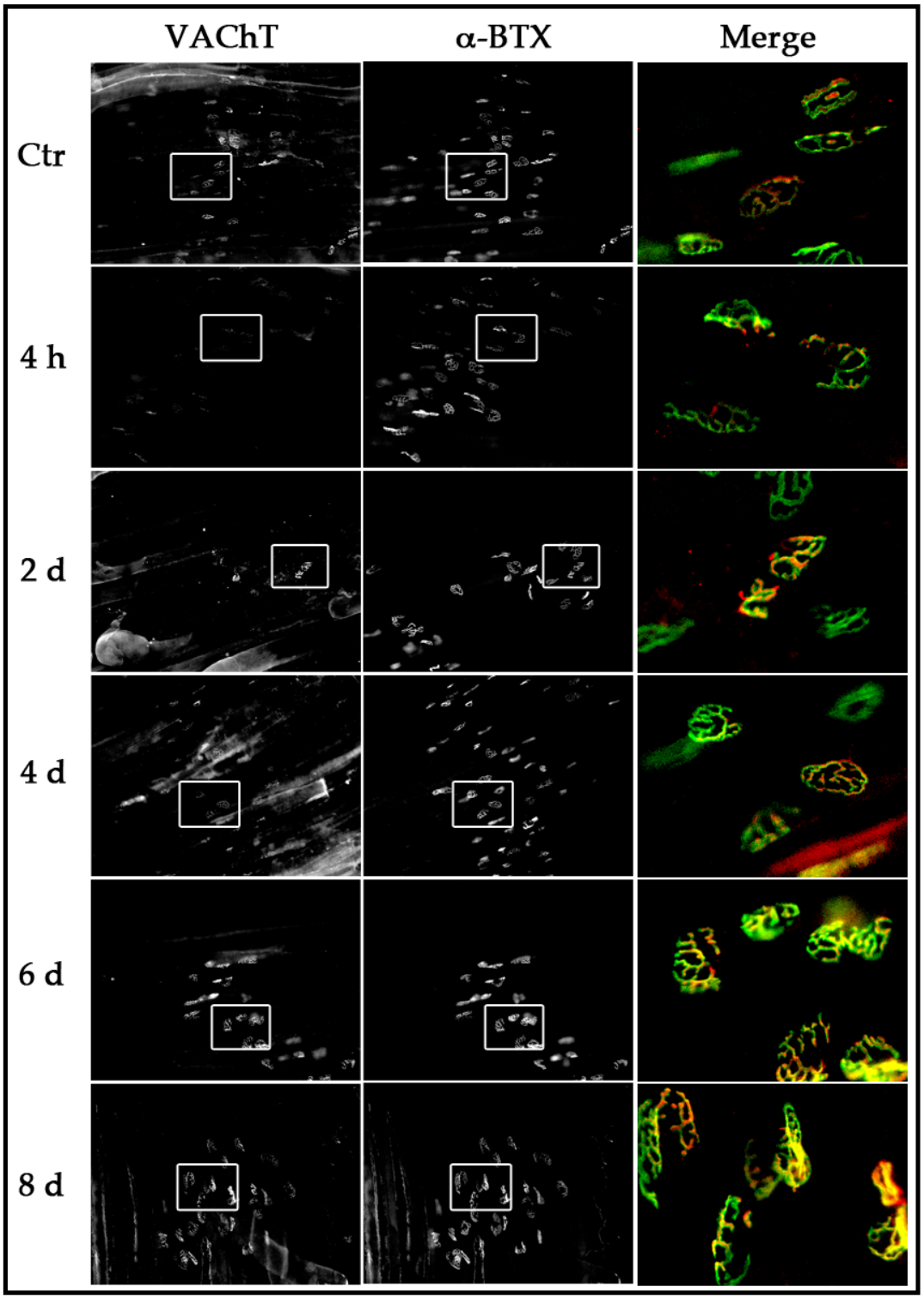

Figure 29 Kinetic of degeneratio/regeneration of nerve terminals in EDL intoxicated with β-BTX Mice hind limbs were injected with β-BTX (10 µg/Kg), dissected at considered time points and processed for indirect Iimmunohistochemistry. VAChT staining (left column) shows an asyncronous degeneration of nerve terminals starting 4 h post-injection with persistent patches of non degenerated nerve terminal. At 6 d, almost all NMJs are reinnervated. No morphological modifications of the postsynaptic element of the NMJ stained with α-BTX (middle column) were observed. Colocalization of pre- and postsynaptic markers is shown in the right column (magnification of the highlighted region). Scale bars: 10 µm

As for α-LTX, no differences in the kinetic of nerve terminal degeneration/regeneration in intoxicated NMJs is observed between fast (EDL) and slow (soleus) muscles and no morphological alterations of the postsynaptic specialization labelled with α-BTX is observed. The kinetic data are summarized in Table 3.

Differenty from α-LTX-poisoning, nerve terminals degeneration at NMJs intoxicated with β-BTX is not synchronous, since patches of still innervated NMJs are present, even in absence of extention reflex (DAS 4).This VAChT labelling pattern does not allow to discriminate between nerve terminals that are still degenerating and nerve terminals that begin to regenerate.

For this reason we decided to perform further experiments in muscles intoxicated only with α-LTX which causes a syncronous and fast degeneration of nerve terminals. Moreover, since there is no difference in kinetic between fast and slow muscle, we chose EDL as a model since it is possible to obtain up to four samples from a single dissected muscle.

4.3.4 α-LTX diffusion in injected EDL

The kinetic analysis of nerve terminal degeneration/regeneration process at NMJs intoxicated with presynaptic neurotoxins was performed on whole muscle. To demonstrate that α-LTX diffuses in each of the four portions of EDL, we injected the toxin at the same concentration of the previous experiments, dissected the EDL after 6 h, time at which nerve terminals are completely degenerated (see Table 2) and performed an immunohistological analysis using VAChT and α-BTX as markers.

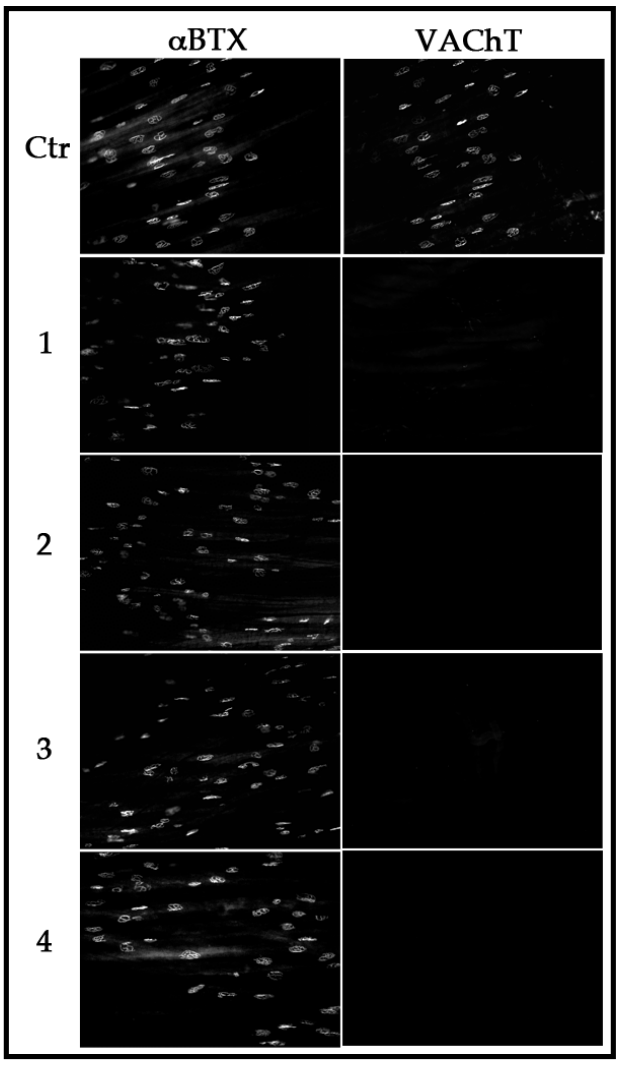

Figure 30 Diffusion of α-LTX in the different portion of EDL. Mice hind limbs were injected with α-LTX dissected at 6 h and processed for indirect immunohistochemistry. As underlined by the lack of VAChT labelling (right column), α-LTX diffuses in all EDL portions inducing degeneration of nerve terminals.

Fig. 30 shows the resulting labelling of the four samples obtained from the same EDL. As expected, VAChT staining disappears in each sample and the postsynaptic labelling is not affected.

The same experiment was performed with α-BTX by injecting an Alexa-conjugated α-BTX (10 μg/Kg) and dissecting the muscle 4 h after injection. Also in this case the four samples obtained from one EDL were equally labelled (data not shown).

4.3.5 Perisynaptic Schwann cells response to NMJ intoxication by α-LTX in EDL muscle

Once determined the correct time window and the best model to work on (EDL intoxicated with α-LTX), we checked for PSCs activation during the time-course of nerve terminal degeneration/regeneration by a pan Schwann cells marker named S100, whose intensity is known to decrease upon cell activation.

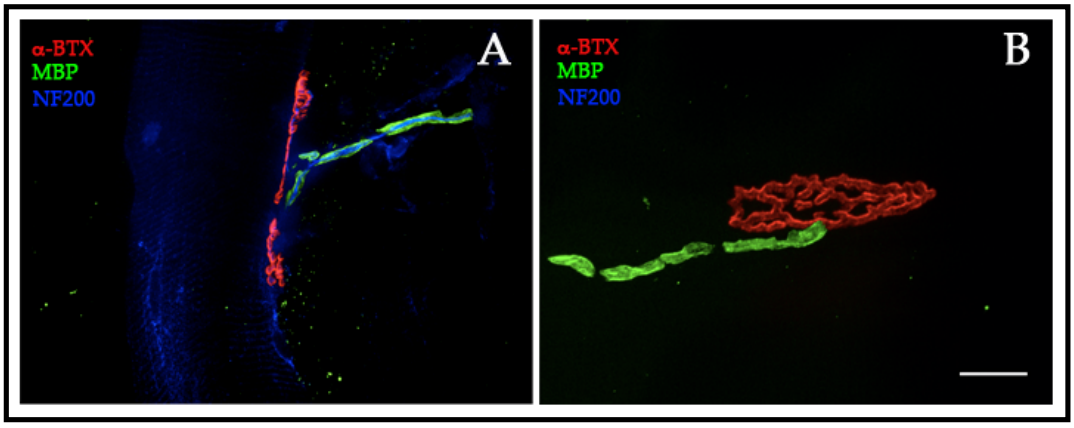

Figure 31 Effect of α-LTX on myelinating Schwann cells activation. Mice hind limbs were injected with α-LTX and processed for indirect immunohistochemistry after 2 d. α-LTX causes degradation of neurofilaments (blue), wheras no changes in myelin basic protein (green) was observed, indicating that myelinating Schwann cells are not activated. No morphological modifications of the postsynaptic element of the NMJ stained with α-BTX (red) were observed. Scale bars: 10 μm.

Comparing the two stainings in Fig. 32, it is evident that the intensity of PSCs labeling decreases after treatment with α-LTX with respect to control conditions and this reduction is maintained up to 2d post injection. The intensity of S100 staining increases 3 d post injection and reaches a level comparable to that of the control after 7 d. To check the correspondence between S100 labelling intensity variation and nerve

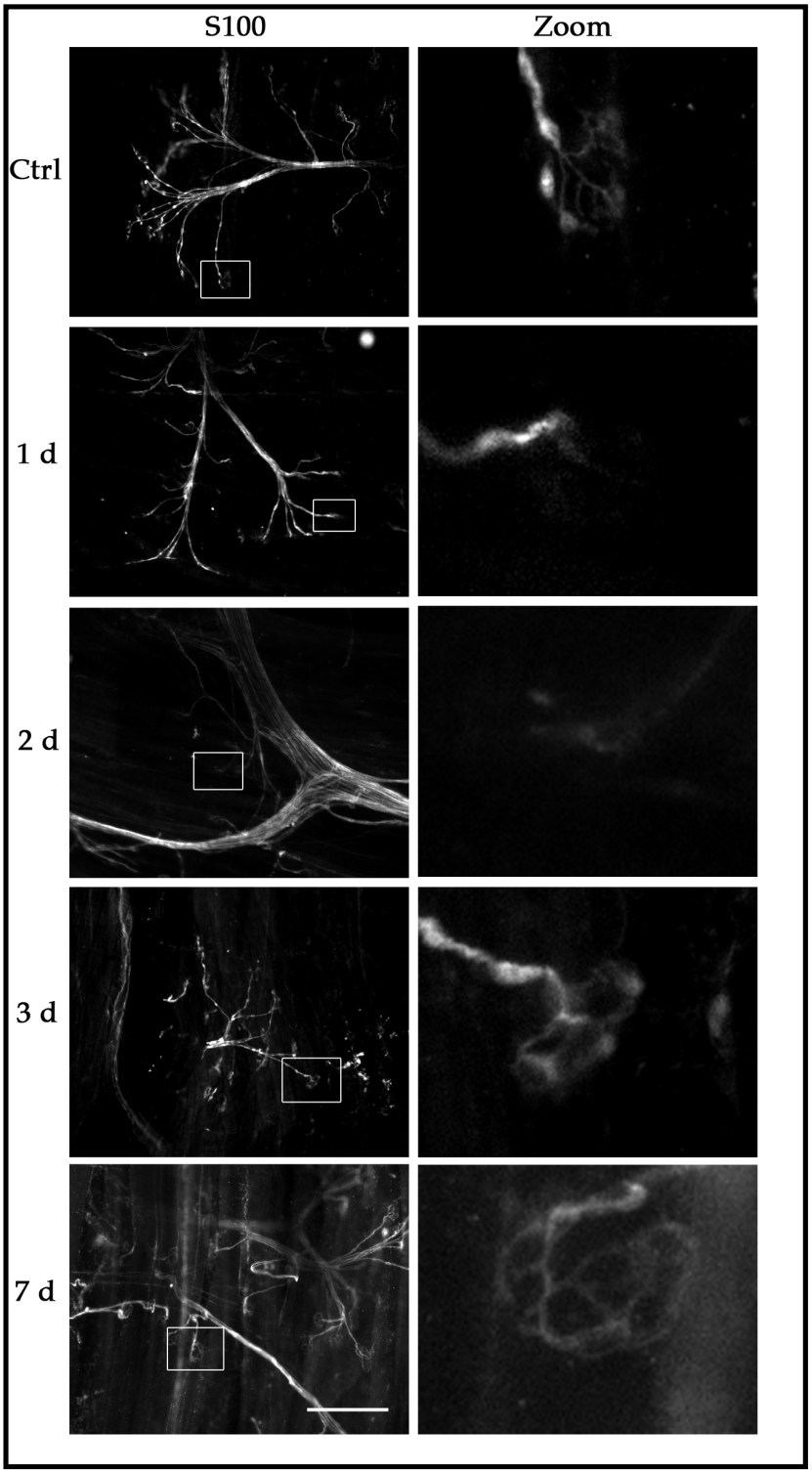

Figure 32 Perisynaptic Schwann Cells activation in α-LTX intoxicated EDL. Mice hind limbs were iinjected with α-LTX , EDL dissected at considered time points and processed for indirect immunohistochemistry. Kinetic of PSCs activation has been monitor by changes in S100 labelling. In α-LTX injected muscles we observed a loss in S100, indicating SCs activation; this phenotyper is specific of PSCs, as shown by magnification of highlighted areas (right column) since S100 staining in myelinating Schwann cells is not affected.. Scale Bar: 10 μM.

terminal process of degeneration/regeneration, one EDL portion was labeled with VAChT and αBTX.

Relevantly, PSCs activation data are strictly coincident with those obtained with the functional muscle assay and immunohistochemistry. Moreover, no decrease in S100 labeling intensity is observed at the level of myelinating Schwann cells. Also MBP labeling of myelinating SCs was not lost (Fig. 31). This indicates that, at the considered time point, activation of PSCs α-LTX-induced degeneration is restricted to the perisynaptic subtype.

Activated PSCs undergo also morphological changes upon nerve terminal damage. Indeed, activated PSCs protrude prolongations to favour reinnervation that act as a guide for the nerve terminals.

We therefore analyzed the same sample at higher magnification (60X) with a confocal microscope in order to check for these possible alterations. Despite the evidence of PSCs activation provided by the decrease of S100 labelling intensity, we failed to observe any prolongation coming from these cells at any considered time point, even when the reinnervation was complete (as assessed by immunohistochemical co-labeling of VAChT and α-BTX).

4.3.6 Perisynaptic Schwann cells response to surgical denervation by α-LTX in EDL muscle

To understand if the absence of prolongations by activated PSCs was dependent on our experimental setup or it underlined a non previously characterized PSCs behaviour, we performed the cut of the sciatic nerve, that represents a positive control of our system, since it is well documented that this procedure activates PSCs The cut was preferred to the crush because the first method usually reproduces a condition similar to that obtained with the injection of α-LTX, that is a syncronous degeneration of the nerve terminals.

As for NMJs intoxicated with α-LTX, 3 d after denervation the nerve terminals are degenerated nerve terminal labelling disappears but,

differently from what observed with α-LTX intoxicated NMJs, the myelin sheat labeled with MBP is lost, indicating an activation of the myelinating Schwann cell. No evident alterations in postsynaptic specialization morphology is observed (Fig. 33).

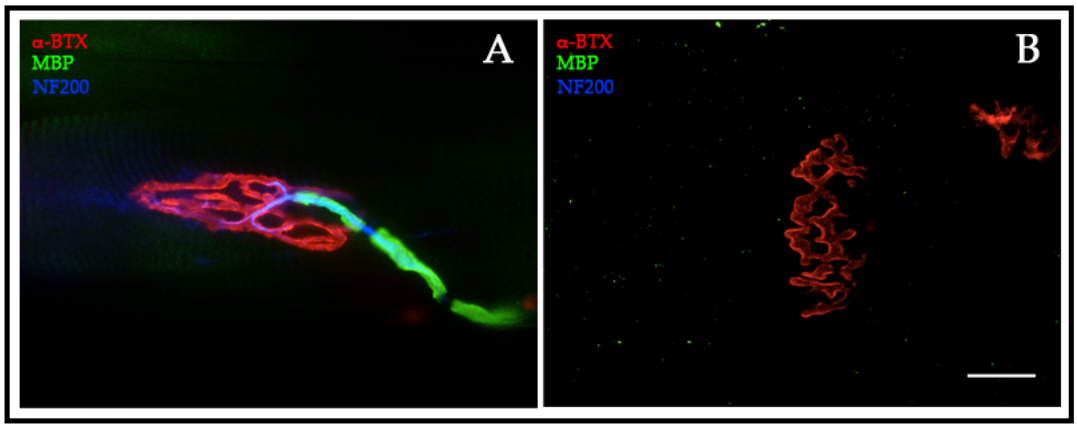

Figure 33 Effect of denervation on myelinating Schwann cells activation. Mice hind limbs were denervated and processed for indirect immunohistochemistry after 7 d. α-ltx cause degradation of neurofilaments (blue) and myelin basic protein (green) is completely degradated indicating myelinating Schwann cells activation. No morphological modifications of the postsynaptic element of the NMJ stained with α-BTX (red) were observed. Scale bars: 20 μm.

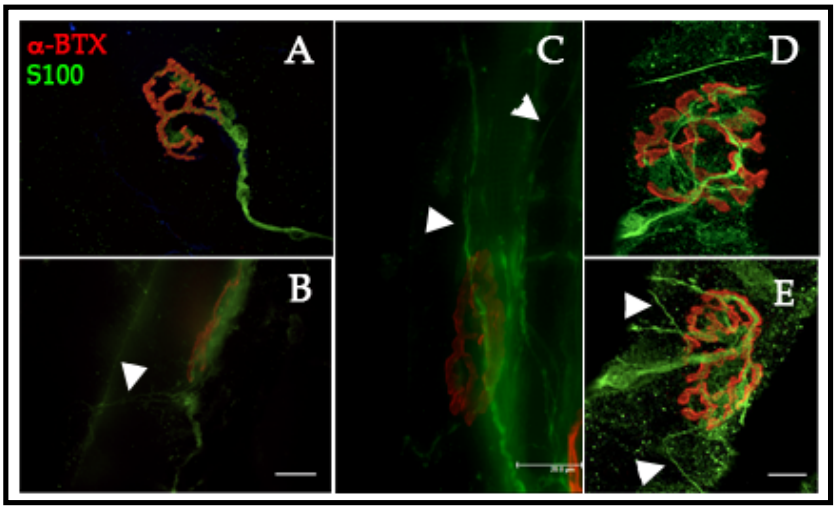

Figure 34 Perisynaptic Schwann cells prolongations protrusion at NMJs of denervated EDL. Mice hind limbs were denervated and processed for indirect immunohistochemistry after 7 d. A) In control samples no prolongations were observed while (B, C) long prolongations (white arrow head) coming from PSCs are evident 3 d post operation. D, E) Confocal images of activated PSCs at NMJs in denervated muscle samples. Scale Bar 10 μm

Considering that the cut of the sciatic nerve was performed at the level of the coxo-femural articulation and, in opposition to the nerve crush paradigm, no compensatory innervation from non damaged axon is possible, we expected a gradual decrease in PSCs and myelinating

Schwann cell S100 intensity labelling. The data obtained confirm our expectation since 3 day after denervation the intensity of S100 labeling of

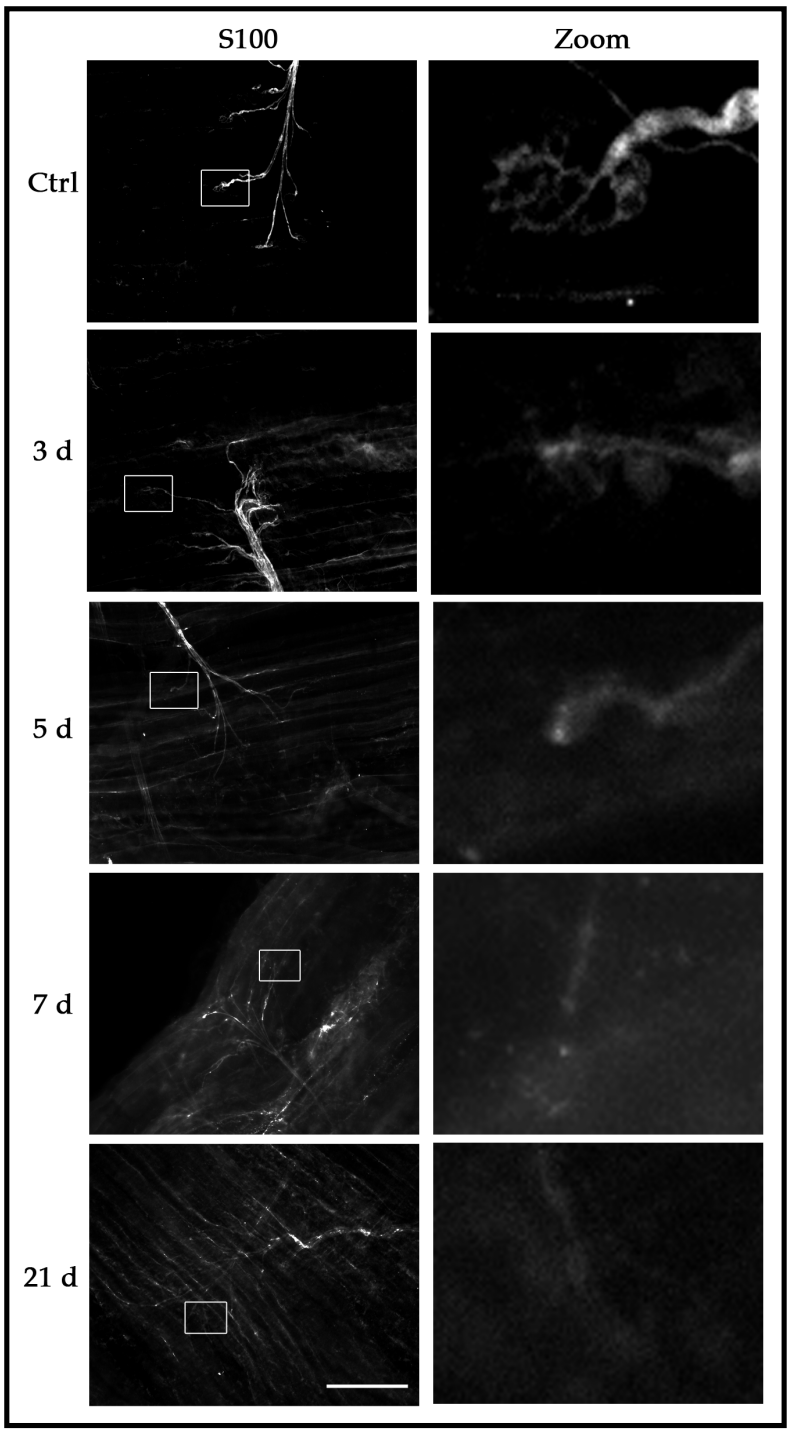

Figure 35 Perisynaptic Schwann Cells activation in denervated EDL. Mice hind limbs were denervated, EDL dissected at considered time points and processed for indirect immunohistochemistry. Kinetic of PSCs activation has been determined by S100 labelling. In opposition to α-LTX, S100 signal loss, indicating SCs activation, is observed both in PSCs, as shown by magnification of highlighted areas (right column), and myelinatin Schwann cells. (left column) at considered times. Scale Bar: 10 μM.

the PSCs decreases. The same is observed for myelinating Schwann cell but a decrease is evident only at longer time point (see the decrease progession from day 3 to 21), probably as Wallerian degeneration advances (Fig. 35).

At 10X magnification no morphological variation in PSCs was evident, therefore we analyzed our samples at higher magnification (60X). As expected, prolongations protruding from PSCs were evident (see Fig. 34). This observation rules out the possibility that the lack of protrusions in α-LTX intoxicated muscles may be due to problems of our experimental setup.

4.4 Discussion and Perspectives

The most common experimental model used to study the nerve terminal degeneration/regeneration process and the activation of PSCs is the mechanical damage through the cut or the crush of the sciatic nerve. One of the major problem of this model is the activation of the Wallerian degeneration, a process that leads to the release of several mediators and the recruitment of different cell types. Under this condition, dissecting the role of arachidonic acid and its derivates on PSCs activation would be very difficult. The model proposed here, that is the intoxication of the NMJs with presynaptic neurotoxins (α-LTX and β-BTX as a SPANs), provides a more controllable system since the damage is confined to the nerve terminal and only cells in close contact with it are affected by mediators released nearby.

As this model has been applied for the first time in this PhD project, we needed to carefully characterize it by determining the time window of nerve terminal degeneration/regeneration and the possible variability coming from the employment of muscles with different physiological properties.

To our knowledge no comparison in intoxication kinetic of our toxins between fast and slow muscle has ever been performed. From the point of view of the predator this comparison could provide interesting data since the venom (from which these toxins are extracted) is used to rapidly immobilize the prey. No differences in the considered kinetic have been highlighted between the intoxication of fast and slow muscle by our experiments.

On the other side, differences in intoxication kinetic have been observed between α-LTX and β-BTX independently from the muscle type. α-LTX provides a fast and syncronous degeneration of nerve terminals while it is asyncronous in β-BTX-injected muscle with a patch-like pattern. This difference could be explained taking into account the different mechanism of action of the two toxin classes. α-LTX is a pore-forming toxin that provokes a massive and rapid influx of Ca^{2+} exploiting its electrochemical gradient. Only few toxin tetramers inserted into the

membrane are needed to cause the degeneration of the nerve terminal. Differently from α-LTX, β-BTX and the other SPANs are enzymes that probably require a high concentration at the nerve terminal of their PLA2 activity products, fatty acids and lysophospholipids, to exert their neurotoxic effect.

In the light of the considerations described above, we decided to use EDL intoxication and α-LTX as a model. The activation of PSCs have been followed by labelling the cells with a well known SCs marker, S100. It is known that the intensity of S100 staining is dependent on the activation state of SCs: when SCs are activated (for example during dedifferentiation), S100 staining intensity decreases (Magill et al., 2007). The kinetic of nerve terminal degeneration/regeneration at the level of NMJs in α-LTX intoxicated EDL revealed a peculiar behaviour of PSCs. As evident from the decrease in S100 intensity, PSCs activate upon nerve terminal degeneration but, differently from what is described in literature following denervation, no protrusion of sprouting elements was observed. We therefore asked whether these differences could be ascribed to our experimental setup. Extensive protrusion of sprouting elements from PSCs was evident in denervated muscle.

A possible explanation for the absence of protrusion in PSCs activated following α-LTX intoxication could be that reinnervation (that is: regeneration) is faster than PSCs processes formation. If this was the case, PSCs could still be activated and partecipate in debris removal without extending any process. In nerve cut experiment protrusions are observed 3 d post operation; at this time point, the NMJs are already reinnervated in α-LTX treated muscle. The molecular cue guiding the reinnervation could be provided in our case by PSCs or from the third component of the tripartite system: the muscle fiber. NT-3, for example, is known to serve as a survival factor for SCs at developing NMJ [18].

To better assess this PSCs peculiar behaviour it would be necessary to extend the analysis to markers of PSCs other than that already used.

It would be interesting to work with transgenic animal in which a fluorescent protein is expressed under the S100B gene promoter or, even better, with transgenic mice in which fluorescent proteins are

constitutively expressed in PSCs and nerve. This model would easily overcome the limitation imposed by the comparison of complex immunohistological samples in which the read out of PSCs activation is the decrease of the signal of a marker. Another interesting model to work with could be the setting up of co-cultures of SCs and neurons since they represent an even more controllable system; however, this model has two major limitations: 1) at present, it is possible to induce immature SCs differentiation only towards the myelinating phenotipe and 2) the absence of the muscular component of the NMJs significantly limits the complex net of interaction between the components of the tripartite system.

The clinical relevance of the possible activation of PSCs by arachidonic acids and its derivatives is remarkable. Up to now, injuries that lead to nerve damage at the level of the peripheral nervous system, i.e. motorbike crush, are usually treated with massive doses of antinflammatory drugs possibly hindering the healing process.

4.5 RESULTS (Part III)

4.5.1 Primary Schwann cells culture Purity

The portion of sciatic nerve dissected to prepare the primary culture of SCs contains different cell types. Among them, SCs, fibroblast and macrophages can proliferate, leading to a mixed primary culture. To improve the purity of our preparation we performed a complement-mediated immunocytolysis step. The efficiency of this step was tested via an indirect immunocytochemistry, using S100 to label SCs and Hoechst to label all nuclei. The presence of "contaminating" cell types was determined by the non-colocalization of the two markers (Fig. 36), yielding an overall purity superior to 98%.

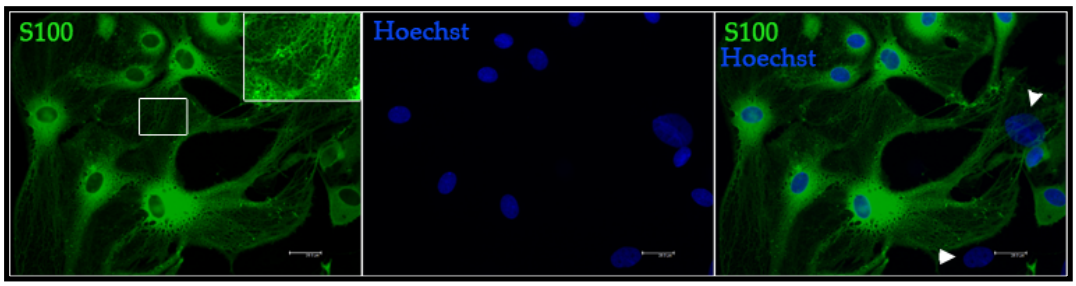

Figure 36 Immunohistochemical characterization of primary Schwann cells culture. 1 day after seeding SCs culture purity was determined by indirect immunofluoresce. SCs were labeled with an antibody against S100 (left) while nuclei were labelled with Hoechst (middle panel). Cell types other than SCs are indicated by the white arrow head). Scale bar: 20 µm.

SCs differentiation towards myelinating phenotype was suggested by the presence of cytoplasmic fenestration in S100 labeled-SCs (see magnification of the highlighted field in Fig. 36 left panel) as described by Stevens & Fields [154].

4.5.2 Morphological and cytoskeletal modification in MTDs and FMLP-treated Schwann cells

SCs are highly plastic cells not only for their ability to dedifferentiate but also because they are able to modify their morphology when activated (i.e. the protrusion of sprouting elements by PSCs). Therefore morphological variations in SCs phenotype could be a reliable marker of activation. We performed time-lapse experiments in SCs treated

with MTDs (150 μg/ml, that contain both mitochondrial DNA (mDNA) and formylated peptides), or FMLP (100 nM), an analogue of formylated peptides. Results are summarized in Fig. 37.

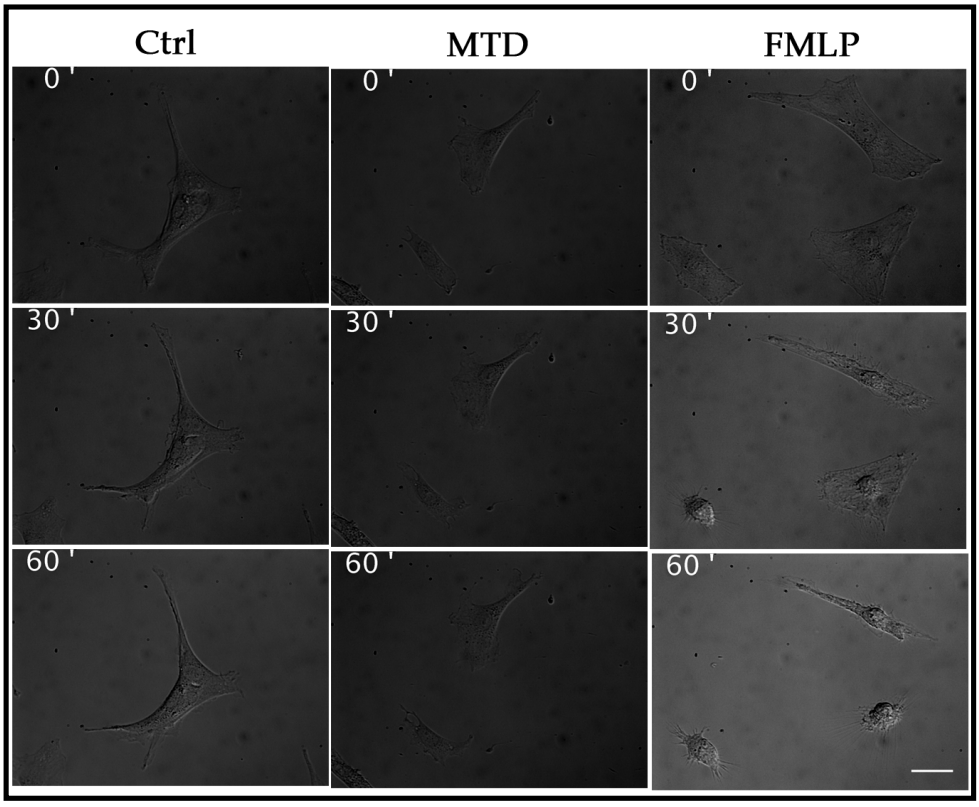

Figure 37 Morphological variation in MTDs and FMLP treated SCs. SCs were incubated at 37°C in KRH medium and images were acquired every 5′ for 1h. MTDs and FMLP were added at t=5′. No evident morphological variations were observed in control and MTDs treated SCs (left and middle column) while a rapid shrinkage was observed in FMLP-treated SCs (right column).

No morphological variation were observed in MTDs-treated SCs, while treatment with FMLP provoked a rapid shrinkage of the cells (arrowhead in Fig. 37). SCs viability was not affected by FMLP during 1 hour incubation as confirmed by the viability assay (data not shown).

Phalloidin labeling revealed a deep cytoskeleton reorganization in both MTDs and FMLP treated SCs as shown in Fig. 38 with disappearance of stress fibers. No changes in cytoskeleton of control samples were detected.

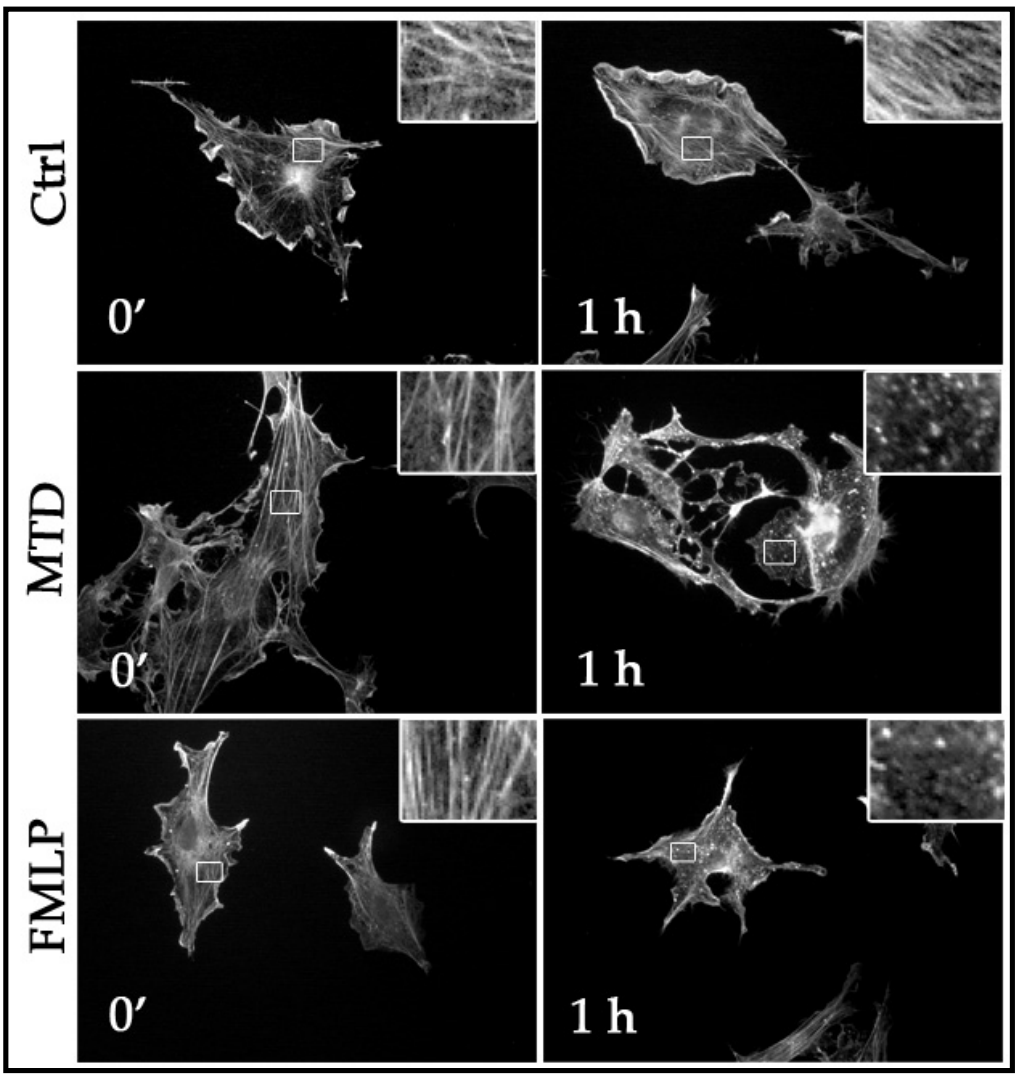

Figure 38 Effect of MTDs and FMLP treatement on SCs cytoskeletal organization. SCs were treated with MTDs and FMLP, fixed at considered time points and processed for indirect immunofluorescence. Actin cytoskeleton was stained with an Alexa-conjugated phalloidin. No changes in cytoskeletal organization was observed in control SCs (top row) with evident stress fibers (see magnification of highlighted fields). In MTDs and FMLP treated SCs (middle and bottom row), stress fibers disappeared.

4.5.3 Immunocytochemical localization of TLR9 and FPR1 in Schwann cells

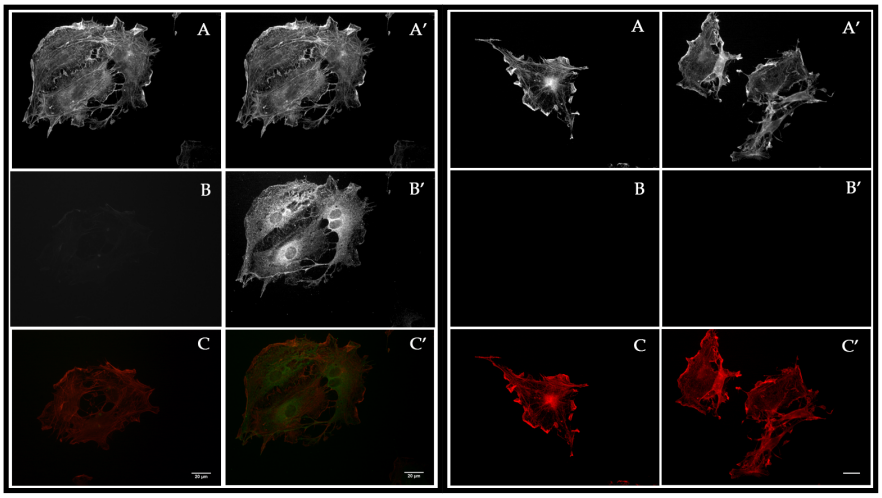

Figure 39 Immunocytochemical characterization of TLR9 and FPR1 presence in SCs. SCs were fixed and processed for indirect immunoflurescence. Left Panel: A,A′) SCs actinic cytoskeleton labelling with Alexa-conjugated phalloidin; B, negative control (no primary Ab) and B′) primary Ab treated sample; C, C′) Merge. TLR9 present a diffure and punctuated staining. Right Panel: A,A′) SCs actinic cytoskeleton labelling with Alexa-conjugated phalloidin; B, negative control (no primary Ab) and B′) primary Ab treated sample; C, C′) Merge. Scale bar: 20 μm.

To determine whether TRL9 and FPR1 were expressed in SCs we performed immunocytochemical labeling with commercially available antibodies and results are shown in Fig. 39. TLR9 staining results in specific and punctuate pattern, diffused to the entire SCs cytoplasm and its specificity was checked by a negative control (Fig. 39, Left Panel). No labelling was observed is SCs stained for anti-FPR1.

4.5.4 TLR9 colocalization with endosomes and endoplasmic reticulum marker

TLR9, differently from other TLRs as TLR 2,3,4, is not a plasma membrane receptor. In resting condition, it is localized at the level of the endoplasmic reticulum and, upon activation by mDNA or CpG (small nucleotidic sequence mimicking mDNA), it moves to endosomal compartments where TLR9 is proteolitically activated.

Taking into consideration this localization shift, we performed some colocalization experiments using Calreticulin as ER marker and

Early Endosomes Associated protein (EEA1) as a marker for the endosomal compartment. We were expecting an increase in colocalization of TLR9 with EEA1 and a decrease with Calreticulin in MTDs-treated SCs; on the contrary, no evident changes in distribution among these markers were observed in MTDs treated samples with respect to control (Fig. 40).

4.5.5 Western Blot analysis

In order to exclude that the negative results obtained by immunocytochemistry of SCs cells are due to the characteristic of the antibodies used, we compared TLR9 and FPR1 patterns in control and MTD-treated SCs by western blot with that of human blood monocyte which are cells known to possess both kind of receptors (Figure 41 C).

In SCs (Fig. 42 A) TLR9 antibody labeled a band of about 55 kDa both in controls, MTDs and FMLP treated samples with an expected molecular weight for unprocessed TLR9 of 130 kDa (black arrowhead in Figure 42 A and B) (dependent on its glycosilation state). In TLR9 antibody's datasheet, the same 55 kDa labeled band is reported in human, rat and murine intestin (red box in Fig. 42 C). No labeling at the expected molecular weight is observed even in control monocytes samples (Fig. 42 B).

No labeling at all was present in immunoblots against FPR1 (expected molecular weight 36 kDa), neither in control and in treated SCs nor in control monocytes samples (black arrowhead in Fig. 43).

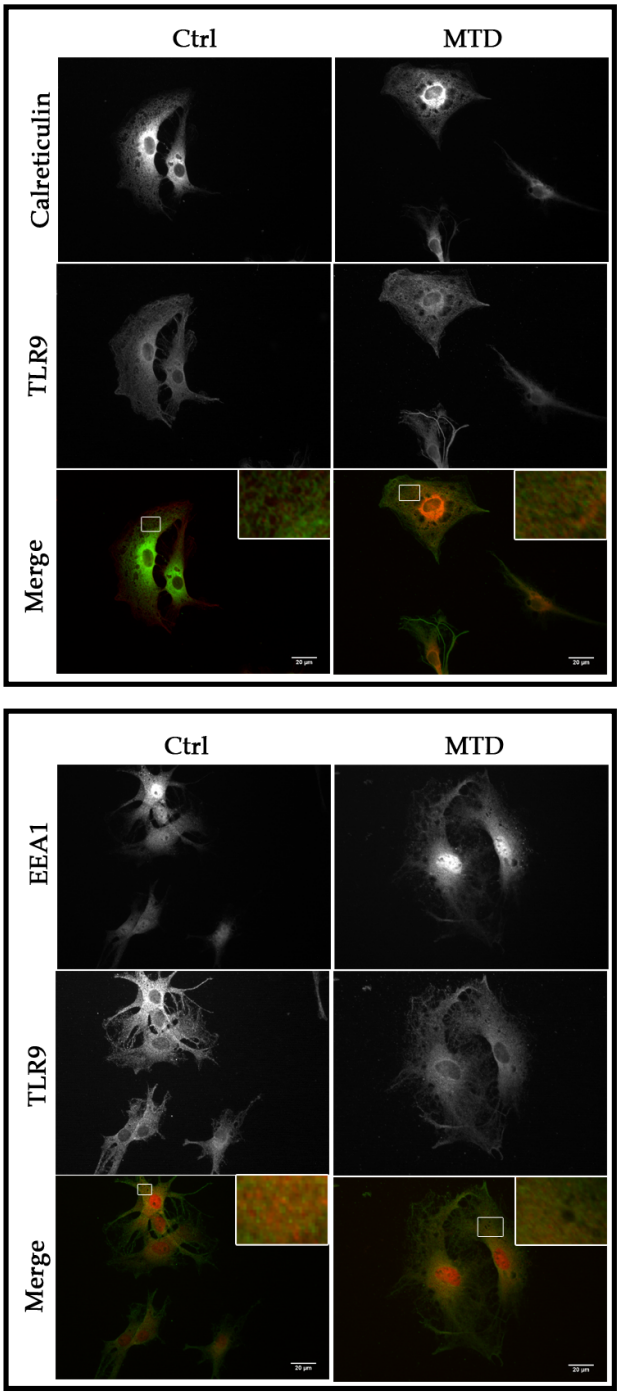

Figure 40 TLR9 colocalization with an endosomal compartment marker (EEA1) and an endoplasmic reticulum marker (calreticulin). SCs were treated with MTDs for 1h, fixed and processed for indirect immunofluorescence. Top Panel) The expected TLR9 localization changes, shown by a decrease in colocalization, was not observed (see magnification of merge highlighted areas). Also the increase in EEA1 and TLR9 colocalization was not observed upon MTDs treatment. (Bottom Panel). No differences were evident also at later cosidered time points (3-6 h). Scale bar: 20 μm.

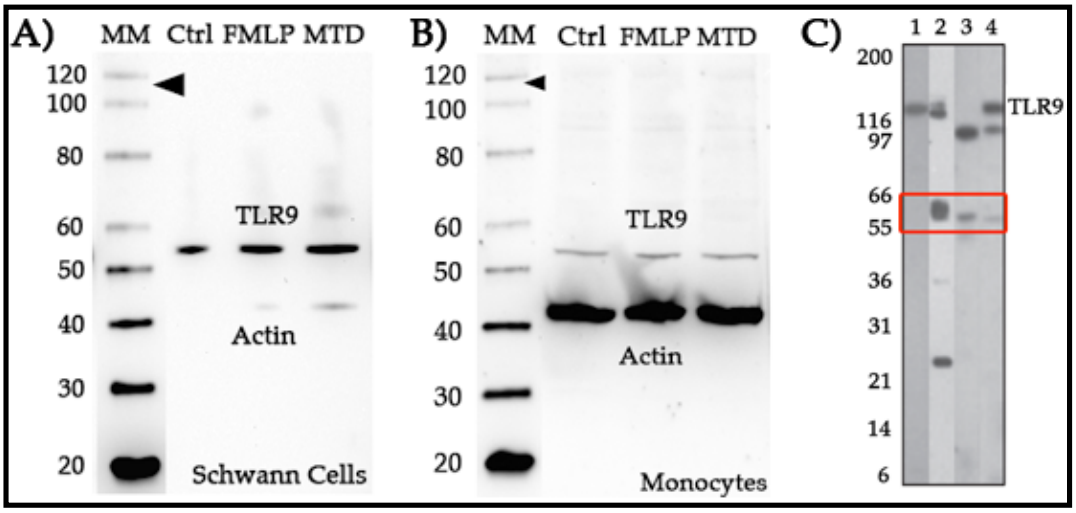

Figure 41 Biochemical analysis of TLR9 expression in MTDs and FMLP treated SCs and monocytes. A) Western blot of MTDs and FMLP treated SCs. TLR9 antibody labelled a band of about 55 kDa in both control and treated samples. No labelling was observed at the TLR9 expected molecular weight (see black arrowhead). B) Western blot of MTDs and FMLP treated monocytes. As for SCs, only a band at about 55 kDa was labelled in all considered conditions. No band at TLR9 expected molecular weight was observed (black arrowhead). C) Datasheet of TLR9 labelling patter in samples from different species'tissues. 1) Human Peripheral Blood Mononucleated Cells, 2) Human Intestine, 3) Murine Intestineand 4) Rat Intestine. Molecular weights (MM) are reported in kDa.

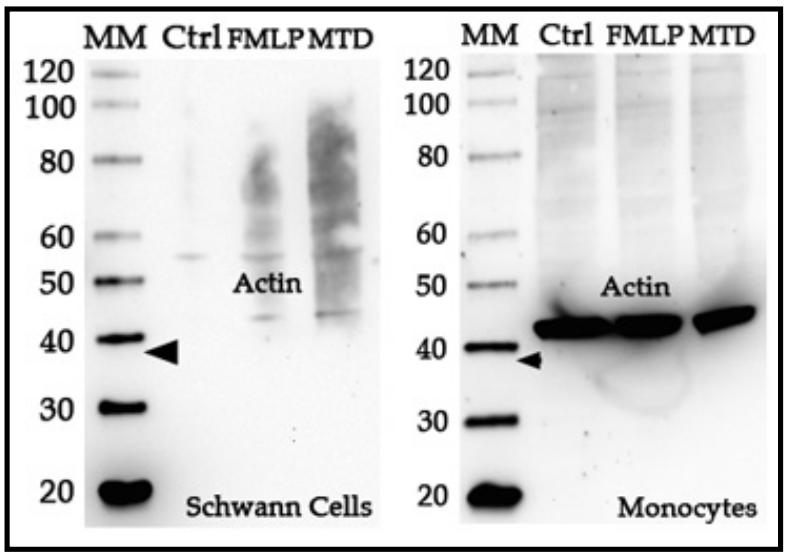

Figure 42 Biochemical analysis of FPR1 expression in MTDs and FMLP treated SCs and monocytes. A) Western blot of MTDs and FMLP treated SCs. No specific staining was observed in both control and treated samples at the expected FPR1 molecular weight (see black arrowhead). B) Western blot of MTDs and FMLP treated monocytes. As for SCs, no bands at FPR1 molecula weight (black arrowhead) were observed in all considered conditions. Molecular weights (MM) are reported in kDa.

4.5.6 Calcium response of SCs treated with FMLP and MTDs.

Due to the unclear results obtained with antibodies, we decided to demonstrate the existance of a FPR1 signalling pathway in SCs by a different approach, that is calcium imaging in cells.

FPR1 signalling leads to calcium release from ER by activating IP_3 receptor [155]. It is therefore possible to determine if FPR1 is expressed and functional in SCs by this powerful technique.

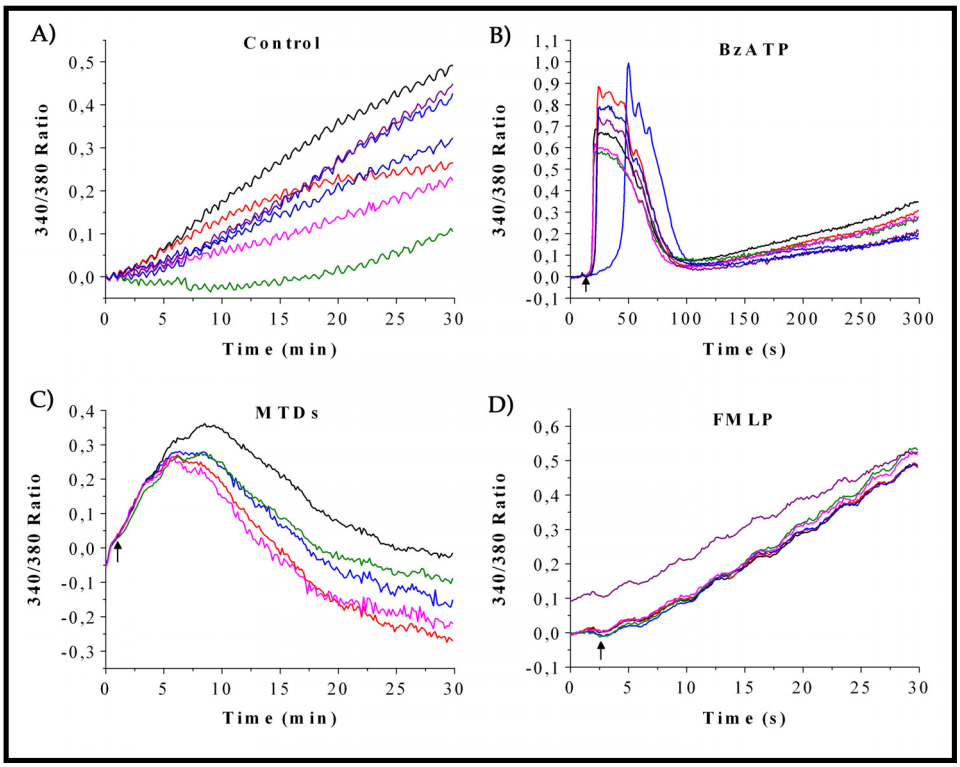

Figure 43 SCs calcium response to MTDs and FMLP. Fura2-AM- loaded SCs were incubated with control medium (A), BzATP (B), MTDs (C) and FMLP (D). In C) calcium response shows a wave-shaped patter while the response in D) is similar to control. Arrows indicated time points of stimulus application.

As a poritive control of our experimental setup we stimulated cultured Schwann cells with benzoil-ATP (BzATP), an ATP analog. The response to ATP is present but less evident, as reported in Verderio et al., 2006 [156] (Fig. 43 B). We then tested the effect to MTDs treatment on calcium response. Surprisingly, we obtained a wave-shaped response (Fig. 43 C), completely different from the spiked one observed by Zhang et al, 2010 [42] in polymorphonucleated neutrophils. Considering that the only MTDs

fraction able to activate FPR1 is the formylated proteins, we tried to stimulate SCs with FMLP, without any significant response (Fig. 43 D).

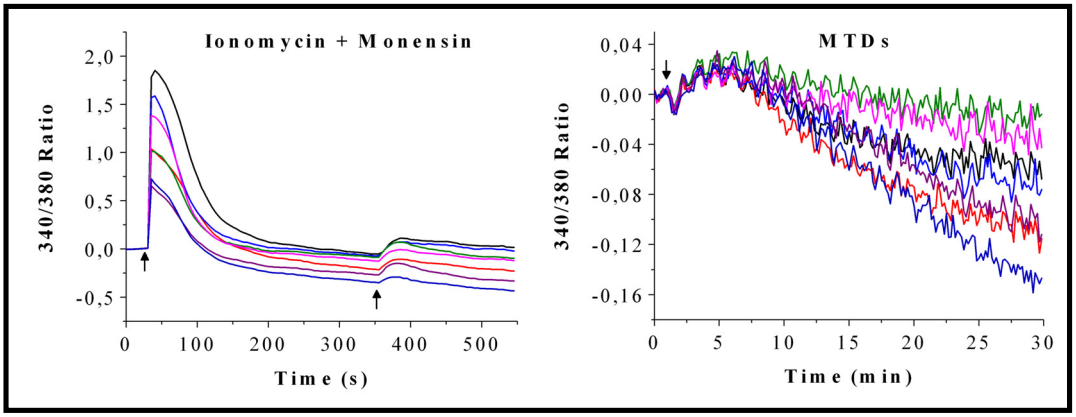

Figure 44 SCs calcium response to MTDs stimulation after calcium stores depletion. Experiments were performed on Fura2-AM-loaded SCs in Ca^{2+}-free KRH plus EGTA (150 μM). Left panel: ionomycin and monensin were applied to deplete calcium stores. The same sample was treated with MTD an calcium response recorded (right panel). Even under this condition a wave-shaped patter was observed (even with lower amplitude). Arrows indicates the time point of stimulus application.

To determine if the wave-shaped response observed upon MTDs treatment was Ca^{2+}-dependent, we depleted calcium stores with ionomycin and monensin in EGTA-medium before treatment (Fig. 44, left panel) and then we treated the samples with MTDs. A wave-shaped response was still observed even if lower in amplitude (Fig. 44, right panel). Thanks to the ratiometric properties of Fura2-AM calcium indicator, the analysis of the recorded traces at 340 and 380 nm allowed us to conclude that SCs response to MTDs is not calcium dependent since both signal decrease (Fig 45 B, B'), with signal at 380 nm decreasing more than that at 340 nm.

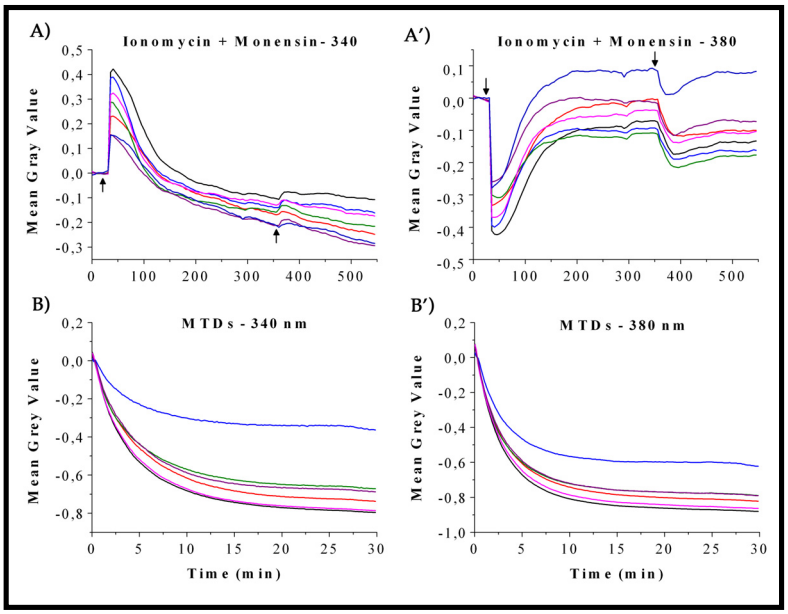

Figure 45 Analysis of 340 and 380 nm traces in MTDs-exposed SCs after ionomycin + monensin pre-treatmentand. Fura2-AM signal intensity increase at 340 nm (A) and decrease at 380 nm (A') following ionomycin and monensin treatment (black arrows) indicate a calcium response while in MTDs-treated SCs both wavelenghts decreased excluding any specific calcium variation.

4.5.7 Calcium response of PSCs to ATP and acetylcholine

SCs primary culture is not a suitable model to study the effect of MTDs on PSCs activation because the complex network between the three components of the NMJs is lost. A good trade-off between the optimal model (the *in vivo* situation) and the *in vitro* culture is represented by the *ex-vivo* soleus preparation which has been chosen for calcium imaging experiments with the calcium indicator Fluo4-AM.

Fig. 46 shows the PSCs response to ACh and ATP that are stimuli known to elicit a calcium response in this kind of cell. The results are comparable to those described in literature, with the intensity of response to ACh decreasing after successive stimulation (see Fig. 46 Left).

Pseudocolor representation of images acquired in the time frame highlighted by the black box in Fig. 46 are shown in Fig. 47 and 48. PSCs were localized with the superimposition of Fluo-4AM and that of the postsynaptic marker α-BTX and stimulated with a puff of ACh or ATP (300 ms and 0.5 atm). PSCs responded to both stimuli with a fast and prolonged increase in cytosolic calcium concentration (represented in pseudocolors by a progressive transition from blue to green to red), lasting up to 10 seconds (Fig. 47 and 48).

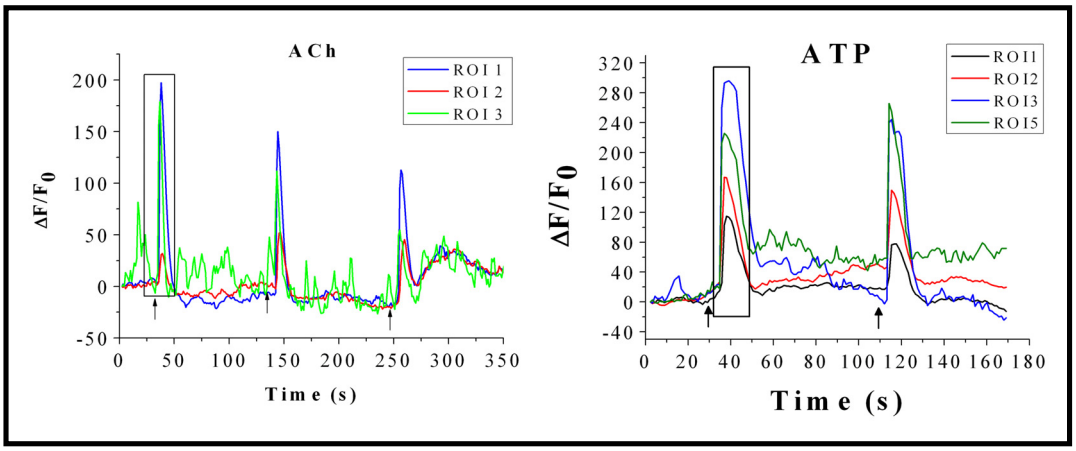

Figure 46 PSCs calcium response to ACh and ATP. After dissection, PSCs were loaded with Fluo4-AM and postsynaptic specialization labeled with Alexa-647 conjugated α-BTX. Once individuated by the superimposition of Fluo4 and BTX signals, PSCs were stimulated with ACh (20 μM) (left) and ATP (1 mM), either of which is a well known PSCs calcium response inducing stimulus. The obtained responses parallel those reported in literature confirming the responsiveness of our preparation. PSCs calcium response to ACh decreased upon repetitive stimulation and its magnitude was inferior to the one elicited by ATP stimulation. Arrows indicated the time points of stimulation. Images were acquired every 1.12″ in both experiments. Pseudocolor images of the time frames highlighted by the black boxes were shown in Fig. (ACh) and in Fig. (ATP). The traces colour paralles those of the empty circles in Fig 45 and 46.

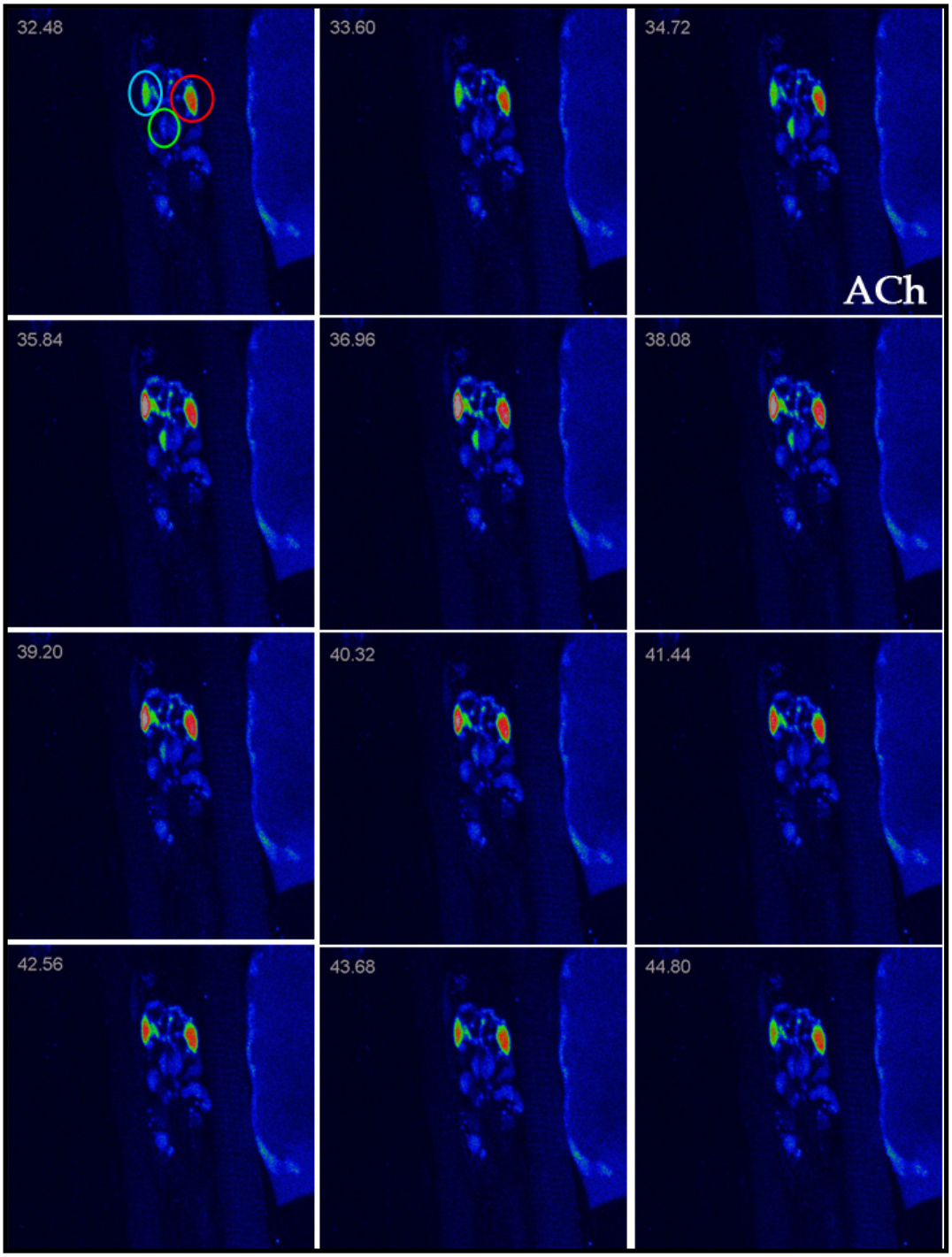

Figure 47 Pseudocolor representation of a representative calcium response of PSCs elicited by ACh. After Fluo-4 loading and Alexa-647 conjugated α-BTX labelling, dissected soleus muscles were pinned in a heated (30 °C) chamber and perfused with Rees buffer. PSCs were stimulated with an ACh (20 μM) puff (0.5 ATM, 300 ms).). The kinetic shows PSCs response in the time frame highlighted by the black box in Figure 44, left panel. PSCs response to ACh by a cytosolic calcium increase that lasted almost 10″ (see in the response of PSC encircled by the cyan and green empty circle).

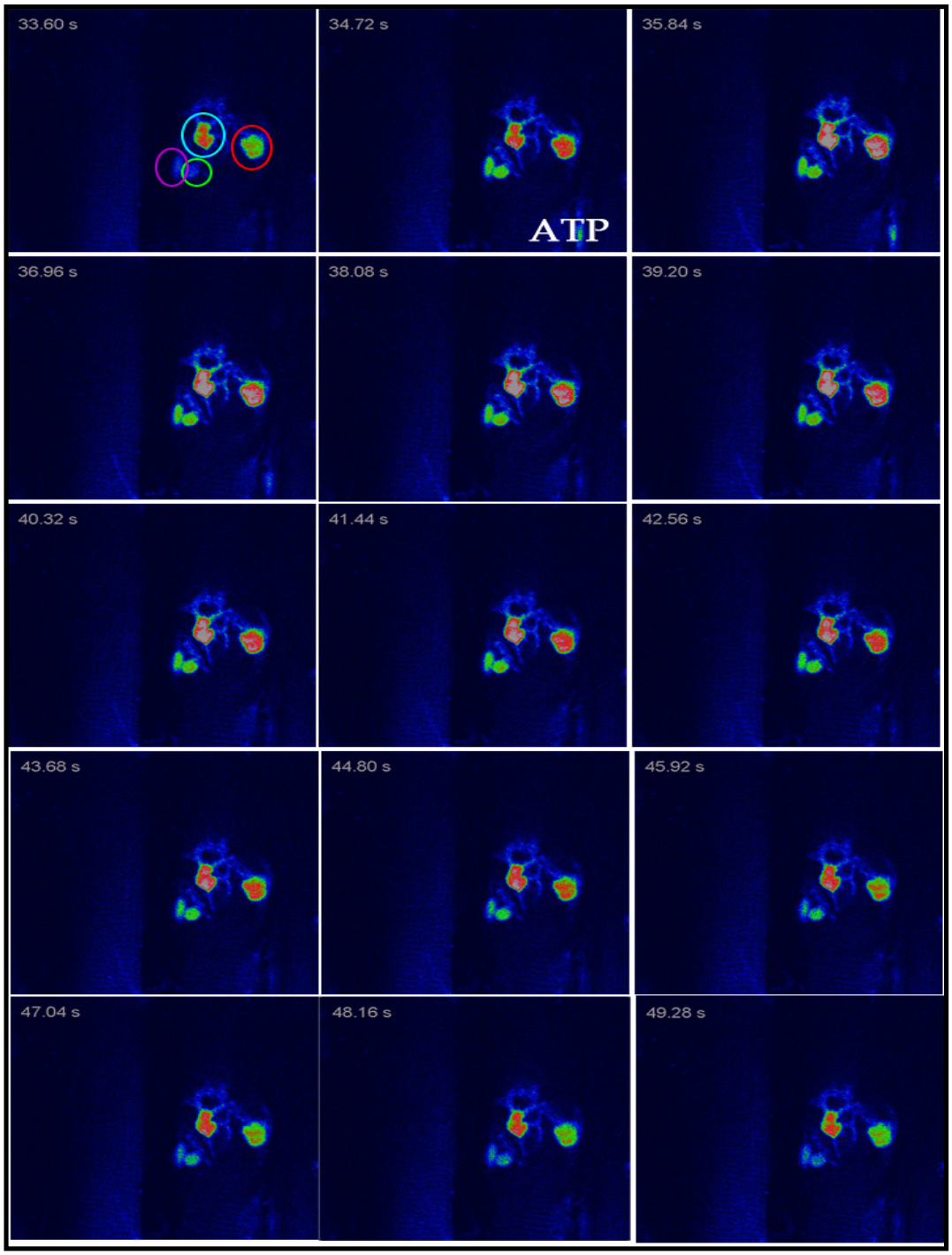

Figure 48 Pseudocolor representation od a PSCs calcium response elicited by ACh. After Fluo-4 loading and Alexa-647 conjugated α-BTX labeling, dissected soleus muscles were pinned in a heated (30 °C) chamber and perfused with Rees buffer. PSCs were stimulated with an ATP puff (1 mM) (0.5 atm, 300 ms). The kinetic shows PSCs response in the time frame highlighted by the black box in Fig. 44, right panel. PSCs responce to ATP rapidly by a cytosolic calcium increase that lasted almost 10" (see the response of PSC encircled by the cyan and green empty circle).

4.5.8 Calcium response of PSCs to α-LTX

Considering that our model of nerve terminal controlled degeneration is based on neurotoxins injection, we tried to poison soleus NMJs in *ex vivo* preparation with focal application of α-LTX to determine if PSCs response could be observed with calcium imaging. A representative trace of PSCs response to α-LTX nerve terminal poisoning is shown in Fig. 49.

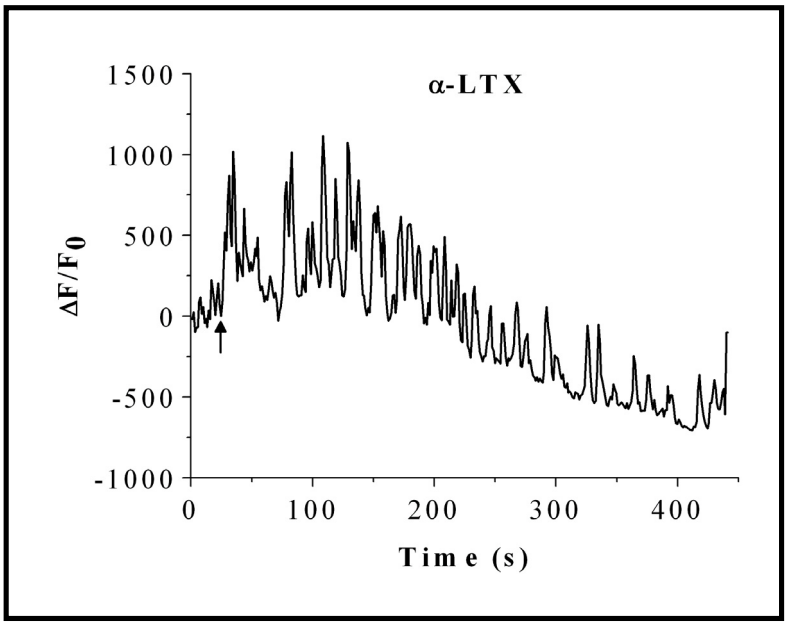

Figure 49 PSCs calcium response to α-LTX poisoning of NMJ. After dissection, PSCs were loaded with Fluo4-AM and postsynaptic specialization labeled with Alexa-647 conjugated α-BTX. Once individuated by the superimposition of Fluo4 and BTX signals, PSCs were stimulated with α-LTX (1 nM). Repetitive calcium spikes were observed. Arrows indicated the time points of stimulation.

Consequently to α-LTX application (black arrow), repetitive spikes were observed, as if PSCs cytosolic calcium concentration was oscillating. However, this data is very preliminar since no data on α-LTX action at the nerve terminal is available in this *ex vivo* preparation. More evidences will be provided by the kinetic coupled recording of PSCs and nerve terminal calcium response to α-LTX poisoning.

4.6 Discussion and Perspectives

SCs are well known to play a fundamental and active role during the process of nerve degeneration and regeneration. Briefly, upon damage they activate, acquiring a macrophagic-like activity [51], and, along recruited macrophages, remove the debries left by the degenerating nerve. Among the various structure and organelles interested by the degenerative process, mitochodria are of particular interest since they represent a sort of "enemy within". Mitochondria gain this threatening definition because of their origin; in fact they are, from the point of view of evolution, endocytosed bacteria and, following damage, they could start the immune response by releasing immunoactive molecules (i.e lipolysaccharide (LPS)) and macromolecules (i.e. formylated proteins and mDNA). Recently Zhang et al, 2010 [42] demonstrated that the aseptic SIRS (Systemic Inflammatory Response Shock), developed in heavily traumatized patience without guts injury, is due to release of mitochondria macromolecules from damaged cells. In particular, they focused their attention on mitochondrial DNA and formylated proteins. In fact, both macromolecule types could activate different cell types, among which macrophages, by interacting with their receptor: TLR-9 for mDNA and FPR1 for formylated peptide.

Interestingly, Schwann cell, as for macrophages, are known to possess a certain degrees of immunocompetence [74]. They can present antigens to the leukocytes, terminate and regulate the immune response and, very importantly, they can recognize the antigen via some already identified Toll like receptor like the 2,3,4. Considering the SCs antigen recognition ability and the release of mitochondria content during nerve degeneration we started wondering if released MTDs could participate in the activation of SCs.

We tried to address this question via different approaches. From a morphological point of view, MTDs seems not to activate cultured SCs while FMLP, a formylated peptide mimicking the effect of formylated proteins, provokes a fast shrinking of cells, not dependent on toxic effect of FMLP. On the other side, phalloidin staining reveals that treatment with either MTDs or FMLP leads to cytoskeletric reorganization. Interestingly,

the same phenotype has been already described for SCs stimulated with another PAMPs, the lipopolysaccharide LPS [157].

The immunocytochemistry approach gave interesting result about TLR9 with a diffuse, punctate staining of SCs. TLR9 change its subcellular localization upon mDNA binding, switching from endoplasmic reticulum to endosomes [158], so we could underline its activation by performing some colocalization experiments with an endosomal marked (EEA1) and a ER marker (calreticulin). Considering the complex staining patterns provided by the selected marker, we planned to perform a subcellular fractionation to obtain a more defined result.

Unfortunately, comparative western blot analysis between SCs and monocytes, known to possess TLR9 [159], highlighted some limitation of the antibody used to stain the mDNA receptor. We expected to observe a molecular weight shift of TLR9 band upon treatment with MTDs. In fact, once in the endosomal compartment, TLR9 is processed by proteolysis and became active. Independently of cell type and condition (control or treated), anti-TLR9 antibody always stained one band at 55kDa with no sign of the full length form. A labeled band of 55 kDa is also reported in the producer datasheet. The same comparison was performed for FPR1, yielding comparable result. Also in this case no bands at 36 kDa, the molecular weight of FPR1, was observed, even in monocytes [160]. In this case, the biochemical analysis paralleled the immunocytochemical ones since no staining was observed in SCs.

On the other side calcium imaging experiments seems to rule out FPR1 receptor presence in SCs and, in this regards, it is worth of mention that rat macrophages, the cells with which SCs seems to share many feature, seems to lack FPR1 [161] so that they are not able to respond to formylated protein.

However, SCs are not macrophages so, given the results obtained until now, it is not possible to confirm the presence or the abscence of TLR9 and FPR1 in SCs. We will try to address the problem by performing RT-PCR experiments and checking the effect of MTDs treatment on TLR9 signalling pathway, focusing our attention on p38 and IkB phosphotilation and the latter level of degradation. Moreover TLR9 presence and

activation in SCs will be probed with fluorescent CpG, small nucleotidic sequence that mimics mDNA.

The possible activation of SCs by MTDs is also important from the point of view of PSCs at NMJs, in particular in the light of our experimental model. In fact, both SPANs and α-LTX promote a necrotic-like degeneration of the nerve terminal leading to release of mitochondria content after their degradation. However PSCs cannot be studied in an *in vitro* model because until now only differentiation towards the myelinating phenotype has been achieved. On the other hands, the poor reliability of tested markers limits the *in vivo* experimentation. A possible response to this problems comes from *ex vivo* preparation. In fact, this system is more controllable than the *in vivo* one and it keeps unaltered the organization of the NMJs, overcoming the limitations imposed by *in vitro* cultures. *Ex vivo* preparation of soleus NMJs has been extensively used to study calcium response of PSCs to nerve activity and to determine the nature of mediators activating this response. In particular, taking into consideration the signalling pathway of FPR1 described above, calcium imaging seems a reasonable method to study the possible activation of PSCs by formylated proteins. Therefore we adapted a protocol from Robitaille et al., 2010 [34], to perform calcium imaging experiments on PSCs. Up to now we have only tested the system with stimuli known to elicit a calcium response in PSCs, ACh and ATP, obtaining response compatible to those observed in literature (citazione). We also observed PSCs calcium oscillation in response to α-LTX (data not shown), but this data has to be considered carefully because no informations on α-LTX action kinetic are available for this model. We are planning to solve this problem by loading nerve terminals with dextrane conjugated Calcium-Green 1, a calcium-sensitive dye already used for this kind of application [33,60].

The study of the possible PSCs activation by mDNA via TLR9 in more difficult because no variation in cytosolic calcium concentration is elicited. A possible approach is to observe the localization shift of the proinflammatory factor NF-kB from the cytoplasm to the nucleus. However, to observe this transition either *in vivo* and in *ex vivo* preparation transgenic mice with fluorescent NF-kB are needed.

5 References

[1] Jessen, K. R. & Mirsky, R. Origin and early development of Schwann cells. *Microscopy Research and Technique* **41**, 393-402 (1998).

[2] Jessen, K. R. *et al.* The Schwann cell precursor and its fate: A study of cell death and differentiation during gliogenesis in rat embryonic nerves. *Neuron* **12**, 509-527 (1994).

[3] Jessen, K. R. & Mirsky, R. The origin and development of glial cells in peripheral nerves. *Nature Reviews Neuroscience* **6**, 671-682 (2005).

[4] Herrera, A. A., Qiang, H. & Ko, C.-P. The role of perisynaptic Schwann cells in development of neuromuscular junctions in the frog (Xenopus laevis). *Journal of Neurobiology* **45**, 18 (2000).

[5] Kelly, A. M. & Zacks, S. I. in *The Journal of Cell Biology* Vol. 42 154-169 (1969).

[6] Linden, D. C., Jeriana, S. M. & Letinsky, M. S. Neuromuscular junction development in the cutaneous pectoris muscle of *Rana catesbeiana*. *Experimental Neurology* **99**, 26 (1988).

[7] Hirata, K., Zhou, C., Nakamura, K. & Kawabuchi, M. Postnatal development of Schwann cells at neuromuscular junctions, with special reference to synapse elimination. *Journal of Neurocytology* **26**, 11 (1997).

[8] Love, F. M. & Thompson, W. J. Schwann cells proliferate at rat neuromuscular junctions during development and regeneration. *The Journal of Neuroscience* **18** 9376-9385 (1998).

[9] Lin, W. *et al.* Aberrant development of motor axons and neuromuscular synapses in erbB2-deficient mice. *PNAS* **97**, 1299-1303 (2000).

[10] Morris, J. K. *et al.* Rescue of the cardiac defect in ErbB2 mutant mice reveals essential roles of ErbB2 in peripheral nervous system evelopment. *Neuron* **32**, 273-283 (1999).

[11] Riethmacher, D. *et al.* Severe neuropathies in mice with targeted mutations in the ErbB3 receptor. *Nature* **389**, 725-730 (1997).

[12] Woldeyesus, M. T. *et al.* Peripheral nervous system defects in erbB2 mutants following genetic rescue of heart development. *Genes & Development* **13**, 2538-2548 (1999).

[13] Wolpowitz, D. *et al.* Cysteine-rich domain isoforms of the neuregulin-1 gene are required for maintenance of peripheral synapses. *Neuron* **25**, 79-91 (2000).

[14] Hayworth, C. R. *et al.* Induction of neuregulin signaling in mouse Schwann cells in vivo mimics responses to denervation. *The Journal of Neuroscience* **26**, 6873-6884 (2006).

[15] Trachtenberg, J. T. & Thompson, W. J. Schwann cell apoptosis at developing neuromuscular junctions is regulated by glial growth factor. *Nature* **379**, 174-177 (1996).

[16] Reddy, L. V., Koirala, S., Sugiura, Y., Herrera, A. A. & Ko, C.-P. Glial cells maintain synaptic structure and function and promote development of the neuromuscular junction in vivo. *Neuron* **40**, 563-580 (2003).

[17] Trachtenberg, J. T. & Thompson, W. J. Nerve terminal withdrawal from rat neuromuscular junctions induced by neuregulin and Schwann cells. *The Journal of Neuroscience* **17 (16)**, 6243-6255 (1997).

[18] Hess, D. M. *et al.* Localization of TrkC to Schwann cells and effects of neurotrophin-3 signaling at neuromuscular synapses. *The Journal of Comparative Neurology* **501**, 465-482 (2007).

[19] Halstead, S. K. *et al.* Anti-disialosyl antibodies mediate selective neuronal or Schwann cell injury at mouse neuromuscular junctions. *Glia* **52**, 177-189 (2005).

[20] Astrow, S. H., Qiang, H. & Ko, C.-P. Perisynaptic Schwann cells at neuromuscular junctions revealed by a novel monoclonal antibody. *Journal of Neurocytology* **27**, 667-681 (1998).

[21] Frostick, S. P., Yin, Q. & Kemp, G. J. Schwann cells, neurotrophic factors, and peripheral nerve regeneration. *Microsurgery* **18**, 397-345 (1998).

[22] Fu, S. Y. & Gordon, T. The cellular and molecular basis of peripheral nerve regeneration. *Molecular Neurobiology* **14**, 67-116 (1997).

[23] Scherer, S. S. & Salzer, J. L. *Axon-Schwann cell interaction during peripheral nerve degeneration and regeneration*. 165-196 (Bios Scientific Publisher Ltd., 1996).

[24] Chiu, S. Y. Functions and distribution of voltage-gated sodium and potassium channels in mammalian schwann cells. *Glia* **4**, 541-558 (1991).

[25] Sontheimer, H. Voltage-dependent ion channels in glial cells. *Glia* **11**, 156-172 (1994).

[26] Verkhratsky, A. & Steinhäuser, C. Ion channels in glial cells. *Brain Research Reviews* **32**, 380-412 (2000).

[27] Jahromi, B. S., Robitaille, R. & Charlton, M. P. Transmitter release increases intracellular calcium in perisynaptic schwann cells in situ. *Neuron* **8**, 1069-1077 (1992).

[28] Reist, N. E. & Smith, S. J. Neurally evoked calcium transients in terminal Schwann cells at the neuromuscular junction. *Proceedings of the National Academy of Sciences of the United States of America* **89**, 7625-7629 (1992).

[29] Rochon, D., Rousse, I. & Robitaille, R. Synapse–glia interactions at the mammalian neuromuscular junction. *The Journal of Neuroscience* **21**, 3819-3829 (2001).

[30] Bourque, M.-J. & Robitaille, R. Endogenous peptidergic modulation of perisynaptic Schwann cells at the frog neuromuscular junction. *The Journal of Physiology* **512**, 197-209 (1998).

[31] Robitaille, R. Modulation of synaptic efficacy and synaptic depression by glial cells at the frog neuromuscular junction. *Neuron* **21**, 847-855 (1998).

[32] Robitaille, R., Jahromi, B. S. & Charlton, M. P. Muscarinic Ca^{2+} responses resistant to muscarinic antagonists at perisynaptic Schwann cells of the frog neuromuscular junction. *The Journal of Physiology* **504**, 6716-6726 (1997).

[33] Castonguay, A. & Robitaille, R. Differential regulation of transmitter release by presynaptic and glial Ca^{2+} internal stores at the neuromuscular synapse. *The Journal of Neuroscience* **21**, 1911-1922 (2001).

[34] Todd, K. J., Darabid, H. & Robitaille, R. Perisynaptic glia discriminate patterns of motor nerve activity and influence plasticity at the neuromuscular junction. *The Journal of Neuroscience* **30**, 11870-11882 (2010).

[35] Waller, A. Experiments on the section of the glossopharyngeal and hypoglossal nerves of the frog, and observations of the alterations produced thereby in the structure of their primitive fibres. *Philosophical Transactions Royal Society London* **140**, 423-429 (1850).

[36] Blanchette, A. R., Ballinger, M. L., Fishman, H. M. & Bittner, G. D. Calcium entry initiates processes that restore a barrier to dye entry in severed earthworm giant axons. *Neuroscience Letters* **272**, 147-150 (1999).

[37] Eddleman, C. S., Ballinger, M. L., Smyers, M. E., Fishman, H. M. & Bittner, G. D. Endocytotic formation of vesicles and other membranous structures induced by Ca^{2+} and axolemmal injury. *The Journal of Neuroscience* **18**, 4029-4041 (1998).

[38] Fishman, H. M. & Bittner, G. D. Vesicle-mediated restoration of a plasmalemmal barrier in severed axons. *News in Physiological Science* **18**, 115-118 (2003).

[39] McNeil, P. L. & Kirchhausen, T. An emergency response team for membrane repair. *Nature Reviews* **6**, 499-505 (2005).

[40] Kerschensteiner, M., Schwab, M. E., Lichtman, J. W. & Misgeld, T. *In vivo* imaging of axonal degeneration and regeneration in the injured spinal cord. *Nature Medicine* **11**, 572-577 (2005).

[41] Vargas, M. E. & Barres, B. A. Why is wallerian degeneration in the CNS so slow? *Annual Review of Neuroscience* **30**, 153-179 (2007).

[42] Zhang, Q. *et al.* Circulating mitochondrial DAMPs cause inflammatory responses to injury. *Nature* **464**, 104-107 (2010).

[43] Harboe, M., Aseffa, A. & Leekassa, R. Challenges presented by nerve damage in leprosy. *Leprosy Reviews* **76**, 5-13 (2005).

[44] Kieseier, B. C. *et al.* Advances in understanding and treatment of immune-mediated disorders of the peripheral nervous system. *Muscle & Nerve* **30**, 131-156 (2004).

[45] Köller, H., Kieseier, B. C., Jander, S. & Hartung, H.-P. Chronic inflammatory demyelinating polyneuropathy. *The New England Journal of Medicine* **352**, 1343-1356 (2005).

[46] Lee, H. *et al.* Necrotic neuronal cells induce inflammatory Schwann cell activation via TLR2 and TLR3: Implication in Wallerian degeneration. *Biochemical and Biophysical Research Communications* **350**, 742-747 (2006).

[47] Oliveira, R. B. *et al.* Expression of Toll-Like Receptor 2 on human Schwann cells: a mechanism of nerve damage in leprosy. *Infection and Immunity* **71**, 1427-1433 (2003).

[48] Zimmerman, U. P. & Schlaepfer, W. W. Multiple forms of Ca-activated protease from rat brain and muscle. *The Journal of Biological Chemistry* **259**, 3210-3218 (1984).

[49] Guertin, A. D., Zhang, D. P., Mak, K. S., Alberta, J. A. & Kim, H. A. Microanatomy of axon/glial signaling during wallerian degeneration. *The Journal of Neuroscience* **25**, 3478-3487 (2005).

[50] Murinson, B. B., Archer, D. R., Li, Y. & Griffin, J. W. Degeneration of myelinated efferent fibers prompts mitosis in Remak Schwann cells of uninjured C-fiber afferents. *The Journal of Neuroscience* **25**, 1179-1178 (2005).

[51] Duchen, L. W., Gomez, S. & Queiroz, L. S. The neuromuscular junction of the mouse after black widow spider venom. *The Journal of Physiology* **316**, 279-291 (1981).

[52] Dennis, M. J. & Miledi, R. Electrically induced release of acetylcholine from denervated Schwann cells. *The Journal of Physiology* **237**, 431-462 (1974).

[53] Lundy-Ekman, L. *Neuroscience: Fundamentals for Rehabilitation*. 3rd edn, (2007).

[54] He, Z. & Koprivica, V. The Nogo signaling pathway for regeneration block. *Neuroscience* **27**, 341-468 (2004).

[55] Turner, J. E. & Glaze, K. A. The early stages of Wallerian degeneration in the severed optic nerve of the newt (*Triturus viridescens*). *Anatomical Record* **187**, 291-310 (1976).

[56] Heumann, R., Korsching, S., Bandtlow, C. & Thoenen, H. Changes of nerve growth factor synthesis in nonneuronal cells in response to

sciatic nerve transection. *The Journal of Cell Biology* **104**, 1623-1631 (1987).

[57] Lindholm, D., Heumann, R., Hengerer, B. & Thoenen, H. Interleukin 1 increases stability and transcription of mRNA encoding nerve growth factor in cultured rat fibroblasts. *The Journal of Biological Chemistry* **263**, 16348-16351 (1988).

[58] Thomas, P. K. & King, R. H. M. The degeneration of unmyelinated axons following nerve section: An ultrastructural study. *Journal of Neurocytology* **3**, 497-512 (1974).

[59] Araki, T. & Milbrandt, J. Ninjurin, a novel adhesion molecule, is induced by nerve injury and promotes axonal growth. *Neuron* **17**, 353-361 (1996).

[60] Georgiou, J., Robitaille, R. & Charlton, M. P. Muscarinic control of cytoskeleton in perisynaptic glia. *The Journal of Neuroscience* **19**, 11 (1999).

[61] Son, Y.-J. & Thompson, W. J. Nerve sprouting in muscle is induced and guided by processes extended by schwann cells. *Neuron* **14**, 133-141 (1995).

[62] Lubischer, J. L. & Thompson, W. J. Neonatal partial denervation results in nodal but not terminal sprouting and a decrease in efficacy of remaining neuromuscular junctions in rat soleus muscle. *The Journal of Neuroscience* **19**, 8931-8944 (1999).

[63] Kawabuchi, M. *et al.* The spatiotemporal relationship among schwann cells, axons and postsynaptic acetylcholine receptor regions during muscle reinnervation in aged rats. *The Anatomic Record* **264**, 183-202 (2001).

[64] Personius, K. E. & Sawyer, R. P. Terminal Schwann cell structure is altered in diaphragm of *mdx* mice. *Muscle & Nerve* **32**, 656-663 (2005).

[65] Jessen, K. R., Thorpe, R. & Mirsky, R. Molecular identity, distribution and heterogeneity of glial fibrillary acidic protein: an immunoblotting and immunohistochemical study of Schwann cells, satellite cells, enteric glia and astrocytes.
The Journal of Neurocytology **13**, 14 (1984).

[66] Georgiou, J. & Charlton, M. P. Non-myelin-forming perisynaptic Schwann cells express protein zero and myelin-associated glycoprotein. *Glia* **27**, 9 (1999).

[67] Hassan, S. M., Jennekens, F. G. I., Veldman, H. & Oestreicher, B. A. GAP-43 and $p75^{NGFR}$ immunoreactivity in presynaptic cells following neuromuscular blockade by botulinum toxin in rat. *Journal of Neurocytology* **23**, 10 (1994).

[68] Kang, H. *et al.* Regulation of the intermediate filament protein nestin at rodent neuromuscular junctions by innervation and activity. *The Journal of Neuroscience* **27**, 10 (2007).

[69] Woolf, C. *et al.* Denervation of the motor endplate results in the rapid expression by terminal Schwann cells of the growth-associated protein GAP-43. *Journal of Neuroscience* **12**, 12 (1992).

[70] Zuo, Y. *et al.* Fluorescent proteins expressed in mouse transgenic lines mark subsets of glia, neurons, macrophages, and dendritic cells for vital examination. *The Journal of Neuroscience* **24**, 11 (2004).

[71] Oda, R. *et al.* A novel marker for terminal Schwann cells, homocysteine-responsive ER-resident protein, as isolated by a

single cell PCR-differential display. *Biochemical and Biophysical Research Communication* **308**, 872-877 (2003).

[72] Young, P. *et al.* LNX1 is a perisynaptic Schwann cell specific E3 ubiquitin ligase that interacts with ErbB2. *Molecular and Cellular Neuroscience* **30**, 238-248 (2005).

[73] Ko, C.-P. A lectin, peanut agglutinin, as a probe for the extracellular matrix in living neuromuscular junctions. *Journal of Neurocytology* **16**, 10 (1987).

[74] Hörste, G. M. Z., Hu, W., Hartung, H.-P., Lehmann, H. C. & Kieseier, B. C. The immunocompetence of Schwann cells. *Muscle Nerve* **37**, 3-13 (2008).

[75] Janeway, C. A. & Medzhitov, R. Innate immune recognition. *Annual Reviews of Immunology* **20**, 197-216 (2002).

[76] Takeda, K., Kaisho, T. & Akira, S. Toll-like receptors. *Annual Review of Immunology* **21**, 335-376 (2003).

[77] Cook, D. N., Pisetsky, D. S. & Schwartz, D. A. Toll-like receptors in the pathogenesis of human disease. *Nature Immunology* **5**, 975-979 (2004).

[78] Hoebe, K., Janssen, E. & Beutler, B. The interface between innate and adaptive immunity. *Nature Immunology* **5**, 971-974 (2004).

[79] Iwasaki, A. & Medzhitov, R. Toll-like receptor control of the adaptive immune responses. *Nature Immunology* **5**, 987-995 (2004).

[80] Hase, A. *et al.* Characterization of glial cell line-derived neurotrophic factor family receptor α-1 in peripheral nerve Schwann cells. *Journal of Neurochemistry* **95**, 537-543 (2005).

[81] Migeotte, I., Communi, D. & Parmentier, M. Formyl peptide receptors: A promiscuous subfamily of G protein-coupled receptors controlling immune responses. *Cytokine & Growth Factor Reviews* **17**, 501-519 (2006).

[82] Ye, R. D. *et al.* International union of basic and clinical pharmacology. LXXIII. Nomenclature for the formyl peptide receptor (FPR) family. *Pharmacological Reviews* **61**, 119-161 (2009).

[83] Le, Y., Murphy, P. M. & Wang, J. M. Formyl-peptide receptors revisited. *Trends in Immunology* **23**, 541-548 (2002).

[84] Panaro, M. A. *et al.* Biological role of the N-formyl peptide receptors. *Immunopharmacology and Immunotoxicology* **28**, 103-127 (2006).

[85] Braun, M. C., Wang, J. M., Lahey, E., Rabin, R. L. & Kelsal, B. L. Activation of the formyl peptide receptor by the HIV-derived peptide T-20 suppresses interleukin-12 p70 production by human monocytes. *Blood* **97**, 3531-3536 (2001).

[86] Tedesco, E. *et al.* Calcium overload in nerve terminals of cultured neurons intoxicated by alpha-latrotoxin and snake PLA2 neurotoxins. *Toxicon* **54**, 7 (2009).

[87] Duan, Z. G. *et al.* Extraction and protein component analysis of venom from the dissected venom glands of *Latrodectus tredecimguttatus*. *Comparative Biochemistry and Physiology Part B: Biochemistry and Molecular Biology* **145**, 350-357 (2006).

[88] Grishin, E. V. Black widow spider toxins: the present and the future. *Toxicon* **36**, 1693-1701 (1998).

[89] Rosenthal, L. & Meldolesi, J. α-Latrotoxin and related toxins. *Pharmacology & Therapeutics* **42** (1989).

[90] Kiyatkin, N. I., Dulubova, I. E., Chekhovskaya, I. A. & Grishin, E. V. Cloning and structure of cDNA encoding α-latrotoxin from black widow spider venom. *Federation of European Biochemical Societies Letters* **270 (1)**, 127-131 (1990).

[91] Cavalieri, M., Corvaja, N. & Grasso, A. Immunocytological localization by monoclonal antibodies of α-latrotoxin in the venom gland of the spider *Latrodectus tredecimguttatus*. *Toxicon* **28**, 341-346 (1990).

[92] Smith, D. S. & Russell, F. E. *Structure of the venom gland of the black widow spider Latrodectus mactans. A preliminary light and electron microscopic study.*, 1-15 (Pergamon, 1966).

[93] Kirill E. Volynski, E. D. N., Yuri A. Ushkaryov, Eugene V. Grishin. Functional expression of α-latrotoxin in baculovirus system. *FEBS* **442**, 4 (1999).

[94] Ichtchenko, K. *et al.* α-Latrotoxin action probed with recombinant toxin: receptors recruit α-latrotoxin but do not transduce an exocytotic signal. *The EMBO Journal* **17 (21)**, 6188-6199 (1998).

[95] Kiyatkin, N. I., Kulikovskaya, I. M., Grishin, E. V., Beadle, D. J. & King, L. A. Functional characterization of black widow spider neurotoxins synthesised in insect cells. *European Journal of Biochemistry* **230**, 854-859 (1995).

[96] Ashton, A. C. *et al.* α-Latrotoxin, acting via two Ca^{2+}-dependent pathways, triggers exocytosis of two pools of synaptic vesicles. *The Journal of Biological Chemistry* **276 (48)**, 44695-44703 (2001).

[97] Orlova, E. V. *et al.* Structure of α-latrotoxin oligomers reveals that divalent cation-dependent tetramers form membrane pores. *Nature Structural Biology* **7**, 48-53 (2000).

[98] Finkelstein, A., Rubin, L. L. & Tzeng, M. C. Black widow spider venom: effect of purified toxin on lipid bilayer membranes. *Science* **193**, 1009-1011 (1976).

[99] Krasil'nikov, O. V., Ternovskiĭ, V. I. & Tashmukhamedov, B. A. [Channel formation properties of black widow venom]. *Biofizika* **27**, 72-75 (1982).

[100] Mironov, S. L., Sokolov, Y. V., Chanturiya, A. N. & Lishko, V. K. Channels produced by spider venoms in bilayer lipid membrane: mechanisms of ion transport an toxic action. *Biochimica et Biophysica Acta - Biomembranes* **862**, 185-198 (1986).

[101] McMahon, H. T., Rosenthal, L., Meldolesi, J. & Nicholls, D. G. α-Latrotoxin releases both vesicular and cytoplasmic glutamate from isolated nerve terminals. *Journal of Neurochemistry* **55**, 2039-2047 (1990).

[102] Deri, Z., Bors, P. & Adam-Vizi, V. Effect of α-Latrotoxin on acetylcholine release and intracellular Ca^{2+} concentration in synaptosomes: Na^{+}-dependent and Na^{+}-independent components. *The Journal of Neurochemistry* **60**, 1065-1072 (1993).

[103] Davletov, B. A. *et al.* Vesicle exocytosis stimulated by α-latrotoxin is mediated by latrophilin and requires both external and stored Ca^{2+}. *The EMBO Journal* **17**, 3909-3920 (1998).

[104] Wanke, E., Ferroni, A., Gattanini, P. & Meldolesi, J. α-Latrotoxin of the black widow spider venom opens a small, non-closing cation channel. *Biochemical and Biophysical Research Communications* **134**, 320-325 (1986).

[105] Hurlbut, W. P., Chieregatti, E., Valtorta, F. & Haimann, C. α-Latrotoxin channels in neuroblastoma cells. *Journal of Membrane Biology* **138**, 91-102 (1994).

[106] Scheer, H., Prestipino, G. & Meldolesi, J. Reconstitution of the purified α-latrotoxin receptor in liposomes and planar lipid membranes. Clues to the mechanism of toxin action. *The EMBO Journal* **5**, 2643-2648 (1986).

[107] Ushkaryov, Y. A., Petrenko, A. G., Geppert, M. & Sudhof, T. C. Neurexins: synaptic cell surface proteins related to the alpha-latrotoxin receptor and laminin. *Science* **257**, 50-56 (1992).

[108] Davletov, B. A., Krasnoperov, V., Hata, Y., Petrenko, A. G. & Südhof, T. C. High affinity binding of α-latrotoxin to recombinant neurexin I α. *The Journal of Biological Chemistry* **270**, 23903-23905 (1995).

[109] Sugita, S., Khvochtev, M. & Südhof, T. C. Neurexins are functional α-latrotoxin receptors. *Neuron* **22**, 489-486 (1999).

[110] Davletov, B. A., Shamotienko, O. G., Lelianova, V. G., Grishin, E. V. & Ushkaryov, Y. A. Isolation and biochemical characterization of a

Ca^{2+}-independent α-latrotoxin-binding protein. *The Journal of Biological Chemistry* **271**, 23239-23245 (1996).

111 Krasnoperov, V. G. *et al.* The calcium-independent receptor of α-latrotoxin is not a neurexin. *Biochemical and Biophysical Research Communications* **227**, 868-875 (1996).

112 Krasnoperov, V. G. *et al.* α-Latrotoxin stimulates exocytosis by the interaction with a neuronal G-protein-coupled receptor. *Neuron* **18**, 925-937 (1997).

113 Lelianova, V. G. *et al.* α-Latrotoxin receptor, latrophilin, is a novel member of the secretin family of G protein-coupled receptors. *The Journal of Biological Chemistry* **272 (34)**, 21504-21508 (1997).

114 Sugita, S., Ichtchenko, K., Khvotchev, M. & Südhof, T. C. α-Latrotoxin receptor CIRL/Latrophilin 1 (CL1) defines an unusual family of ubiquitous G-protein-linked receptors. *The Journal of Biological Chemistry* **273 (49)**, 32715-32724 (1998).

115 Ichtchenko, K. *et al.* A novel ubiquitously expressed α-latrotoxin receptor is a member of the CIRL family of G-protein-coupled receptors. *The Journal of Biological Chemistry* **274 (9)**, 5491-5498 (1999).

116 Matsushita, H., Lelianova, V. G. & Ushkaryov, Y. A. The latrophilin family: multiply spliced G protein-coupled receptors with differential tissue distribution. *Federation of the Societies of Biochemistry and Molecular Biology Letters* **443**, 348-352 (1999).

[117] Krasnoperov, V. *et al.* Protein-tyrosine phosphatase-σ is a novel member of the functional family of α-latrotoxin receptors. *The Journal of Biological Chemistry* **277 (39)**, 35887-35895 (2002).

[118] Matteoli, M. *et al.* Differential effect of alpha-latrotoxin on exocytosis from small synaptic vesicles and from large dense-core vesicles containing calcitonin gene-related peptide at the frog neuromuscular junction. *Proceedings of the National Academy of Sciences of United States of America* **85**, 7366-7370 (1988).

[119] Ushkaryov, Y. A., Rohou, A. & Sugita, S. in *Pharmacology of Neurotransmitter Release* Vol. 184 eds Thomas C. Südhof & Klaus Starke) 171-206 (Springer Berlin Heidelberg, 2008).

[120] Liu, W.-H., Kao, P.-H., Lin, S.-R. & Chang, L.-S. Membrane-damaging activity with A chain and B chain of β-bungarotoxin. *Toxicon* **53**, 262-268 (2009).

[121] Yang, C. C. *Chemical modification and functional sites of phospholipases A2 in venom phospholipase A2 enzymes.*, (John Wiley & Sons, 1997).

[122] Kini, R. M. *Venom phospholipase A2 enzymes.*, (John Wiley & Sons, 1997).

[123] Harris, J. B., Grubb, B. D., Maltin, C. A. & Dixon, R. The neurotoxicity of the venom phospholipase A2, notexin and taipoxin. *Experimental Neurology* **161**, 517-526 (2000).

[124] Prasarnpun, S., Walsh, J. & Harris, J. B. β-bungarotoxin-induced depletion of synaptic vesicles at the mammalian neuromuscular junction. *Neuropharmacology* **47**, 304-314 (2004).

[125] Prasarnpun, S., Walsh, J., Awad, S. S. & Harris, J. B. Envenoming bites by kraits: the biological basis of treatment-resistant neuromuscular paralysis. *Brain* **128**, 2987-2996 (2005).

[126] Montecucco, C., Rossetto, O. & Schiavo, G. Presynaptic receptor arrays for clostridial neurotoxins. *Trends in Microbiology* **12**, 442-446 (2004).

[127] Keller, J. E., Cai, F. & Neale, E. A. Uptake of botulinum neurotoxin into cultured neurons. *Biochemistry* **43**, 526-532 (2004).

[128] Rummel, A., Mahrhold, S., Bigalke, H. & Binz, T. The H_{CC}-domain of botulinum neurotoxins A and B exhibits a singular ganglioside binding site displaying serotype specific carbohydrate interaction. *Molecular Microbiology* **51**, 631-643 (2004).

[129] Rigoni, M. *et al.* Equivalent effects of snake PLA2 neurotoxins and lysophospholipid-fatty acid mixtures. *Science* **310**, 1678-1680 (2005).

[130] Fuller, N. & Rand, R. P. The influence of lysolipids on the spontaneous curvature and bending elasticity of phospholipid membranes. *Biophysical Journal* **81**, 243-254 (2001).

[131] Chernomordik, L. V. & Kozlov, M. M. Protein-lipd interplay in fusion and fission of biological membranes. *Biochemistry* **72**, 175-207 (2003).

[132] Hamilton, J. A. Fast flip-flop of cholesterol and fatty acids in membranes: implications for membrane transport proteins. *Current Opinion in Lipidology* **14**, 263-271 (2003).

[133] Chernomordik, L. V., Leikina, E., Frolov, V., Bronk, P. & Zimmerberg, J. An early stage of membrane fusion mediated by the

low pH conformation of influenza hemagglutinin depends upon membrane lipids. *The Journal of Cell Biology* **136**, 81-93 (1997).

[134] Abe, T., Limbrick, A. R. & Miledi, R. Acute muscle denervation induced by β-bungarotoxin. *Proceedings of Royal Society of London B* **194**, 545-553 (1976).

[135] Chen, I.-L. & Lee, C. Y. Ultrastructural changes in the motor nerve terminals caused by β-bungarotoxin. *Virchows Archiv B Cell Pathology Zell-Pathologie* **6**, 318-325 (1970).

[136] Cull-Candy, S. G., Fohlman, J., Gustavsson, D., Lüllmann-Rauch, R. & Thesleff, S. The effects of taipoxin and notexin on the function and fine structure of the murine neuromuscular junction. *Neuroscience* **1**, 175-180 (1976).

[137] Dixon, R. W. & Harris, J. B. Nerve terminal damage by β-bungarotoxin: its clinical significance. *The American Journal of Pathology* **154**, 447-455 (1999).

[138] Gopalakrishnakone, P. & Hawgood, B. J. Morphological changes induced by crotoxin in murine nerve and neuromuscular junction. *Toxicon* **22**, 791-804 (1984).

[139] Aoki, K. R. A comparison of the safety margins of botulinum neurotoxin serotypes A, B, and F in mice. *Toxicon* **39**, 1815-1820 (2001).

[140] Arce, V. *et al.* Cardiotrophin-1 requires LIFRβ to promote survival of mouse motoneurons purified by a novel technique. *The Journal of Neuroscience Research* **55**, 119-126 (1999).

[141] Monje, P. V. *et al.* Non-antagonistic relationship between mitogenic factors and cAMP in adult Schwann cell re-differentiation. *Glia* **57**, 947-961 (2009).

[142] Giacomello, M. *et al.* Reduction of Ca2+ stores and capacitative Ca2+ entry is associated with the familial Alzheimer's disease presenilin-2 T122R mutation and anticipates the onset of dementia. *Neurobiology of Disease* **18**, 638-648 (2005).

[143] Young-Jin Son, J. T. T. a. W. J. T. Schwann cells induce and guide sprouting and reinnervation of neuromuscular junctions. *Trend in Neuroscience* **19**, 280-285 (1996).

[144] Rigoni, M. *et al.* Snake presynaptic neurotoxins with phospholipase A2 activity induce punctate swellings of neurites and exocytosis of synaptic vesicles. *The Journal of Cell Science* **117**, 3561-3570 (2004).

[145] Pennuto, M., Dunlap, D., Contestabile, A., Benfenati, F. & Valtorta, F. Fluorescence resonance energy transfer detection of synaptophysin I and vesicle-associated membrane protein 2 interactions during exocytosis from single live synapses. *Molecular Biology of the Cell* **13**, 12 (2002).

[146] Rigoni, M. *et al.* Calcium influx and mitochondrial alterations at synapses exposed to snake neurotoxins or their phospholipid hydrolysis products. *The Journal of Cell Biology* **282**, 11238-11245 (2007).

[147] Rossetto, O. & Montecucco, C. Presynaptic neurotoxins with enzymatic activities. *Handbook of Experimental Pharmacology* **184**, 129-170 (2008).

[148] Ceccarelli, B., Hurlbut, W. P. & Mauro, A. Depletion of vesicles from frog neuromuscular junctions by prolonged tetanic stimulation. *The Journal of Cell Biology* **54**, 30-38 (1972).

[149] Ceccarelli, B. & Hurlbut, W. P. Vesicle hypothesis of the release of quanta of acetylcholine. *Physiological Reviews* **60**, 396-441 (1980).

[150] Lee, C. Y., Tsai, M. C., Chen, Y. M., Ritonja, A. & Gubensek, F. Mode of neuromuscular blocking action of toxic phospholipases A2 from Vipera ammodytes venom. *Archives Internationales de Pharmacodynamie et de Therapie* **268**, 313-324 (1984).

[151] Pungerčar, J. & Križaj, I. Understanding the molecular mechanism underlying the presynaptic toxicity of secreted phospholipases A2. *Toxicon* **50**, 871-892 (2007).

[152] Rigoni, M. *et al.* Snake phospholipase A2 neurotoxins enter neurons, bind specifically to mitochondria, and open their transition pores. . *The Journal of Biological Chemistry* **283**, 34013-34020 (2008).

[153] Robbins, N., Kuchynski, M., Polak, J. & Grasso, A. Motor nerve terminal restoration after focal destruction in young and old mice. *International Journal of Developmental Neuroscience* **8**, 667-678 (1990).

[154] Stevens, B. & Fields, R. D. Response of Schwann cells to action potentials in development. *Science* **287**, 2267-2271 (2000).

[155] Selvatici, R., Falzarano, S., Mollica, A. & Spisani, S. Signal transduction pathways triggered by selective formylpeptide analogues in human neutrophils. *European Journal of Pharmacology* **534**, 1-11 (2006).

[156] Verderio, C. *et al.* Cross talk between vestibular neurons and Schwann cells mediates BDNF release and neuronal regeneration. *Brain Cell Biology* **35**, 187-201 (2006).

[157] Barber, S. C., Mellor, H., Gampel, A. & Scolding, N. J. S1P and LPA trigger Schwann cell actin changes and migration. *European Journal of Neuroscience* **19**, 3142-3150 (2004).

[158] Latz, E. *et al.* TLR9 signals after translocating from the ER to CpG DNA in the lysosome. *Nature Immunology* **5**, 190-198 (2004).

[159] Hoene, V., Peiser, M. & Wanner, R. Human monocyte-derived dendritic cells express TLR9 and react directly to the CpG-A oligonucleotide D19. *Journal of Leukocyte Biology* **80**, 1328-1336 (2006).

[160] Durstin, M., Gao, J. L., Tiffany, H. L., Mcdermott, D. & Murphy, P. M. Differential expression of members of the n-formylpeptide receptor gene cluster in human phagocytes. *Biochemical and Biophysical Research Communications* **201**, 174-179 (1994).

[161] Walker, B. A., Seiler, A. J., Owens, C. A., Hagenlocker, B. E. & Ward, P. A. Absence of FMLP receptors on rat macrophages. *Journal of Leukocyte Biology* **50**, 600-606 (1991).